# Chitin and the Gel Within the Electrosensory Organs of Cartilaginous Fishes

**Molly Berkley Phillips**

A dissertation

submitted in partial fulfillment of the

requirements for the degree of

Doctor of Philosophy

University of Washington

2020

Reading Committee:

Chris T Amemiya, Chair

Martha Bosma

Joseph A Sisneros

Program Authorized to Offer Degree:

Biology

University of Washington

**Abstract**

# Chitin and the Gel Within the Electrosensory Organs of Cartilaginous Fishes

Molly Berkley Phillips

Chair of the Supervisory Committee:
Chris T Amemiya
Department of Biology

In 1678, the Italian physician, Stefano Lorenzini discovered a mysterious set of tubular organs inside an electric ray. The function of these organs, named Ampullae of Lorenzini (AoL), was unknown for almost three centuries until physiological and behavioral studies revealed that they were sensitive to weak electric fields. AoL have been observed in all cartilaginous fishes and are used to detect electric fields emitted by other animals and possibly for navigation using the earth's magnetic field. They are comprised of open pores that lead into tubular canals filled with a viscous hydrogel and terminate distally in lobed structures containing specialized electrosensory cells. External field stimuli must pass through the AoL's space-filling gel to reach the distal electrosensory cells, yet we do not understand what role the material plays in the process. Further, some recent studies have documented some of the gel's constituents and properties, but its complete molecular makeup and physical structure remain unknown.

In this dissertation, I present biological, physicochemical, and structural evidence that chitin is a component of AoL gel in diverse cartilaginous fish species. This is surprising because, until the recent discovery of endogenous chitin within several fish and amphibian

species, it was thought that the structural polysaccharide was not synthesized by vertebrates. Due to the novelty of this field of study, I carried out diverse experiments to satisfy the burden of proof that chitin is prevalent within the AoL and corresponds with the expression of genes that code for chitin synthesizing enzymes (chitin synthases). Chitin binding histochemical probes localized specifically to the gel inside the AoL and treatment with chitin digesting enzymes (chitinases) subsequently eliminated probe binding completely. *In situ* hybridization studies on chitin synthase genes revealed an overt spatial correspondence between chitin synthase expression and chitin binding probes in the AoL. Additionally, analytical techniques confirmed that the gel material exhibited characteristic chitin signatures. Using the little skate (*Leucoraja erinacea*) as my experimental system, I documented the developmental onset of the AoL themselves and the appearance of chitin within AoL gel. Subsequently, I observed some surprising features of developing AoL and discovered a curious population of chitinous structures widespread across the skin of developing little skate embryos. Finally, ever interested in the function of chitin within AoL gel, I worked collaboratively with researchers in the Physics and Materials Sciences departments at UC Merced as well as electrical engineers at UC Santa Cruz to provide a descriptive report of the molecular structure of gel from spotted ratfish (*Hydrolagus colliei*) specimens. Imaging with atomic force and scanning electron microscopy revealed that ratfish gel is seemingly colloidal in nature – composed of aggregating spherical particles. X-ray scattering analyses, proton conductivity assays, and further imaging studies were carried out to investigate the differences between native gel and gel that had been digested with proteolytic enzymes. With these experiments, I learned that proteins are critical for the maintenance of both the gel's stiffness and organized polymeric network and upon their removal, the remaining material readily forms crystalline structures similar in morphology to published images of chitin nanocrystals.

# Table of Contents

# List of Figures & Tables

## Acknowledgments

I will start by thanking the fishes. As an animal lover, having had to sacrifice numerous fishes, tiny and large, young and old, was by far the most taxing part of graduate school. The animals themselves taught me more than any person ever could and I will forever remain indebted to them for their involuntary participation in my research. I only hope that the findings laid out here will benefit future fishes in one way or another.

My list of mentors and supporters is lengthy and ever-expanding! Before I landed at UW, my trajectory was shaped by a handful of influential experiences – working as a technician at MBL in charming Woods Hole, MA, scrambling through the rainforests of Malaysia as a field guide for Ecofieldtrips, and studying at the Oregon Institute of Marine Biology where my childhood passion for "all things ocean" evolved into a concrete foundation for my future. I would not have pursued a graduate degree in biology had it not been for the many people and places I encountered during these phases of my life.

I began my tenure at UW as a student in the embryology course at Friday Harbor Laboratories on San Juan Island, a magical place. There I spent the summer with Zander Fodor, my first UW friend and colleague. I am grateful for his guidance as I sorted out how to start grad school, for his contagious affection of squishy inverts, and for his efforts to bring tie dye back! Zander left us too soon and his memory has and will always motivate me. Zander, Josh Swore, Shawn Luttrell, and Billie were my first welcome into the UW community. I am grateful to Billie for hosting me as a rotation student and for always being the first person to "cheers" with me at departmental happy hours!

To my advisor Chris Amemiya. Soon after I joined his lab, Chris said in an email: "we shouldn't be ashamed to pursue knowledge for the sake of knowledge… everything else is value added." In a world where grant awards, reviewer comments, and red tape can often dictate our productivity, my enthusiastic mentor always allowed curiosity to drive my experiments. I am so lucky to have been showered by Chris' positivity and encouragement throughout this process; his support, in so many different ways, has been overwhelming.

I had the privilege to work alongside a number of talented, interesting scientists in the Amemiya lab at Seattle's Benaroya Research Institute and at UC Merced. I want to thank Lauren Vandepas for keeping our lab full of energy (and fun music). Thanks to Mike Rego for his quiet support and patience on the days that I struggled and for always filling the room with his infectious laugh. Thanks to many other Amemiya lab members including

Aline Dragalzew, Athena Avalos, Natalia Buceta, Murat Kaya, Leesa Hagerman, Kyle Rekedal, and Hailey Harkness for technical help and comradery – to be lab mates is to be family. I am grateful to Daniel Ocampo Daza for giving me many lessons on genome evolution, computation, and all things pop culture. It can be isolating when you work in a niche field of study and when Daniel arrived in our lab, already very familiar with chitin synthases and the Ampullae of Lorenzini, it was such a relief. I want to thank Joyce Tang for showing me how to use the microscopes and analyze images with ImageJ, how to manage the lab, the list goes on and on… Joyce introduced me to many of the biological methodologies that I employed for this dissertation and even though I only had her with me for my first two years, she remained a thoughtful mentor and friend throughout my graduate career. Finally, with the exception of Chris, Hassan Khan has been my only constant in graduate school. Each day I could rely on his mood to be positive and level-headed. For five straight years, he never failed to put down his pencil or pipet and help me overcome a problem. Hassan, thank you for always checking my math (no matter how simple) without judgment. I will forever cherish our countless discussions as we stared out the window at the rolling hills skirting the distant Sierras.

I want to thank the many collaborators I worked with both at UW and UCM, including Linda Hirst, Manping Jia, Richard Johnson, Linda Hirst, Valerie Leppert, Matthew Robinson, Marco Rolandi, Joel Spencer, and Alauna Wheeler. The work described in this dissertation is a product of many great ideas from an incredible group of scientists and these studies would not have progressed without their help. I also want to thank Clare Baker and Andrew Gillis for sharing protocols and offering experimental advice in my times of need. Andrew took particular interest in helping me make progress on the content described in Chapter 2 and I would have approached all of my skate work blindly had it not been for his careful and generous guidance.

Thank you to my dissertation committee, Dave Raible, Joe Sisneros, Marti Bosma, and Lorenz Hauser. I spent more than half of graduate school as a long-distance student, so I am appreciative to have maintained close relationships with my committee members. They could easily have bailed when my scenario got complicated, but they didn't. Thanks especially to Lorenz for letting me rotate in his lab, where I had the pleasure of working with the lovely, Eleni Petrou. I loved spending time with you fishy people.

To the incredible Biology department at the University of Washington. Thank you to Marissa Heringer and Krista Clouser for answering my seemingly constant questions

about how to be a long-distance graduate student. And thanks to Ben Kerr for offering me much needed advice (and popcorn!) when I met some challenges. To the staff, faculty, postdocs, and grads that I was lucky to teach with, especially Mandy Schivell and Christopher Wells – teaching "Inverts" alongside you was rewarding and wonderful. Although our lab's relocation to California meant that I was only at UW in person for two years of graduate school, the friendships I made there are lifelong. Biograds, collectively you are some of the funniest, most talented, impressive people I have ever met! To Livy Kosterlitz, Ana Maria Bedoya, Lyda "Tootsie" Harris, Meera Lee Sethi, Mo Turner, Claire Rusch, and many others, your love and laughter kept this process fun even in the low lows.

To my UC Merced family. It was challenging and isolating moving to rural California in the middle of a semester and in the middle of my degree. A handful of very warm, welcoming grads made the transition easier. Thanks to Angel Kongsomboonvech, Eli Isael Maciel, Cristie Donham, Alauna Wheeler, Paniz Rahmani, Zach Petrak, and especially Amanda Tan. I don't think I would have made it to the end without those cookie & Disney nights! And thank you to my precious parking lot pup, Tug, who made me smile every day and gave me some well-needed purpose during lonely times.

Thanks to Megan, Elisa, Shannon, Eunice, Victoria "Squishy," Amitai, David, Tyler, and Monica. You never failed to keep these past five years full of joy and you showed interest in my research even in the rare times that I myself found it dull!

Finally, I want to thank my family. To my brother, Casey. I am who I am because of your influence. To my dad, Rob, whose support knows no bounds. There is no one else with your work ethic and motivation. You taught me to push myself, and I did! To mama. Thank you for showing me how to stop and appreciate the wonder of nature and for filling my life with so much magic. Thank you for always listening – no matter how long the ramble, no matter how senseless the point, no matter how strange the topic. Now, of course, to my Scotty. I have been following a path paved by science from the day we met, and all along your magnanimity and patience never wavered. Since we began our coevolution as teeny boppers, you have endured years and years of living at great distances, tremendous lows, trials, and even a breaking point. You adapted to the lifestyle graduate school required of me (more elegantly than I) and you never let a single day pass without making me laugh. I thank you and I love you fiercely.

**In memory of Ryder Buck**

"Life takes crazy twists and turns, but sometimes they're for our betterment, and we can't realize why until much further down the road.

# Introduction

*Introduction to electroreception*

There are many sources of both animate and inanimate electric fields, from earth's magnetic field, to a small swimming copepod. In aquatic environments, differences in ion concentrations between the inside of a living organism and the surrounding water generate weak bioelectric fields that are modulated by movements including ventilation (Collin & Whitehead 2004, Kalmijn 1974, Wilkens & Hofmann 2005). These electric fields are detectable by electroreceptive animals. Ample evidence suggests that a form of electroreception, the extraordinary ability to detect electric fields, evolved in the ancestors to all vertebrates over 500 million years ago (Bullock et al 1983, New 1997). Ancestral electroreceptive capabilities have been maintained in some extant vertebrate clades and lost in others such as anurans, teleost fishes, and amniotes. Interestingly, analogous electrosensory abilities subsequently evolved in a few different teleost lineages as well as some amniote species (Baker et al 2013, Czech-Damal et al 2013, Lissman 1951, Pettigrew 1999). It is thought that the ability to detect electric fields exists solely in animals that inhabit aqueous or moist environments, because the trait is dependent on the electrical resistivity of surrounding media (Klimley 2010).

*Cartilaginous fishes of the class Chondrichthyes*

The ancestral form of vertebrate electroreception has been most rigorously studied in the organisms that are the main subjects of this dissertation, namely the cartilaginous fishes (class Chondrichthyes), a class of aquatic animals divided into two subclasses:

Elasmobranchii and Holocephali (Figure I.1). The elasmobranchs are further split into two clades, the Selachii, an informal group of animals containing all of the familiar sharks that you have possibly grown to admire (or fear), and the Batoidea, a superorder containing the "flattened sharks," or skates and rays. Holocephalans are likely less familiar cartilaginous fishes, many of which inhabit deep, benthic ecosystems. Holocephalans diverged from elasmobranchs some 400 million years ago and are generally referred to as chimaeras or ghost sharks (Inoue et al 2010).

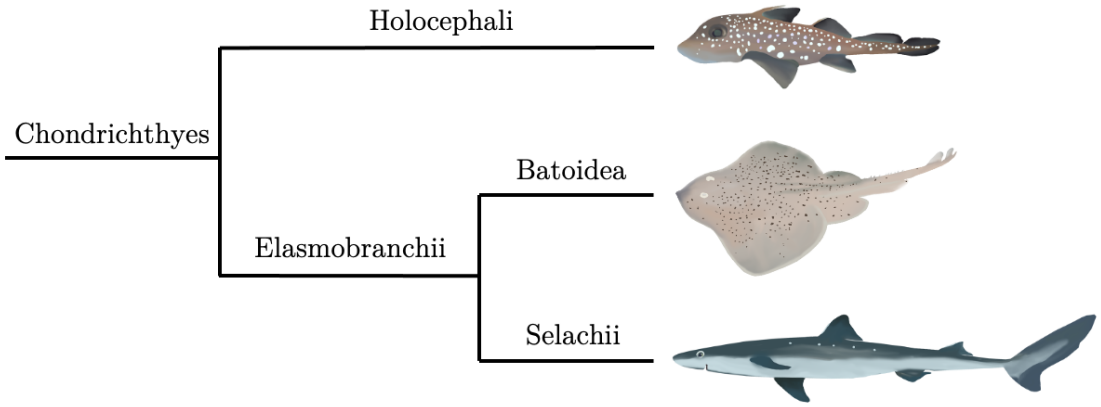


**Figure I.1** A simplified phylogeny showing the names of major taxonomic groups of cartilaginous fishes. Cartoon images depict a single representative species from the subclass Holocephali (spotted ratfish, *Hydrolagus colliei*), the superorder Batoidea (little skate, *Leucoraja erinacea*), and the clade Selachii (spiny dogfish, *Squalus acanthias*). Note that cartoons are not drawn to scale.

*Introduction to the electroreceptive Ampullae of Lorenzini (AoL) of cartilaginous fishes*

The detection of electric fields is made possible by a network of sensory organs that contain specialized electroreceptive cells. In the 17$^{th}$ century, the organs were first discovered inside an electric ray by the Italian physician, Stefano Lorenzini but remarkably, their electrosensory function wasn't determined until the 1960s (Lorenzini 1678, Murray 1960, Murray 1962). The electroreceptive organs found in cartilaginous fishes are called Ampullae of Lorenzini (also known as ampullary organs or "AoL"). The number and distribution of

AoL in many species have been meticulously counted and mapped and show a broad morphological diversity amongst cartilaginous fishes. In very general terms, the AoL of sharks and chimaeras are most concentrated rostrally and ventrally, whereas in the batoids, while still most concentrated rostrally, AoL are more widespread across the ventral and dorsal body surfaces (Kempster et al 2012, Raschi 1986). Cartilaginous fishes use their AoL for a variety of purposes including the identification of prey, the localization of conspecifics for mating, and perhaps even for navigation (Collin & Whitehead 2004, Kalmijn 1974, Newton & Kajiura 2017, Tricas et al 1995). These activities are referred to as "passive electroreception."

The detailed morphology of the AoL in many chondrichthyan species has been well documented using electron and light microscopy (Camilieri-Asch et al 2013, Fields 1993, Fishelson & Baranes 1998, Raschi 1986, Tavares Schafer et al 2012, Waltman 1966). In general, a single AoL contains a tubular canal surrounded by an insulating collagenous sheath, open on one end to the environment *via* a pore in the skin (Figure I.2A,B). As mentioned earlier, many AoL features, including pore diameter and canal length, vary significantly and are highly dependent on species, environment, and anatomic location (Newton et al 2019). In little skates (*Leucoraja erinacea*), a species that was studied extensively for this dissertation, I found that AoL pores in embryos are ~10-20 $\mu$m in diameter whereas those in adults are ~100 $\mu$m. AoL canals are lined on the inside by two layers of squamous epithelial cells (Waltman 1966, Whitehead et al 2015). At the distal end of the canal is a round, lobed structure called an alveolus and the whole organ is filled with an acellular viscous hydrogel that can be removed from AoL pores and studied (Figure I.2B). The alveolus contains specialized electrosensory cells that are surrounded by support

cells and innervated by afferent nerve fibers of specific rami from the anterior lateral line nerve (Bodznick & Schmidt 1984, Szabo 1974).

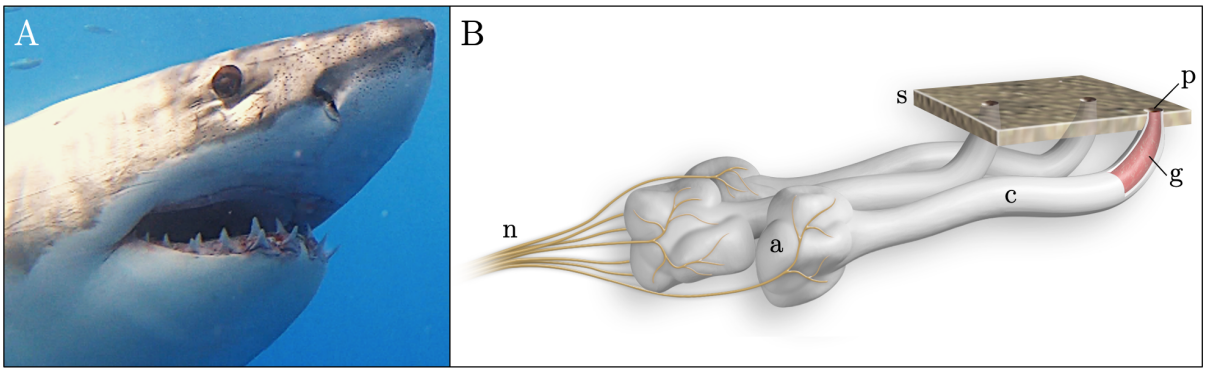


**Figure I.2** Distribution and anatomy of Ampullae of Lorenzini. **A)** An adult great white shark (*Carcharodon carcharias*) with AoL pores covering its snout. **B)** Diagram depicting the general anatomy of three simplified AoL (a: alveolus (pl. alveoli)); c: canal; g: gel; n: nerves; p: pore; s: skin surface).

Electrosensory cells inside AoL share many morphological, developmental, transcriptional, and physiological similarities with mechanosensory hair cells of the lateral line, which supports the likelihood that the two cell types share an evolutionary origin (Baker 2019, Baker et al 2013, Modrell et al 2017, Szabo 1974). There have been a number of elegant electrophysiological studies on the anatomy and the response properties of the neurons that innervate chondrichthyan electrosensory systems (Bodznick & Montgomery 2005, Bodznick & Northcutt 1980, Bodznick & Schmidt 1984, New 1990, Northcutt 1997). Further, signal transduction in skate electrosensory cells has been recently characterized. The simplified order of events begins with the opening of specialized voltage-gated $Ca^{2+}$ channels on the apical surface of the electrosensory cells in response to environmental electric fields (specifically, low-frequency cathodal fields). The entry of $Ca^{2+}$ leads to the depolarization of both apical and basal cell membranes leading to the opening of other $Ca^{2+}$ channels and the basal release of glutamate via the exocytosis of synaptic vesicles. The $Ca^{2+}$ influx also triggers the opening of $Ca^{2+}$-activated $K^{+}$ channels on the apical cell surfaces,

which repolarize the membrane (Bellono et al 2017, King et al 2016, Leitch & Julius 2019, Modrell et al 2017).

After Murray determined that chondrichthyan AoL perform an electrosensory function, Adrianus Kalmijn discovered that the fish are behaviorally sensitive to electrodes emitting a voltage gradient as low as 5 nV/cm (Kalmijn 1982, Murray 1960)! Interestingly, this minute field strength is weaker than the minimum voltage required for a physiological response from the AoL afferent neurons (Dijkgraff & Kalmijn 1962, Dijkgraff & Kalmijn 1966, Kalmijn 1974). Despite the many studies that have been conducted on the electrosensory systems of cartilaginous fishes alone, it remains unknown how changes in weak electric fields are transmitted from the environment through the AoL and how the gel inside the organs is involved in the process.

*Embryonic development of AoL*

In vertebrates, many anatomic structures develop from specific thickenings of ectodermal cells known as placodes that develop in stereotypical positions. There are various types of placodes in vertebrates that each give rise to a specific population of structures and/or tissue types (Graham & Shimeld 2013). In a 2012 study, Gillis et al injected dye into lateral line placodal cells of developing little skate embryos to track their trajectories over developmental time (Gillis et al 2012). These so-called, "fate-mapping studies" demonstrated that cells within maturing AoL (and mechanosensory neuromasts) originate from lateral line placodes and migrate to the eventual location where the organs are then formed (Gillis et al 2012). These findings along with the results of some transcriptomic studies, collectively led researchers to conclude that the electrosensory cells in ampullary organs share common ancestry with lateral line hair cells (Baker & Modrell 2018). Two published studies documented early-stage AoL developing from initial invaginations in the

skin surface, but otherwise I am not aware of any further descriptions of AoL development in cartilaginous fishes (Freitas et al 2006, Gillis et al 2012). Therefore, there is a large gap in our understanding of how these initial invaginations evolve into complex and widespread mature electrosensory organs.

*Electrosensory organs in other taxa*

Chondrichthyan electrosensory organs share homology with those of coelacanths, lungfishes, some amphibians, and "basal branching" ray-finned fishes including sturgeons, bichirs, and paddlefishes. The electrosensory systems of these fishes all respond to cathodal stimuli, are innervated by anterior lateral line nerves that project onto the medulla, and will hereafter be referred to as "ancestral ampullary" organs (Baker et al 2013). These ancestral ampullary organs were subsequently lost in hagfishes, amniotes, anurans (frogs & toads), and in the Neopterygii, a clade containing most familiar bony fishes (Figure I.3). Electrosensory organs have never been observed in hagfish, but lampreys possess organs known as "end buds," that are thought to be homologous to ancestral ampullary organs because they both share similar response properties and innervation (although they have very different morphologies) (Bullock et al 1983). Because of this suspected homology, ampullary electroreception may have evolved in the ancestors to all vertebrates (jawed and jawless) although as Baker et al point out, embryonic studies need to be carried out in lampreys in order to confirm this claim (Baker et al 2013). As far as we know, the only invertebrates that may be able to detect electric fields are two species of freshwater crayfish (Patullo & Macmillan 2010).

As mentioned earlier in the introduction, some teleost clades independently evolved electrosensory systems after ancestral ampullary organs had been lost somewhere in the lineage leading to all neopterygian fishes (Figure I.3). There are two distinct groups of

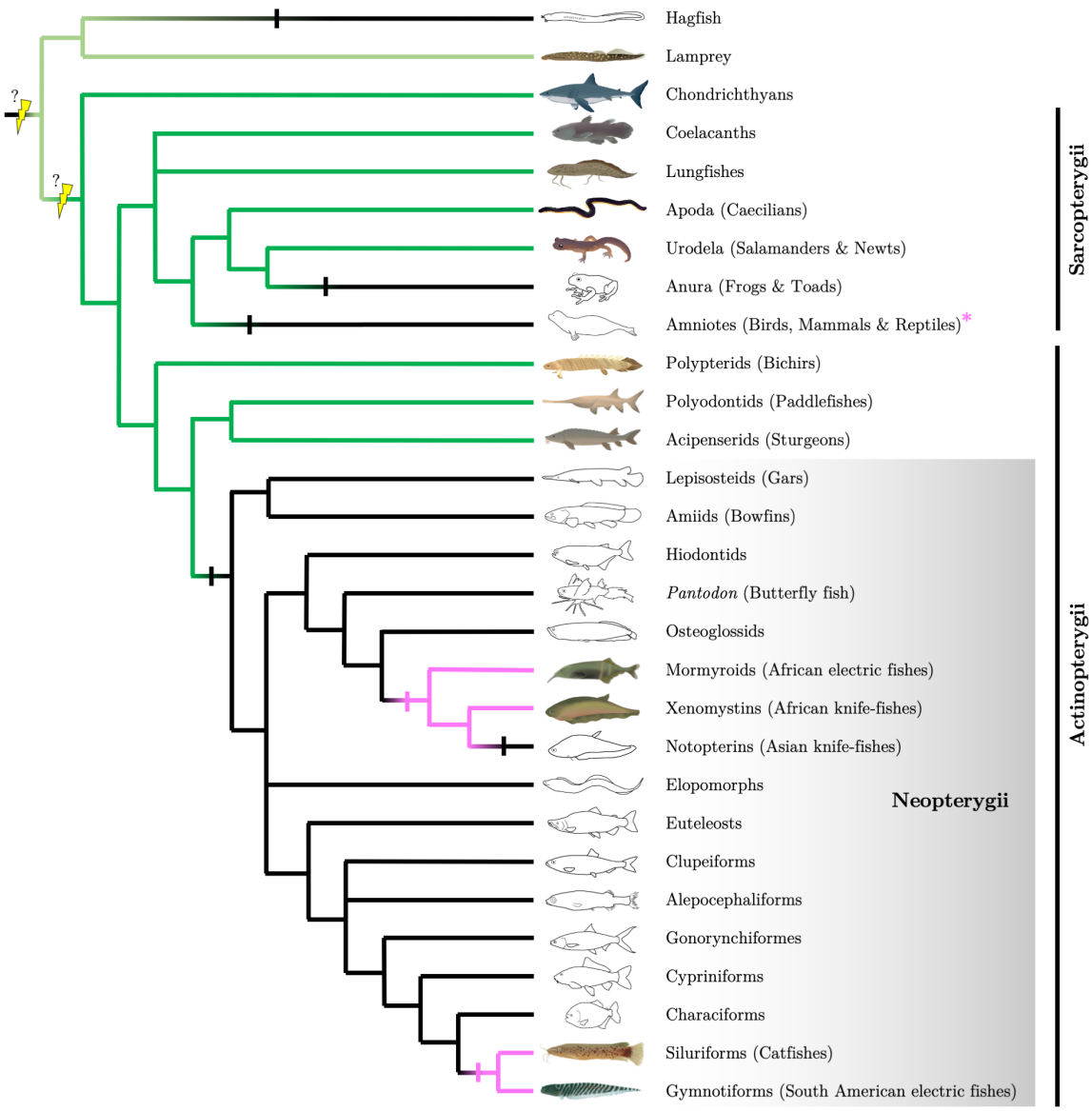


**Figure I.3** A phylogeny showing the distribution of electroreception amongst extant vertebrates. Yellow lightning bolts represent two hypothetical origins of ancestral ampullary organs. If lamprey electrosensory organs share homology with other fishes such as chondrichthyans, as suggested by the shared innervation and sensory mechanisms of the two types of organs, then hagfishes would have lost electrosensory abilities and all green branches would indicate clades that possess the ancestral form of electroreception. If, however, lampreys independently evolved endbud electrosensory organs, as suggested by their unique morphology, then ampullary electrosensory organs would have originated in the ancestors to all jawed vertebrates and were maintained only in those lineages at the tips of bright green branches (Baker et al 2013). Black hash marks represent losses of electroreception based on parsimony. The ancestral electrosensory system was likely lost several times over evolutionary time including in the ancestors to all amniotes (although pink asterisk indicates that monotremes and Guiana dolphins independently evolved electrosensory organs), in the ancestors to anurans, and before the divergence of the Neopterygii, which includes the majority of ray-finned fishes. Black branches correspond to clades that are not electroreceptive, visually shown by black/white animals which represent a single species within each clade. Pink hash marks indicate the independent origins of teleost ampullary-type electrosensory organs and pink branches show lineages that maintained electroreceptive abilities. Colored animals depict a representative species from each of the electroreceptive clades. Figure modified from (Lavoue et al 2012).

electroreceptive teleost fish. The first group consists of mormyroids (which comprises fish in the family Mormyridae and the single species within the family Gymnarchidae) along with African and Asian knifefishes, while the gymnotiforms (South American knifefishes) and catfishes of the order Siluriformes make up the second group (Figure I.3) (Baker 2019). Despite their independent origins, the electrosensory organs of the fishes in these two distinct groups are similar in that they respond to anodal stimulation. Interestingly, fishes belonging to the family Mormyridae and the order Gymnotiformes both possess electrogenic organs which they use to communicate and interact with their environment. These fishes have evolved ampullary organs that are fairly similar in anatomy to those of their cartilaginous relatives and used to detect environmental electric fields (passive electroreception). They also possess a secondary set of electroreceptors called tuberous organs which receive and interpret discharges emitted from their own electric organs (an act referred to as active electroreception) (Baker 2019). There are a few types of tuberous electroreceptors found within these fishes and they will be briefly described in Chapter 1.

Although ancestral ampullary organs were lost in the lineage that gave rise to the amniotes, we know of a few amniote groups that independently evolved electrosensory organs. These include the monotremes (echidnas and platypus) and one species of cetacean, the Guiana dolphin. Unlike fishes, monotremes and Guiana dolphins each developed their own unique type of electroreceptive organs. Of the monotremes, at least two of the four echidna species have electrosensory organs but they are far less numerous than those of their cousin, the platypus (which is likely a product of their different life history strategies) (Czech-Damal et al 2013). Interestingly, monotreme electrosensory organs are seemingly modified mucous and serous glands that use free nerve endings from the trigeminal system as electroreceptor cells (Asahara et al 2016, Czech-Damal et al 2013). In contrast, the electrosensory organs of Guiana dolphins consist of a dozen ampulla-shaped gel-filled

vibrissal crypts that are innervated by branches of the trigeminal nerve. It is unclear how the dolphins detect electric fields as they do not appear to possess specialized electrosensory cells nor bare nerve endings as are seen in the monotremes (Czech-Damal et al 2012).

*The unknown function of AoL gel*

Although admittance data demonstrated that AoL gel does not facilitate the movement of electrons (Brown et al 2005), the material was shown to have a proton conductivity of 2 mS/cm, the highest value of any biological substance yet reported (Josberger et al 2016). This remarkably high proton conductivity was documented in gel from three different cartilaginous fish species (one shark and two skates) and was attributed to keratan sulfate, a polysaccharide that with known proton conductive properties that was recently identified in the gel (and described in more detail later in this introduction) (Josberger et al 2016, Selberg et al 2019). This study described some very compelling new characteristics of AoL gel, however we still don't understand how the proton conductive gel contributes to the overall function of the AoL in cartilaginous fishes. It is possible that the gel plays a direct role in the movement of signals from the environment to the distal electrosensory cells, but it is mechanistically unclear, to me at least, how this would work. There are a few other hypothetical roles of the gel within the AoL. For example, it is possible that the gel confers resistance to infection from pathogens that could easily invade from the environment. Alternatively, perhaps the gel's viscoelasticity provides rigidity necessary to build the tubular AoL during development and maintain their shape over time. This potential function is explored in Chapter 2 of this dissertation.

*The protein component of AoL gel*

Not surprisingly, studies have reported that there are clear signatures of proteins within AoL gel, however their specific identities have remained elusive (How & Jones 1969, How et al 1970). Zhang et al recently generated a proteome using gel extracted from big skate (*Raja binoculata*) and identified a number of candidate gel component proteins (Zhang et al 2018). Interestingly, they identified actin, tropomyosin, and keratin within their proteome, all proteins that are known to exist intracellularly and/or in the extracellular matrix (Zhang et al 2018). Further, a type of mucin, which is a major component of mucosal substances, was also present in the published proteome. Although these findings were compelling, it is possible that these proteins could have resulted from cellular contamination as cells readily slough off from the epithelium during the gel removal process. This topic will be addressed in more detail in Chapter 3.

*The polysaccharide component of AoL gel*

AoL gel from marine elasmobranchs is made of ~95% water with an ionic composition very similar to that of seawater (Murray & Potts 1961). The concentrations of urea and $K^+$ increase marginally in a gradient from pore to alveolus, likely due to mixing with environmental media at the pore interface (Murray & Potts 1961). Over fifty years ago, Doyle studied the materials making up AoL gel from a dogfish shark (*Squalus acanthias*), and classified the major non-water components as "mucopolysaccharides," with glucosamine and galactosamine (monosaccharides) observed in a ratio of approximately 4:1 (Doyle 1967, Doyle 1968). However, when Doyle compared the gel components of several diverse cartilaginous fishes, the monosaccharide ratios were actually quite variable amongst species (Doyle 1968). Doyle also noted that gel exhibited a greater stiffness in species that possessed

larger AoL pore diameters, which corresponded to a higher concentration of sugars (Doyle 1967, Doyle 1968).

Since then, it has been confirmed that keratan sulfate, namely the type called KS I, exists as a component of AoL gel from skates (Josberger et al 2016, Zhang et al 2018). Keratan sulfates are glycosaminoglycans (GAGs) that consist mostly of repeating dimers of sulfated N-acetylglucosamine and galactose (Figure I.4A). There are three classes of keratan sulfate, called KS I, KS II, and KS III, each with different oligosaccharides connecting them to core proteins of various types depending on location and function (Uchimura 2015). Josberger et al inferred the presence of keratan sulfate in AoL gel using Fourier transform infrared spectroscopy (FTIR) in addition to a compositional analysis with AoL gel from a skate, and like Doyle, they observed a higher abundance of glucosamine as compared to galactose and galactosamine (Doyle 1967, Josberger et al 2016).

Following the initial discovery of keratan sulfate in AoL gel by Josberger et al, Zhang et al studied the glycosaminoglycan content of big skate gel specifically and found that keratan sulfate was definitively the only glycosaminoglycan present (Josberger et al 2016, Zhang et al 2018). This was an unexpected finding as multiple glycosaminoglycans are typically found comprising animal tissues (Zhang et al 2018). Importantly, the study by Zhang et al focused on glycosaminoglycans specifically, and their extraction methods using a strong anion exchange membrane would have excluded uncharged polysaccharides (Zhang et al 2018). Therefore, despite the apparent variability in polysaccharide composition amongst chondrichthyans, evidence suggests that AoL gel contains polysaccharides and/or monosaccharides in addition to keratan sulfate. Chapter 1 of this dissertation will focus entirely on the identification of chitin, another type of polysaccharide, within AoL gel.

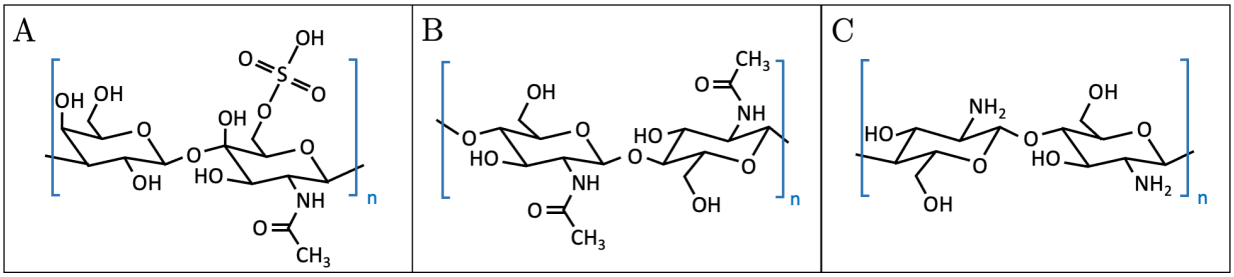


**Figure I.4** Chemical structures of three relevant polysaccharides. **A)** Keratan sulfate consists of repeating dimers of galactose and *N*-acetylglucosamine 6-sulfate, with a variable protein binding oligosaccharide region on one end (not shown). **B)** Chitin consists of repeating units of $\beta$-(1-4)-linked *N*-acetylglucosamine. **C)** Chitosan is made of $\beta$-(1-4)-linked *N*-glucosamine (although the degree of acetylation varies).

*Chitin*

Chitin, a polysaccharide composed of repeating units of *N*-acetylglucosamine, is found abundantly in the biosphere and is a key component of structures such as fungal cell walls and arthropod exoskeletons (Figure I.4B). Chitin is a very durable, water insoluble material. When chitin is deacetylated, by chemical and/or enzymatic means, it becomes far more reactive, soluble, and biodegradable and is known as chitosan (Figure I.4C) (Roy et al 2017). The degree of deacetylation, which can be determined by various methods, is an important metric that dictates the properties of chitin or chitosan and although published definitions of the copolymers vary, it is generally accepted that when >90% of the glucosamine monomers are acetylated, the molecule can be referred to as chitin (Roy et al 2017, Sato et al 1998). Chitin is one of the world's most abundant polymers, yet due to the wide distribution of chitinases, a group of enzymes that digest chitin, it isn't found dramatically accumulating in the environment (Rathore & Gupta 2015). Chitinases are found in bacteria, plants, fungi, and animals alike and can be broadly broken up into two categories: endochitinases, which break chitin up into multimers, and exochitinases, which digest chitin or chitin multimers into trimers, dimers (called chitobiose) and monomers of *N*-acetylglucosamine (Hamid et al 2013).

Chitin synthase (CHS) enzymes belong to a family of glycosyltransferases and are critical for chitin synthesis. *CHS* genes are present in the vast majority of invertebrates and were recently discovered in the genomes of fishes and amphibians (Tang et al 2015, Zakrzewski et al 2014). Whereas the presence of these genes is suggestive that endogenous chitin is being synthesized, the actual cellular process for chitin biogenesis is complex and involves many enzymes and precursors (Merzendorfer 2011). Researchers in our lab used developmental, histological, and chemical evidence to show definitively that chitin is indeed synthesized by vertebrates, a finding that went counter to the long-held tenet that the molecule is not generated in these organisms (Tang et al 2015). Endogenous chitin was found in multiple anatomic locations in both fish and amphibians, including the gut and integument of zebrafish. *In situ* hybridization showed that the expression of *CHS* genes correlated with signal from CBD, a home-made fluorescent probe containing the chitin binding domain from a bacterial chitinase (Tang et al 2015). Since then, it has been implicated that chitin forms a barrier in the gut of tunicates, hagfish, lancelets, and a ray-finned fish (tilapia), which separates the gut epithelium from ingested microbes (Nakashima et al 2018). Daniel Ocampo Daza, a postdoc in our lab, recently analyzed the distribution of *CHS* genes in vertebrates and confirmed the generalized assumption that chitin synthases were lost in the ancestors of amniotes and possibly coelacanths, which explains why we have been unable to identify chitin in these animals (unpublished data). Still, despite the recent advances in our understanding of chitin's distribution in select vertebrate species, the distribution and function of endogenous chitin within the many diverse anatomical systems of other vertebrate clades remains unknown.

*A summary of the studies conducted in this dissertation*

The Amemiya lab actively studies chitin synthesis in fishes. Having grown up completely mesmerized by sharks and their kin, when I joined the Chris Amemiya's group in my first year of graduate school, I was eager to investigate the presence of chitin in cartilaginous fishes specifically. When I arrived on the scene, our lab had recently used chitin-binding histochemical reagents (CBD) on skate embryos and observed signals in the gel that fills AoL lumens. This preliminary evidence of chitin in the AoL was completely unexpected as chitin had not been observed as a component of a gelatinous material in any biological system. Given that the structure and function of AoL gel has remained poorly understood, I was eager to test these initial findings and explore their implications within the electrosensory system of cartilaginous fishes. Therefore, to test the hypothesis that chitin is synthesized endogenously in the AoL, I used several methods and most of my five years of graduate school! I describe these experiments and my specific findings in great detail in Chapter 1 of this dissertation and conclude that chitin, in some form, is synthesized endogenously by diverse chondrichthyan species.

Very few studies have documented the embryonic development of AoL in cartilaginous fishes. In fact, the developmental timing and the progressional patterns of AoL growth have remained entirely unknown. As I collected evidence of evidence in the AoL gel of several fish species, I also considered the potential functions of chitinous gel within the grand scheme of the electrosensory system. Ever interested in embryonic development, I chose to document the early development of AoL within my preferred experimental animal, the little skate, and examined the developmental effects of impeding chitin synthesis. In Chapter 2, I document the onset of chitin synthesis in little skate embryos and describe the distribution of chitin, as evidenced by chitin-binding histochemical reagents and chitin synthase expression patterns, over developmental time. When I began strategizing how to

investigate the function of chitin in the AoL of cartilaginous fishes, I quickly realized the limitations of the "non-model animals" I have always been so fond of. Methodologically speaking, injection-based gene perturbation experiments were not practical with the little skate system. Therefore, to explore the possible developmental functions of chitin synthesis in chondrichthyan embryos, I reared little skate in chitin synthase-inhibiting drugs. Although drug exposure did not induce any repeatable effects on chitin synthesis, I also document my extensive observations on the rearing of little skate embryos in two kinds of drugs in Chapter 2.

The more I examined AoL gel, the more interested I became in uncovering the unknown molecular structure of the mysterious substance. Recent studies have documented some of the components of AoL gel, but our current understanding of the gel's structure has remained speculative. I collaborated with several researchers from diverse scientific backgrounds, and through the use of various chemical and physical methods, we gained perspective on the polymeric structure of native gel and the type of molecules that confer its observed stiffness (Chapter 3). Finally, with a continued interest in chitin's influence on the gel's properties specifically, I teased apart which of the observed gel properties can be attributed to proteins vs polysaccharides by comparing the structural characteristics of native gel to gel that had been digested with proteolytic enzymes (proteinases).

## Introduction References

Asahara M, Koizumi M, Macrini TE, Hand SJ, Archer M. 2016. Comparative cranial morphology in living and extinct platypuses: Feeding behavior, electroreception, and loss of teeth. *Sci Adv* 2: e1601329

Baker C. 2019. The Development and Evolution of Lateral Line Electroreceptors: Insights from Comparative Molecular Approaches In *Electroreception: Fundamental Insights from Comparative Approaches*, ed. BA Carlson, JA Sisneros, AN Popper, RR Fay. Switzerland: Springer Nature

Baker CV, Modrell MS, Gillis JA. 2013. The evolution and development of vertebrate lateral line electroreceptors. *J Exp Biol* 216: 2515-22

Baker CVH, Modrell MS. 2018. Insights into Electroreceptor Development and Evolution from Molecular Comparisons with Hair Cells. *Integr Comp Biol* 58: 329-40

Bellono NW, Leitch DB, Julius D. 2017. Molecular basis of ancestral vertebrate electroreception. *Nature* 543: 391-96

Bodznick D, Montgomery JC. 2005. The Physiology of Low-Frequency Electrosensory Systems In *Springer Handbook of Auditory Research - Electroreception*, ed. TH Bullock, CD Hopkins, AN Popper, RR Fay

Bodznick D, Northcutt RG. 1980. Segregation of Electro- and Mechanoreceptive Inputs to the Elasmobranch Medulla. *Brain Research* 195: 313-21

Bodznick D, Schmidt AW. 1984. Somatotopy Within the Medullary Electrosensory Nucleus of the Little Skate, Raja erinacea. *The Journal of Comparative Neurology* 225: 581-90

Brown BR, Hughes ME, Russo C. 2005. Infrastructure in the electric sense: admittance data from shark hydrogels. *J Comp Physiol A Neuroethol Sens Neural Behav Physiol* 191: 115-23

Bullock TH, Bodznick DA, Northcutt RG. 1983. The Phylogenetic Distribution of Electroreception: Evidence for Convergent Evolution of a Primitive Vertebrate Sense Modality. *Brain Research Reviews* 6: 25-46

Camilieri-Asch V, Kempster RM, Collin SP, Johnstone RW, Theiss SM. 2013. A comparison of the electrosensory morphology of a euryhaline and a marine stingray. *Zoology (Jena)* 116: 270-6

Collin SP, Whitehead D. 2004. The functional roles of passive electroreception in non-electric fishes. *Animal Biology* 54: 1-25

Czech-Damal NU, Dehnhardt G, Manger P, Hanke W. 2013. Passive electroreception in aquatic mammals. *J Comp Physiol A Neuroethol Sens Neural Behav Physiol* 199: 555-63

Czech-Damal NU, Liebschner A, Miersch L, Klauer G, Hanke FD, et al. 2012. Electroreception in the Guiana dolphin (Sotalia guianensis). *Proc Biol Sci* 279: 663-8

Dijkgraff S, Kalmijn AJ. 1962. Verhaltensversuche zur Funktion Lorenzinischen Ampullen. *Die Naturwissenschaften* 49: 400

Dijkgraff S, Kalmijn AJ. 1966. Versuche Zur Biologischen Bedeutung Der Lorenzinischen Ampullen Bei Den Elasmobranchiern. *Zeitschrift fur vergleichende Physiologie* 53: 187-94

Doyle J. 1967. The 'Lorenzan Sulphates' - A New Group of Vertebrate Mucopolysaccharides. *Biochemical Journal* 103: 325-30

Doyle J. 1968. The Lorenzan Sulphates: A Comparative Study. *Comparative Biochemistry and Physiology* 24: 479-85

Fields RD. 1993. Ampullary sense organs, peripheral, central, and behavioral electroreception in chimeras (Hydrolagus, Holocephali, Chondrichthyes). *Brain, Behavior, and Evolution* 41: 269-89

Fishelson L, Baranes A. 1998. Morphological and Cytological Ontogenesis of the Ampullae of Lorenzini and Lateral Line Canals in the Oman Shark, *Iago omanensis* Norman 1939 (Triakidae), from the Gulf of Aqaba, Red Sea. *The Anatomical Record* 252: 532-45

Freitas R, Zhang G, Albert JS, Evans DH, Cohn MJ. 2006. Developmental origin of shark electrosensory organs. *Evolution & Development* 8: 74-80

Gillis JA, Modrell MS, Northcutt RG, Catania KC, Luer CA, Baker CV. 2012. Electrosensory ampullary organs are derived from lateral line placodes in cartilaginous fishes. *Development* 139: 3142-6

Graham A, Shimeld SM. 2013. The origin and evolution of the ectodermal placodes. *Journal of Anatomy* 222: 32-40

Hamid R, Khan MA, Ahmad M, Ahmad MM, Abdin MZ, et al. 2013. Chitinases: An update. *J Pharm Bioallied Sci* 5: 21-9

How MJ, Jones JVS. 1969. Comparative Studies of Lorenzini Jelly from 2 Species of Elasmobranch .I. Preparation of Glycopeptides. *Carbohydrate Research* 11: 207-&

How MJ, Jones JVS, Stacey M. 1970. Comparative Studies of Lorenzini Jelly From Two Species of Elasmobranch. *Carbohydrate Research* 12: 171-81

Inoue JG, Miya M, Lam K, Tay BH, Danks JA, et al. 2010. Evolutionary origin and phylogeny of the modern holocephalans (Chondrichthyes: Chimaeriformes): a mitogenomic perspective. *Mol Biol Evol* 27: 2576-86

Josberger EE, Hassanzadeh P, Deng Y, Sohn J, Rego MJ, et al. 2016. Proton Conductivity in ampullae of Lorenzini jelly. *Science Advances* 2: e1600112: 1-6

Kalmijn AJ. 1974. The Detection of Electric Fields from Inanimate and Animate Sources Other Than Electric Organs In *Handbook of Sensory Physiology: Electroreceptors and Other Specialized Receptors in Lower Vertebrates*, pp. 147-200

Kalmijn AJ. 1982. Electric and Magnetic Field Detection in Elasmobranch Fishes. *Science* 218

Kempster RM, McCarthy ID, Collin SP. 2012. Phylogenetic and ecological factors influencing the number and distribution of electroreceptors in elasmobranchs. *J Fish Biol* 80: 2055-88

King BL, Shi LF, Kao P, Clusin WT. 2016. Calcium activated K(+) channels in the electroreceptor of the skate confirmed by cloning. Details of subunits and splicing. *Gene* 578: 63-73

Klimley AP. 2010. Electric Fields In *The Encyclopedia of Applied Animal Behaviour and Welfare*, ed. DS Mills. UK: CAN International

Lavoue S, Miya M, Arnegard ME, Sullivan JP, Hopkins CD, Nishida M. 2012. Comparable ages for the independent origins of electrogenesis in African and South American weakly electric fishes. *PLoS One* 7: e36287

Leitch DB, Julius D. 2019. Electrosensory Transduction: Comparisons Across Structure, Afferent Response Properties, and Cellular Physiology In *Electroreception: Fundamental Insights from Comparative Approaches*, ed. BA Carlson, JA Sisneros, AN Popper, RR Fay. Switzerland: Springer

Lissman HW. 1951. Continuous Electrical Signals from the Tail of a Fish, Gymnarchus niloticus. *Nature* 167: 201-02

Lorenzini S. 1678. Osservazioni Intorno Alle Torpedini.

Merzendorfer H. 2011. The cellular basis of chitin synthesis in fungi and insects: common principles and differences. *Eur J Cell Biol* 90: 759-69

Modrell MS, Lyne M, Carr AR, Zakon HH, Buckley D, et al. 2017. Insights into electrosensory organ development, physiology and evolution from a lateral line-enriched transcriptome. *Elife* 6

Murray RW. 1960. Electrical Sensitivity of the Ampullae of Lorenzini. *Nature*: 957

Murray RW. 1962. The response of the ampullae of Lorenzini of elasmobranchs to electrical stimulation. *J Exp Biol* 39: 119-28

Murray RW, Potts WTW. 1961. The Composition of the Endolymph, Perilymph, and Other Body Fluids of Elasmobranchs. *Comparative Biochemistry and Physiology* 2: 65-75

Nakashima K, Kimura S, Ogawa Y, Watanabe S, Soma S, et al. 2018. Chitin-based barrier immunity and its loss predated mucus-colonization by indigenous gut microbiota. *Nat Commun* 9: 3402

New JG. 1990. Medullary electrosensory processing in the little skate. *Journal of Comparative Physiology* 167: 295-307

New JG. 1997. The Evolution of Vertebrate Electrosensory Systems. *Brain Behav Evol* 50: 244-52

Newton KC, Gill AB, Kajiura SM. 2019. Electroreception in marine fishes: chondrichthyans. *J Fish Biol* 95: 135-54

Newton KC, Kajiura SM. 2017. Magnetic field discrimination, learning, and memory in the yellow stingray (Urobatis jamaicensis). *Anim Cogn* 20: 603-14

Northcutt RG. 1997. Evolution of gnathostome lateral line ontogenies. *Brain Behav Evol* 50: 25-37

Patullo BW, Macmillan DL. 2010. Making sense of electrical sense in crayfish. *J Exp Biol* 213: 651-7

Pettigrew JD. 1999. Electroreception in Monotremes. *The Journal of Experimental Biology* 202: 1447-54

Raschi W. 1986. A Morphological Analysis of the Ampullae of Lorenzini in Selected Skates (Pisces, Rajoidei). *Journal of Morphology* 189: 225-47

Rathore AS, Gupta RD. 2015. Chitinases from Bacteria to Human: Properties, Applications, and Future Perspectives. *Enzyme Res* 2015: 791907

Roy JC, Salaun F, Giraud S, Ferri A, Chen G, Guan J. 2017. Solubility of Chitin: Solvents, Solution Behaviors and Their Related Mechanisms In *Solubility of Polysaccharides*, ed. Z Xu: Intech Open

Sato H, Mizutani S, Tsuge S, Ohtani H, Aoi K, et al. 1998. Determination of the degree of acetylation of chitin/chitosan by pyrolysis-gas chromatography in the presence of oxalic Acid. *Anal Chem* 70: 7-12

Selberg J, Jia M, Rolandi M. 2019. Proton conductivity of glycosaminoglycans. *PLoS One* 14: e0202713

Szabo T. 1974. Anatomy of the specialized lateral line organs of electroreception In *Handbook of Sensory Physiology*, ed. A Fessard, pp. 13-58

Tang WJ, Fernandez J, Sohn JJ, Amemiya CT. 2015. Chitin is endogenously produced in vertebrates. *Curr Biol* 25: 897-900

Tavares Schafer B, Malavasi CE, Favaron PO, Ambrosio CE, Miglino MA, et al. 2012. Morphological observations of ampullae of lorenzini in Squatina guggenheim and S. occulta (Chondrichthyes, Elasmobranchii, Squatinidae). *Microsc Res Tech* 75: 1213-7

Tricas TC, Michael SW, Sisneros JA. 1995. Electrosensory optimization to conspecific phasic signals for mating. *Neuroscience Letters* 202: 129-32

Uchimura K. 2015. Keratan Sulfate: Biosynthesis, Structures, and Biological Functions In *Glycosaminoglycans*, ed. K Balagurunathan, H Nakato, UR Desai, pp. 389-400. New York: Springer

Waltman B. 1966. Electrical properties and fine structure of the ampullary canals of Lorenzini. *Acta physiologica Scandinavica* 66: 3-60

Whitehead DL, Gauthier AR, Mu EW, Bennett MB, Tibbetts IR. 2015. Morphology of the ampullae of Lorenzini in juvenile freshwater Carcharhinus leucas. *J Morphol* 276: 481-93

Wilkens LA, Hofmann MH. 2005. Behavior of Animals with Passive, Low-Frequency Electrosensory Systems In *Springer Handbook of Auditory Research - Electroreception*, ed. TH Bullock, CD Hopkins, AN Popper, RR Fay: Springer

Zakrzewski AC, Weigert A, Helm C, Adamski M, Adamska M, et al. 2014. Early Divergence, Broad Distribution, and High Diversity of Animal Chitin Synthases. *Genome Biol Evol* 6: 316-25

Zhang X, Xia K, Lin L, Zhang F, Yu Y, et al. 2018. Structural and Functional Components of the Skate Sensory Organ Ampullae of Lorenzini. *ACS Chem Biol*

# **Chapter 1:** Evidence of Chitin Within the Ampullae of Lorenzini of Cartilaginous Fishes

## 1.1 Abstract

Cartilaginous fishes, including sharks, skates, rays, and chimaeras, possess specialized electrosensory organs used to locate other animals and to navigate. The tubular organs, called Ampullae of Lorenzini (AoL), are open to the environment *via* pores in the skin and filled with a hydrogel known to contain keratan sulfate (a glycosaminoglycan) and various poorly identified proteins. Although many studies have documented the anatomy and electrophysiology of the AoL in various species, it is still unknown how electric field signals move through the organs and what role the interior gel plays in the process. More specifically, even though some chemical analyses have been published, the polysaccharide content of AoL gel has not been fully documented. In this chapter, I report findings from experiments using chitin-binding histochemical reagents and chitinase digestions which suggest that chitin (a polysaccharide) is another component of the gel inside the AoL of cartilaginous fishes. I isolated chitin from spotted ratfish (*Hydrolagus colliei*) gel and used Fourier transform infrared spectroscopy (FTIR) and monosaccharide analyses to corroborate these findings. Further, *in situ* hybridization studies using chitin synthase gene sequences from little skates suggest that chitin is synthesized endogenously by cells within the AoL and not accumulated from the environment. This is the first report of chitin existing as a natural hydrogel component and it is still unclear how the insoluble polysaccharide polymers suspend in the aqueous gel material. These results expand the scope of vertebrate chitin to the cartilaginous fishes and to another anatomic system and beg further investigation into the function of the polysaccharide in electrosensory organs.

## 1.2 Introduction

Several years ago, our lab reported that the polysaccharide, chitin, a key component of arthropod exoskeletons and fungal cell walls, is endogenously produced by fishes and amphibians in spite of the widely held view that it was not synthesized by vertebrates (Tang et al 2015). Chitin is composed of repeating subunits of *N*-acetylglucosamine (GlcNAc) and can exist in several allomeric chemical forms. Since the initial discovery of vertebrate chitin, genes encoding chitin synthase (CHS) enzymes have been found in the genomes of a number of fishes and amphibians and have shown to be correspondingly expressed at the sites where detectable chitin is localized (Nakashima et al 2018, Tang et al 2015, Zakrzewski et al 2014). Our lab has continued to investigate the distribution of *CHS* genes, and discovered that they are widely distributed amongst agnathans, cartilaginous fishes, some ray-finned fishes, and amphibians, but lost in amniotes (unpublished data). The distribution of chitin and *CHS* gene expression has only been described in a handful of species and remains a compelling field of study. Our lab's 2015 paper showed that chitin is synthesized in the gut of zebrafish and in the skin of both salamanders and a few species of teleost fish (Tang et al 2015). Nakashima et al expanded on this initial finding, determining that chitin within the guts of tunicates, lancelets, hagfish, and another species of ray-finned fish forms a barrier membrane, which may protect gastrointestinal tissues from ingested pathogenic microbes (Nakashima et al 2018). More studies are necessary to determine a complete list of vertebrate anatomic systems that synthesize endogenous chitin and to document what various functions it might serve.

In the Amemiya lab's continued investigations into the distribution of vertebrate chitin, attention was turned towards the electrosensory organs of cartilaginous fishes (class Chondrichthyes). These organs, the Ampullae of Lorenzini (AoL), are widely dispersed and

comprise a series of gel-filled canals emanating from surface pores in the skin (Fig. I.2). The canals extend into ovoid (sometimes lobed) structures called alveoli that contain sensory cells capable of detecting subtle changes in electric fields (Kempster et al 2012, Murray 1960, Newton et al 2019). In general terms, AoL detect weak environmental electric fields and transduce them into neuronal signals that project onto the brain. The subsequent topographical map of the organism's electrical surroundings is thought to be used for various functions, most notably the detection of prey, localization of conspecifics for mating, and perhaps even for navigation (Newton et al 2019). Having likely originated in the ancestors to all vertebrates, the electrosensory organs of cartilaginous fishes share homology with those found in other vertebrate lineages including some amphibians and ray-finned fishes, coelacanths, and lungfish. These so-called "ancestral ampullary organs" were lost in some vertebrate groups including a large clade of bony fishes belonging to the subclass Neopterygii. Subsequently, a few groups of neopterygian fishes independently evolved electrosensory organs that exhibit some morphological and functional similarities with the AoL of cartilaginous fishes, despite their analogous origins.

Although much is understood about the anatomy and physiology of AoL in cartilaginous fishes, the mechanism by which electric field signals enter AoL pores and traverse through the gel to the distal electrosensory cells remains to be worked out. Further, we still don't understand what role the AoL gel plays in the process, nor have we uncovered its entire molecular composition. AoL gel is approximately 95% water with an ionic composition very similar to that of seawater (Murray & Potts 1961). Some of the remaining gel components have been historically classified as "mucopolysaccharides" (Doyle 1967, Doyle 1968). Recently published compositional analyses and Fourier transform infrared spectroscopy (FTIR) suggest that keratan sulfate, a polysaccharide composed of repeating subunits of galactose and *N*-acetylglucosamine (with one or both units sulfated), is

synthesized in AoL gel (Josberger et al 2016, Zhang et al 2018). However, the compositional analyses described in two separate studies suggest that there is a larger proportion of glucosamine to galactose in AoL gel, indicating that AoL gel contains a still undescribed polysaccharide component (Doyle 1967, Josberger et al 2016).

Here, I provide several lines of evidence suggesting that chitin is a component of AoL gel in cartilaginous fishes. I used histochemical chitin-binding probes with tissues from several cartilaginous fish species and observed consistent localization of signal to the AoL. To confirm that the probes were indeed binding to chitin, I exposed AoL tissue sections to chitinolytic enzymes and studied the effects of digestion on the labeling of the same chitin-binding probes. Given that AoL are open to an environment filled with chitin, it was still not clear if the fishes were synthesizing chitin endogenously or taking it up from the surrounding water. Therefore, I used both *in situ* hybridization and transcriptomic analyses to examine expression patterns of *CHS* genes inside the AoL of embryonic and adult little skate (*Leucoraja erinacea*) specimens to learn if the sites of *CHS* expression corresponded with chitin signals. Finally, due to the novelty of my claim that chitin is a component of a biological gel, I used physicochemical methods including Fourier transform infrared spectroscopy and monosaccharide analyses to study the polysaccharide components extracted from spotted ratfish (*Hydrolagus colliei*) AoL gel. With these methods, the extracted material exhibited chemical signatures of chitin and these studies offered more confirmatory evidence that chitin is synthesized in the AoL of cartilaginous fishes.

## 1.3 Methods

### *1.3.1 Biological specimens*

Juvenile dogfish (*Squalus acanthias*) and adult skates (*Raja* spp.) were obtained from Carolina Biological Supply Company as formalin-fixed and preserved (Carosafe) specimens. Cleared-and-stained skeletal preparations of embryonic stingray (*Hypanus sabinus*) and little skate (*Leucoraja erinacea*) were obtained from Adam Summers (Friday Harbor Laboratory) and Tsutomu Miyake (Benaroya Research Institute), respectively. Martin Cohn (University of Florida) provided several fixed specimens of embryonic and larval specimens of the small-spotted catshark (*Scyliorhinus canicula*). A preserved freshwater stingray (*Potamotrygon falkneri*) specimen was provided by James Albert (University of Louisiana at Lafayette). Pacific electric ray (*Tetronarce californica*) specimens were collected off the coast of Monterey Bay by John Field (NOAA Southwest Fisheries Center) and his NOAA groundfish assessment team. A spotted ratfish (*Hydrolagus colliei*) was collected by Thomas Quinn (University of Washington) on a research cruise in Puget Sound, and brought to the Benaroya Research Institute for tissue processing. Additional expired and frozen spotted ratfish were obtained from Jason Cope (NOAA), Scott Hamilton (Moss Landing Marine Labs, MLML) and Matthew Jew (MLML). Specimens of live embryonic and adult little skates were obtained from the Marine Resources Center (Marine Biological Laboratory). Freshwater teleost fishes (*Gnathonemus petersii* and *Apteronotus albifrons*) were fixed and provided by Joseph Sisneros (University of Washington). All animal work was conducted under approved IACUC protocols: IACUC16-014 (Benaroya Research Institute) and AUP18-0001 (University of California, Merced). Euthanasia was carried out using tricaine methylsulfonate (Western Chemical Inc., #NC0872873) at 1000 mg/L.

### *1.3.2 Paraffin sections*

Wax sections of formalin-fixed embryonic or adult tissues were prepared using standard processing, embedding and microtomy protocols. If the sections were to be used for *in situ* hybridization, RNase-free reagents were used in the processing.

### *1.3.3 Cryosections*

Fixed tissues were washed in PBS (3 x 10 minutes) and equilibrated in 15% sucrose in PBS for three hours at room temperature. The solution was replaced with 15% sucrose/7.5% gelatin in PBS, and samples were incubated for three hours at 37°C. Samples were then infiltrated with 20% gelatin in PBS overnight at 37°C and embedded in fresh 20% gelatin in PBS using plastic molds. Embedded samples were mounted onto a cryotome chuck with Tissue-Tek O.C.T. compound, flash frozen in liquid nitrogen and sectioned at 10-12 μm on a cryotome and mounted on Superfrost Plus slides (VWR). Sections were de-gelatinized with 0.3% gelatin in 50% ethanol, rinsed several times in PBS and allowed, to air dry before histochemistry and staining.

### *1.3.4 Affinity histochemistry probes*

The two chitin binding probes used in this study were selected on the basis of availability and known efficacy of chitin binding. Most of the experiments used a probe (CBD) that was obtained from New England Biolabs because of the ease of handling (one step method):

AWQVNTAYTAGQLVTYNGKTYKCLQPHTSLAGWEPSNVPALWQLQ (45 aa)

Chitin binding domain from plasmid pYZ205 (*Bacillus circulans*).

Conserved domain superfamily cluster cl00046 (NCBI).

We also used a different chitin probe to independently validate experiments with CBD:

FTCEGKADGLYSDPYQCNMYYECVMYVKYHRPCPTGTVF (39 aa)

Chitin binding domain from VCBP_C (*Ciona intestinalis*, NP_001190979).

Conserved domain superfamily cluster cl02629 (NCBI).

### *1.3.5 Isolation and labeling of SNAP-tag Chitin Binding Domain (SNAP-CBD) fusion protein*

Plasmid pYZ205 containing the SNAP-CBD fusion construct was provided in T7 Express *E. coli* cells and protein isolated on a nickel-NTA agarose resin affinity column as described in Maduzia et al (Maduzia et al 2011). The protein was eluted in 1 mL fractions with elution buffer (50 mM $NaH_2PO_4$, 300 mM NaCl, 250 mM imidazole, pH 8.0), quantified on a Nanodrop spectrophotometer, and electrophoresed by SDS-PAGE to ascertain purity. Fractions with the highest concentration of protein were pooled and dialyzed overnight in phosphate buffer (50 mM $NaH_2PO_4$, 50 mM $Na_2HPO_4$, pH 7.2, 0.1 mM NaCl) containing 1mM DTT, then stored at -80°C. To fluorescently label the fusion protein, 5 $\mu$M SNAP-CBD was incubated with 10 $\mu$M SNAP-Surface Alexa Fluor-488 or -546 (New England Biolabs) and 1 mM DTT in phosphate buffer for one hour at 37°C in the dark, then dialyzed overnight at 4°C in phosphate buffer with 1 mM DTT. An aliquot of the fluorescently labeled SNAP-CBD was electrophoresed by SDS-PAGE and imaged with a Typhoon 9410 Imager (GE Amersham Molecular Dynamics) to ensure successful labeling, then stored at -20°C in 50% glycerol. In order to detect chitin *in situ*, we employed affinity histochemistry using this CBD peptide probe (CBD-488 or CBD-546). Alternatively, aliquots of the SNAP-CBD were labeled with biotin using either SNAP-surface biotin (as above) or through direct conjugation. For the latter, approximately 0.2 mg of SNAP-CBD was labeled with NSH-$PEG_4$-Biotin with EZ-Link Micro NSH-PEG4-Biotinylation Kit (Thermo Scientific), which attaches NSH-$PEG_4$-Biotin to lysine residues and the N-terminus. Unincorporated NSH-

$PEG_4$-Biotin was removed by desalting columns in the Kit. Biotin incorporation was measured using Biotin Quantitation Kit (Thermo Scientific); only samples showing incorporation of one or more biotin per molecule of the SNAP-CBD were used for further experiments. Sections labeled with CBD-Biotin were detected using Streptavidin 546 (Invitrogen S11225A).

### *1.3.6 Chitin affinity histochemistry*

Chitin affinity histochemistry largely followed the protocols outlined in Tang, et al. (Tang et al 2015). Fixed specimens (whole-mount tissue or sectioned material) were washed in PBS-T (PBS with 0.05% Tween-20) at room temperature (3 x 10 minutes), then dehydrated in a graded methanol series and stored at -20°C. For histochemistry, specimens were rehydrated with PBS-T, bleached briefly with 1% $H_2O_2$/0.5% KOH at room temperature to remove pigment, then permeabilized with 1% Triton-X/PBS overnight at 4°C. Specimens were then washed in PBS-T for thirty minutes, and blocked in 1% BSA in PBS for one hour before incubation with fluorescently-labeled CBD-488 or CBD-546 at 4°C for 24-48 hours. For co-detection experiments, specimens were simultaneously incubated with either *Ciona intestinalis* VCBP-C fused with the C-terminal region of human IgG1 Fc (provided by Larry Dishaw, John Cannon and Gail Mueller, University of South Florida) or CBD-biotin (Dishaw et al 2011). For secondary detection of VCBP-C or CBD-biotin, larvae were washed in PBS-T (3 x 10 minutes), blocked for one hour in 1% BSA in PBS or Pierce TBS Blocking Buffer (Thermo Fisher, 37535), then incubated overnight at 4°C with goat anti-human IgG Fc conjugated to Dylight 488 (Abcam) or Streptavidin-488 (Invitrogen), respectively. Samples were then washed in PBS-T (3 x 1 hour), counterstained and imaged. If using slides, samples were mounted in anti-fade mounting medium (Vectashield) prior to imaging.

### *1.3.7 Chitinase digestion of AoL-bearing histological specimens*

Slides containing histological sections were rehydrated in 1X PBS. Several types of chitinase were used but we found that chitinase isolated from a nematode species (*Brugia malayi*) (NEB, P5205 – now discontinued), and the bacterium, *Streptomyces griseus* (Sigma Aldrich, C6137) worked most reliably. Chitinase from *S. griseus* was diluted to 1 mg/mL in 50 mM $KH_2PO_4$ and 10% glycerol. Chitinase from *B. malayi* was diluted 1/100 in prepared buffer (.2 M NaCl, .02 M $NaPO_4$, 1 mM EDTA). Slides were incubated in 300 $\mu$L of chitinase solution under parafilm in a humidified chamber at room temperature (*S. griseus*) or at 37°C (*B. malayi*) for ~36 hours. Samples were washed 3 times for 30 minutes in 1X PBS and then 300 $\mu$L of Pierce TBS Blocking Buffer were added to the slides and incubated for 1 hour at room temperature. Slides were stained with CBD-546 (*B. malayi*) or CBD-biotin + Streptavidin-546 (*S. griseus*) in TBS Blocking Buffer at 4°C overnight. Slides were washed 3 times in 1X PBS and then counterstained with a dilute DAPI solution (in 1X PBS). Slides were washed a few times in 1X PBS, rinsed with $dH_2O$, and mounted with Vectashield before imaging.

### *1.3.8 Pilot transcriptome of the AoL of adult little skate*

Approximately 600 mg of alveoli and canal tissue from the hyoid cluster was dissected from an adult little skate and stored in RNAlater (Life Technologies, #AM-7020) at 4°C. The tissue was homogenized, and total RNA was isolated using Trizol reagent (Life Technologies, #15596-026) and purified with RNeasy MinElute Cleanup kit (Qiagen, #74204) according to manufacturer's instructions. The library was prepared and sequenced by Otogenetics Corporation (Atlanta, GA) using an Illumina HiSeq 2500 sequencer in Rapid Run mode with SBS v2 chemistry. The raw paired read files were quality-trimmed with Trimmomatic and assembled into a *de novo* transcriptome using Trinity v2.2.0. The

sequence data were submitted to the SRA database under the BioProject PRJNA550453 (SRA Experiment SRX6358492).

### *1.3.9 Probe synthesis and in situ hybridization experiments*

RNA was extracted from *L. erinacea* tissue and cDNA was synthesized from the extracted RNA using the SuperScript III First-Strand Synthesis kit from Invitrogen (Life Technologies, #18080-051). Gene-specific primers were designed for segments of two of the little skate chitin synthase genes (*LeCHS1* and *LeCHS3*) identified using our little skate transcriptome (above) and transcriptomes published by Bellono et al (Bellono et al 2017). The *LeCHS1* probe was 645 bp in length and the *LeCHS3* probe was 666 bp long). Probe sequences are given below (magenta and yellow sequences are the PCR primer sequences).

**LeCHS1**

CCACCAAAAGGAGTTCTAGCCATGGTATGCTTCATCGAAGCAATTATCGCACTTGCCACTTCAGTTCTGGTGCTGGTCTGCTTGCC
TCAGTTTGATGTCATCACAAATCTCTGCATTTTGAATGGTGCCTGTCTGTTTCCTTCATTCCTACAAATAATGTATGAGTTGAAAC
ATCTGGGGGGTTGCCTTGCTATTCCCCCTCATTGGTTTTGGGTTGACTTTTCTAGGCCTCTTGCTTTTCATTTTAGTCCACAATTCC
CTGCAGCAATCAGACACCCCTCAATACCTTCAGATGTACGTAGCCATAGCAATAGTTTCCTTAACAGTATTATCTCTCAATTGGTG
GGAAAACTTTACATCCTTCTGTAAAATTGGATTCCTGCAAAATATAAGGGAAAGCCTACGTGGCAATAGAAATCTTACCTACGTTT
GCAGTAGTGCAGTTAGAATTCTCGTCACCTTTGGTGTAGTCGCGGCATGGATTCCAATTAAGAAGTATGACTGGGTAGATTTGAAA
ACAGTCTCTCAATTTGAACTAAATATTGTTTTGGGTCTCTTTGGGGTGCAGGCATGTTCTTCTGTACTTTGCCACTGGTTTGGGGT
CCTGGTGTGCAAAATGCATGCAGTCAGGCGAAGTTTCATGCTG

**LeCHS3**

CCTAATCCTTGGCTGCGTTTTGATCATTCCCAGCATCTTGACCGCCGCAAAATGCCTGTGGAAACACTCACTCCGTCCCGTACCAA
TGCTCTCCGCAAGCAGCCTGATAACGGTGTGCCTGCTGGAAGCAGTTGCATCCTTTGGAACGGCATCTCTGGTTGTCGTCTGCCTT
CCCCAATATGACATCCTCACAATGGTGTTCATTTCCAACAGTATTTGTCTCATCCCATCCATACTACAAGTGATCTCTCTAAACAT
CAGCCATCGCTTCAAAGTTGTAGCCCCTCTGGCCGGGCTTCTCCTTCTCTTGGGCGGCTATAGTCTCTTTCTCTTTGTCCAGATGT
TTTACCTGACGAGACACGATGGGATGTCCTTGGGTCTTGTCATTTTATTCTCAGTTTTAACTTCCCTAACCTGGTGGGAGAACTTC
ATCTCCAACTGGAAGCATCCAGTATTTAGACGTCTGAGATCTGACGTGGATAAATGCAGGAACGTGATGAGCCTGTGCATAAGTGT
AGTGAGAACTCTTGTTACTGTCTGTGTTGTGGGAGCTTTGATTCCTCTTCGGGGGCTGGAGTGGGCAACTATCACTGACGTTGCAT
CCCATGAACTCAGAATAATCCTGGGCCTTCTGGGGGGTGCAGGCGGGAGCATCGGTCTTGTGTTC

The fragments were cloned into a pCR-II-TOPO vector (Invitrogen, #450640) and DIG-labeled probes were synthesized using Ambion's MEGAscript Sp6 and T7 kits (Invitrogen, #1330 & #1334). Probes were stored in hybridization buffer (50% Formamide, 5X SSC, 2% blocking reagent (BBR), 50 $\mu$g/mL heparin, 10 g/mL yeast tRNA, 0.1% CHAPS, 0.1% Triton-X) at a concentration of 100 ng/$\mu$L at -80°C. A probe specific to the *ChAT* gene in

planarians was obtained from Eli Isael Maciel at UC Merced for use as a negative control (see below).

Little skate embryos were fixed in HA fixative (70% ethanol, 5% glacial acetic acid, 4% formaldehyde, 21% water) overnight then moved to RNAse-free methanol and stored at -20°C until use. Snout and fin pieces were dissected from embryos for whole-mount ISH experiments and entire anterior ends were embedded in paraffin for ISH with sections.

For whole-mount ISH, I adapted a protocol from Andrew Gillis (Cambridge University). Embryos were moved to 1X PBT. To permeabilize, the tissues were incubated in proteinase K (5 $\mu$g/mL) for 15 minutes then in glycine (2 mg/mL) for 5 minutes. The tissue was re-fixed in fresh 4% paraformaldehyde (PFA) for 20 minutes. Hybridization buffer (hyb) was added to each tube for ten minutes then replaced with fresh pre-warmed hyb (68°C) and incubated for 3-5 hours. Probes were diluted to a working concentration of 5 ng/$\mu$L in 1 mL hybridization buffer and then denatured for 8 minutes at 80°C. Hybridization buffer was subsequently removed, replaced with probe solution, and the tubes were incubated at 68°C for 70 hours.

2X SSC (10 mL formamide, 4 mL 20X SSC (pH 4.5), 2 mL 10% SDS, 4 mL $dH_2O$), and 0.2X SSC (10 mL formamide, 2 mL 20X SSC (pH4.5), 8 mL $dH_2O$) were pre-warmed to 68°C. Probe was removed, 2X SSC was added quickly to the tissue and washed for 45 minutes at 68°C (this wash was performed two times). Three 0.2X SSC washes were then performed at 68°C for 30 minutes each. Tissue was washed 4 times in MABT (Maleic Acid Buffer + Tween-20) for 10 minutes each. Fresh blocking solution (20% heat inactivated sheep serum + 1% Roche blocking reagent) was prepared and added to the tissue for 4 hours at 4°C. Blocking solution was replaced with anti-DIG AP Fab fragments (Roche, #11093274910) diluted 1:2500 in blocking buffer. Tubes were left at 4°C overnight with gentle rocking.

The next day, samples were washed 3 times in MABT for 5 minutes each and then 5 more times in MABT for one hour each. The samples were left in the last MABT wash overnight at 4°C. Samples were then washed in freshly made NTMT (1 mL 5M NaCl, 5 mL 1M Tris/HCl, 0.2 mL Tween-20, 44 mL $dH_2O$) three times for 10 minutes. Tissue was bathed with BM Purple solution (Roche, 11442074001) rotating in the dark at room temperature. Staining solution was replaced after an hour. After the color reaction was complete, tissues were washed with 1X PBS then post-fixed with 4% PFA and stored in 75% glycerol.

For ISH with tissue sections, slides were rehydrated in 1X PBT then rinsed with 2X SSC in a Coplin jar at room temperature. DIG-labeled probes were diluted to a working concentration of 5 ng/$\mu$L in slide-specific hybridization buffer (50% formamide, 1X salt solution, 10% dextran sulfate, 10 mg yeast tRNA, 1X Denhardt's solution, and DEPC water to 10 ml). The working concentration of probe (5 ng/$\mu$l) was denatured at 80°C for 5 minutes before adding to each slide and covering with a #1 coverslip. Slides were placed in a humidified chamber of 50% formamide, 50% 2X SSC and incubated overnight at 63°C.

The next day, slides were washed twice with a solution of 50% formamide, 1X SSC, and 0.1% Tween-20 at 63°C for 30 minutes. Slides were washed 3 times with 1X MABT solution, placed in blocking solution (1% Roche blocking reagent and 20% sheep serum) for 2 hours, then incubated in anti-DIG-AP antibody at a concentration of 1:1000 in block solution overnight.

Slides were washed every 30-60 minutes with MABT the following day and left in the final wash overnight at 4°C. On the final day, fresh NTMT (0.1 M NaCl, 0.1 M Tris (pH 9.5), 5 mM $MgCl_2$, 0.1% Tween-20) was prepared and used to wash the slides 3 times. Slides were incubated in BM Purple on a shaker for several hours until color was revealed. In some cases, staining continued overnight in order for signal to be observable. Slides were washed

with 1X PBS, post-fixed for one hour with 4% PFA then mounted with glycerol or antifade medium (Vectashield) for imaging.

Sense *CHS* probes were synthesized in tandem with antisense probes as described above. Upon performing ISH experiments with sense probes, I often observed localization of signal to the AoL in the same specific pattern as was seen with antisense probes. Andrew Gillis (personal communication) reported similar observations when performing *in situ* hybridization on chondrichthyan species, presumably due to an abundance of antisense transcripts. I thus used heterospecific probes from another organism as negative controls. I used an antisense probe specific to a cholinergic acetyltransferase (*ChAT*) gene of planaria (*Schmidtea mediterranea*, SMU15019525 in SmedGD database) (complements of Eli Isael Maciel, Oviedo lab, UC Merced). When I performed ISH experiments with *LeCHS* probe using skate tissue, I would use either a second piece of tissue from the same skate specimen or another slide in the case of tissue sections and expose the tissue to probes specific to *ChAT*. Further, when I performed ISH with whole-mount skate tissues, I would also use fixed planarian tissue to confirm that *ChAT* probes hybridized to the expected anatomic locations in the flatworms.

### *1.3.10 Transcriptomics*

An adult female little skate (*Leucoraja erinacea*) was shipped from the Marine Biological Laboratory to our lab and was immediately euthanized with MS222 (Western Chemical Inc., #NC0872873) at 1000 mg/L. Tissues were harvested from specimen on ice and were immediately placed in RNAlater (Ambion #AM7020) and stored at -80°C. The four samples correspond to: 1) AoL pores and surrounding skin located anterior to the upper lip, 2) AoL canals located subdermally on the left side of the mouth, 3) a piece of one of the hyoid clusters containing both alveoli and canals, and 4) AoL-free skin from a pelvic fin. RNA

was isolated and transcriptomes were sequenced by QIAGEN Sciences (Germantown, MD) using Illumina's NextSeq 550 system, which can generate up to 260 million 2 x 100 bp paired-end reads. The RNA Integrity Numbers (RNI) (Schroeder et al 2006) for the isolated RNA spanned between 6.0 and 7.4, with an average of 6.7. Positive polyA selection was used in the preparation of RNA-seq libraries. The final RNA concentrations for the four libraries were 870 pg/$\mu$L (AoL pores), 5560 pg/$\mu$L (AoL canals), 1300 pg/$\mu$L (AoL hyoid cluster), and 146 pg/$\mu$L (pelvic fin skin). RNA quality controls were done using the High Sensitivity D1000 ScreenTape System (Agilent Technologies). Each RNA-seq library was sequenced in four replicates, generating 2 x 9.1–10.1 million (AoL pores), 12.0-13.0 million (AoL canals), 9.5-10.4 million (AoL hyoid cluster), 10.7-11.6 million (pelvic fin skin) paired-end reads. The average length of reads was 98 bp for the AoL samples and 99 bp for the pelvic fin skin sample. This transcriptome data was quality controlled using FastQC (Wingett & Andrews 2018). The Phred scores per base position and read were >30 throughout, which indicates a 1 in 1000 risk of incorrect base call (99.9% base call accuracy). Nevertheless, base pairs 1-13 (5' end) and 98-100 (3' end) of every read were trimmed using Trimmomatic version 0.39 (Bolger et al 2014) to remove remaining adapter sequences and overrepresented sequences in 5', and low-quality (<30 Phred score) base pairs in 3'. This removed between 0.05% and 1.86% of the total reads, where trimming resulted in read lengths below 20 bp. Using these trimmed paired-end reads in four replicates per sample, each transcriptome was assembled *de novo* using Trinity (Grabherr et al 2011, Haas et al 2013) with standard settings, and relative transcript counts were calculated as transcripts per million (TPM) using the Kallisto software (Bray et al 2016, Zhang et al 2017). For the transcript count analysis, the total set of transcript annotations from the little skate genome (leuEri2) was used as an index. The transcriptome assembly and analysis were performed by Daniel Ocampo Daza, a postdoctoral scholar in the Amemiya lab.

### *1.3.11 Imaging*

Stereoscope imaging was done on a Leica M205FA fluorescent stereoscope equipped with a DFC360FX monochrome CCD camera and a DFC425C color CCD camera. Epifluorescent images were taken using either a Leica DMR upright epifluorescent microscope equipped with a SPOT RT Slider cooled 1.4 megapixel color/monochrome CCD camera and an Insight 4 megapixel color CCD camera (Diagnostic Instruments) or a Keyence BZ-X700 microscope workstation equipped with epifluorescence. The latter was also employed for brightfield images. Confocal images were obtained with a Leica TCS SP5 laser scanning confocal microscope. Brightness and contrast adjustments, gamma correction, background subtraction, and confocal image smoothing using the unsharp mask filter were completed in Photoshop CS9 (Adobe) and Fiji (ImageJ, NIH).

### *1.3.12 Collection of gel from the Ampullae of Lorenzini of Hydrolagus colliei*

Isolation of AoL gel was previously described (Josberger et al 2016). Briefly, gel was obtained from multiple freshly caught and recently expired fish by gently pressing on the visible surface pores and collecting the extruded material by scooping it directly into tubes with a pipet tip or scalpel. Samples were stored at -80°C until use.

### *1.3.13 Polysaccharide extraction and analysis by FTIR*

Several milliliters of gel were removed from the AoL pores of expired spotted ratfish (*Hydrolagus colliei*). I carried out a few separate extraction experiments and changed the protocol slightly each time. In one of the extractions, gel was diluted in an equal volume of Proteinase K buffer (0.1 M Tris, 0.05 M EDTA, 0.1% SDS). Proteinase K (Roche Cat No.3115879001) was added to a final concentration of approximately 40 $\mu$g/$\mu$L and the solution was incubated at 50°C for 1-2 hours. I then brought the sample to 75°C for 20

minutes to denature remaining Proteinase K. The sample was moved to a Pur-A-Lyzer Mega 3500 dialysis unit (Sigma Cat No. PURG35015-1KT) and dialyzed against water overnight. In our other extraction rounds, I did not use a Proteinase K treatment, but added the gel directly in the dialysis unit and dialyzed against water overnight. Samples were heated to 50°C in water with gentle spinning then added to pre-heated 1 M HCl and allowed to incubate for 1 hour at 50°C. Sample was brought slowly to room temperature then dialyzed against several rounds of water over the course of a day and overnight. Sample was brought again to 50°C in water, then incubated in 4-7 rounds of 1 M NaOH at 50°C for 1-2 hours, each time. Sample was dialyzed in many changes of water for several days until pH reached approximately 6.5-7. For the extraction round that did involve a Proteinase K step, a subset of the resulting liquid was placed in an Amicon Ultra 100 kD centrifugal filter unit (Millipore Sigma Cat No.UFC510024) and spun-dialyzed with 6 washes of water to remove any small proteins, sugars, or other molecules smaller than 100 kD. Samples were dropped onto glass slides and dried overnight at 62°C.

Chitin from *Sepia sp.* cuttlebone (from pet store) was isolated using an established protocol (Kaya et al 2017a). Cuttlebone chitin, shrimp shell chitin (Sigma, C9752) and polysaccharide extract from ratfish gel (three separate isolations) were dried at 62°C overnight before spectra were recorded with a Bruker Vertex 70 Fourier transform infrared (FTIR) spectrometer with a diamond crystal ATR accessory. In addition, requisite quality control FTIR experiments were also carried out with keratan sulfate and chitosan (75% deacetylated chitin; Sigma, C3646) in order to validate the robustness and fidelity of our AoL chitin extraction method (Selberg et al 2019).

### *1.3.14 Monosaccharide analysis with ratfish gel and polysaccharides extracted from gel*

Samples of shrimp chitin (Sigma, C9752), spotted ratfish (*Hydrolagus colliei*) gel, and extracted ratfish gel (see section 1.3.13 for extraction protocol) were sent to Biswa Choudhury at the University of California, San Diego's GlycoAnalytics Core for analysis. Approximately 0.2 mg of shrimp chitin control was weighed out in a glass hydrolyzing tube and hydrolyzed. 1.5 mg lyophilized ratfish gel was dissolved in 750 $\mu$L of ultrapure water and homogenized to fine suspension. 100 $\mu$g of material was taken for hydrolysis. The stickiness of the extracted ratfish gel prevented it from being weighed so it was dissolved in 500 $\mu$L ultrapure water (clear solution) and 50 $\mu$L was taken for hydrolysis (10% of the total material). All samples were hydrolyzed with 6 N HCl at 100°C for 6 hours, followed by removal of acid by dry nitrogen flush. Finally, dried and hydrolyzed samples were dissolved in water and approximately 0.25 $\mu$g of chitin control, 3 $\mu$g of ratfish gel, and 0.625% of ratfish gel extract were injected on HPAEC-PAD using a Thermo Scientific Dionex Ion Chromatography (IC) Systems HPAEC-PAD/UV/FL Detector. Known amounts of standards (glucosamine and galactosamine) were used for quantification of the monosaccharides.

## 1.4 Results

### *1.4.1 Histochemistry with chitin binding probes*

The spatial distribution of chitin in vertebrates was preliminarily studied using a histochemical reagent containing a chitin binding domain (CBD) cloned from a bacterial (*Bacillus circulans*) chitinase enzyme and a colorimetric or fluorescent label (Tang et al 2015). These histochemical probes can be easily used on whole-mount or sectioned tissues

and were introduced to embryos of several cartilaginous fish species. To my surprise, stereomicroscope imaging of formalin-fixed little skate (*Leucoraja erinacea*) embryos revealed an overt correspondence of CBD signals with the Ampullae of Lorenzini (AoL) (Figure 1.1A,B). Further experiments using confocal fluorescence microscopy showed that although CBD signals were bright throughout the canals, they were absent from the alveoli of early-stage little skate tissue sections (Figure 1.1C). When I used fluorescence microscopy to image tissue sections from late-stage little skate embryos, however, I discovered that CBD signals were clearly visible in the alveoli, indicating that the CBD-positive material must expand over developmental time (Figure 1.1D). Importantly, CBD signals observed with both whole-mount and sectioned materials were specifically localized to the gel filling the acellular lumen of the organs in both embryos and adult specimens (Figure 1.1C-G). AoL-containing tissue sections from embryonic little skate (Figure 1.1F) and juvenile dogfish (*Squalus acanthias*) (Figure 1.1G) demonstrated that although gel volume expands and fills the interior AoL lumen as the animals get older and larger, approximately 2 cell layers line the inside of AoL canals regardless of AoL diameter size. High magnification images of CBD-labeled gel inside a single AoL in a spotted ratfish (*Hydrolagus colliei*) specimen revealed an ordered pattern consisting of many folds (Figure 1.1H). The observed pattern gave the impression that packets of CBD-positive material were being released by canal cells into the interior AoL lumen. This same pattern was also apparent in the tissue section from spotted dogfish (Figure 1.1G).

In addition to CBD, I used another fluorescent probe called VCBP, which contained an unrelated chitin binding domain from an immune receptor protein found in a tunicate species (*Ciona intestinalis*). I used CBD and VCBP (conjugated to different fluorophores) on whole-mount and histological preparations of a few chondrichthyan species, including

spotted ratfish (Figure 1.1G,H). Both probes yielded highly similar patterns despite their disparate amino acid sequences (Dishaw et al 2016, Tang et al 2015).

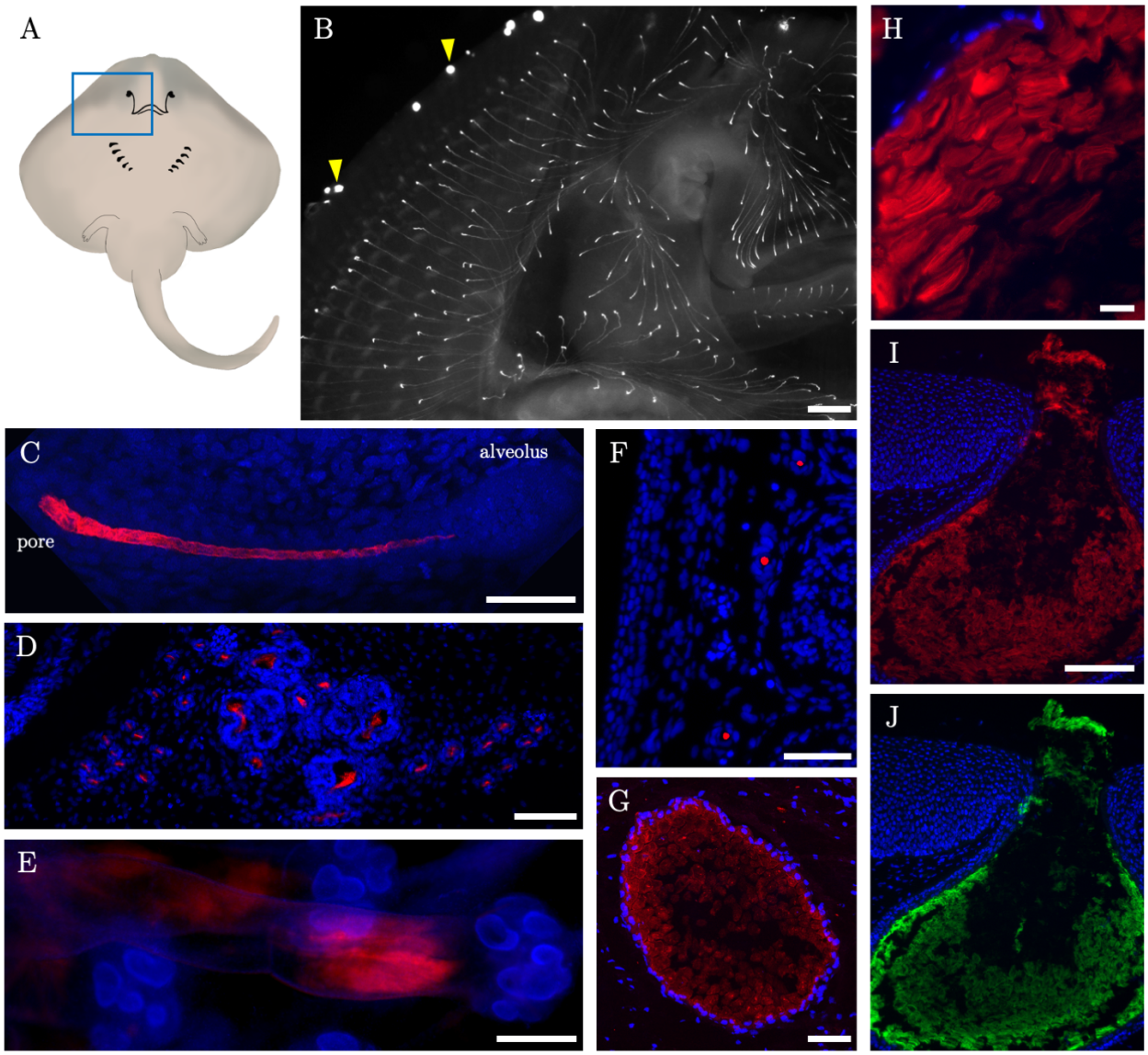


**Figure 1.1** Distribution of signals from chitin binding probes in AoL. **A)** Schematic depicting the ventral surface of a simplified skate embryo. Blue box shows rough anatomic location of image shown in B. **B)** Fluorescent image shows a portion of the anterior ventral surface of a little skate (*Leucoraja erinacea*) embryo labeled with a histochemical reagent (CBD) conjugated with a snap-546 fluorophore (no pseudocolor used in this image). CBD-546 clearly reveals the skate's AoL network. Yellow arrowheads point to structures that I affectionately call, "blobs," which will be discussed in more detail in Chapter 2. **C)** Confocal image of a CBD-labeled AoL from the lip of a stage ~31 embryonic little skate. Nuclei are stained with DAPI (blue) and delineate the canal and alveolus. CBD-546 (red) signal is seen throughout the canal. At this stage, it appears that CBD-labeled gel does not yet fill the inside of the alveolus (right). **D)** Paraffin section of tissue from a stage 32 little skate embryo. Here the section is cut through the hyoid cluster and shows both AoL canals (small circles on either side of the image) as well as some alveoli (large cell dense structure in the center of the image). The

section was labeled with CBD-Biotin + Streptavidin 546 and DAPI, and shows that at this stage of development, CBD-positive signal is visible inside the alveoli. **E)** Stereoscope image of alveoli dissected from the hyoid cluster of an adult little skate specimen. Nuclear stain (blue) outlines three lobed alveoli at the base of tubular canals and CBD-546 signal (red) occupies the interior lumen of the organs. **F)** A paraffin tissue section through the wing of an embryonic little skate showing three AoL cut in cross section. DAPI (blue) signal reveals the 1-2 cell layers lining the inside of each individual AoL, and CBD-positive material (red) occupies the center of the AoL exclusively. **G)** Affinity histochemistry with a cryosection of tissue from a juvenile dogfish shark (*Squalus acanthias*) (0.4 m total length) using CBD-546 and DAPI (counterstain, blue) showing a single AoL in cross section. Similar to (F), approximately 2 layers of cells can be observed surrounding the acellular lumen of the AoL and CBD signal is localized entirely to the AoL gel. **H)** A paraffin tissue section from the snout of an adult spotted ratfish (*Hydrolagus colliei*) showing the inside wall of a single AoL canal in high magnification. The canal wall is lined by DAPI-positive (blue) cells, and the inside lumen is filled with CBD-positive (red) gel. **I,J)** CBD labeling of a paraffin section taken from the snout of a juvenile spotted ratfish using two fluorescent probes consisting of different chitin binding domains. The CBD-546 probe used in (I) contains the chitin binding domain from a chitinase of the bacterium, *Bacillus circulans*, whereas the chitin binding region of the VCBP probe used in (J) came from an immune receptor protein found in the gut of the tunicate, *Ciona intestinalis*. The probes were applied simultaneously to the same histological section and show highly similar fluorescent patterns. Scale bars – B,E: 500 $\mu$m; C,F: 50 $\mu$m; G: 200 $\mu$m; H: 20 $\mu$m D,I: 100 $\mu$m.

Figure 1.1 shows histochemical data from three different species of cartilaginous fish, namely, *Squalus acanthias*, *Leucoraja erinacea*, *and Hydrolagus colliei*. Over the course of my studies, however, I used CBD with either sections or whole-mount tissue from a few other chondrichthyan representatives (as many as I could get my hands on)! My advisor, Chris Amemiya observed CBD in AoL gel from the Southern stingray, *Dasyatis Americana* (data not shown here), and I examined CBD patterns in two other batoids that I obtained surreptitiously. The first, a species of ray, *Potamotrygon falkerni*, lives in freshwater ecosystems and possesses very shallow AoL that are known as, "microampullae" (Szabo et al 1972). These microampullae are somewhat anatomically distinct from the AoL of saltwater-inhabiting chondrichthyans but interestingly, they closely resemble the electrosensory organs that evolved analogously in groups of freshwater teleost fishes (Szabo 1974). CBD labeling of tissue sections from the freshwater ray revealed punctate signals concentrated around the microampullae and diffusely throughout the skin (Figure 1.2A). In this experiment, I used CBD conjugated to biotin detected by Streptavidin-546. Due to the shallow nature of the structures, there is a likelihood that gel was dislodged and lost during

the fixation process as it was difficult to see any obvious gel in the microampullae. However, the prevalence of CBD signals within the cells that make up the structures may be indicative of chitin's presence within the microampullae, but it can't be interpreted as definitive proof. I also investigated the distribution of CBD signals in tissue from Pacific electric ray (*Tetronarce californica*) specimens. This species belongs to a group of rays that possess two sizeable electric organs in their left and right flanks that emit extremely powerful electric discharges to stun prey (Bray & Hixon 1978). I observed that the AoL of this species were distributed differently than those from related chondrichthyans – their canals wrapped around the outside of the electric organs, following the curvature of the animal's disc-like anterior before turning inwards and terminating in egg-shaped alveoli. Using CBD-Biotin & Streptavidin-546 on tissue sections from this species I observed that signal localized to the AoL gel (Figure 1.2B). Imaging of the sample's background autofluorescence using the green channel of our fluorescent microscope showed that red CBD signal inside the AoL lumen was real (Figure 1.2C). As an interesting side note, perhaps due to its composition, the gel inside the electric ray's AoL was reluctant to stick to charged slides as compared to the gel from other chondrichthyan species and I had to perform CBD experiments many times before gel stuck effectively to the slides.

In summary, I studied several species within the class Chondrichthyes and with the exception of the freshwater stingray, all of them very clearly exhibited CBD signals in the gel of their AoL. Figure 1.2D shows a phylogeny of all the currently accepted chondrichthyan orders represented by a schematic of a single species within each order (phylogeny based on data from "Chondrichthyan Tree of Life" at sharksrays.org). In Figure 1.2D, colored fish schematics signify that at least one species from that order exhibited positive CBD labeling within their AoL. I was unable to sample from every chondrichthyan order and so black-and-white fish represent clades that have not yet been sampled.

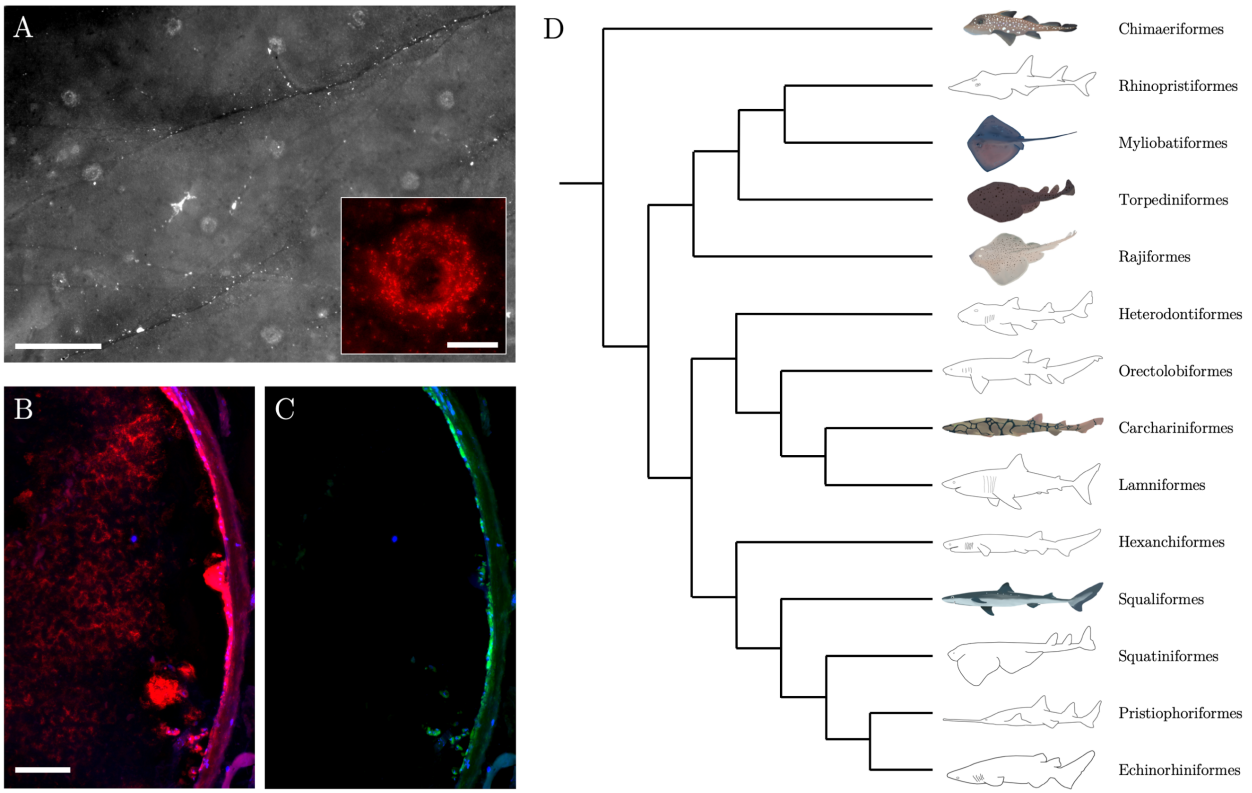


**Figure 1.2** Summary of CBD labeling in AoL of diverse chondrichthyan taxa. **A)** Whole-mount tissue from freshwater stingray (*Potamotrygon falkneri*) specimen (~36 cm in length) labeled with CBD-Biotin and detected with Streptavidin-546. Tissue was dissected from just above the upper lip of the animal. Stereomicroscopy reveals the ray's skin surface with brightest CBD signal observed in a speckled pattern concentrated near the microampullae. Inset shows a single microampullae from the same tissue imaged with compound microscopy and pseudocolored red. Gel was not observed inside the microampullae. **B)** Paraffin section of tissue dissected from the anterior edge of a Pacific electric ray (*Tetronarce californica*) specimen containing AoL canals cut in cross section. Curvature to the right of the image shows the inside wall of a single AoL canal with the acellular canal lumen filling the left side of the image. Red CBD-Biotin + Streptavidin-546 signal was observed inside the lumen. **C)** The same section as shown in (B) using green channel to show background autofluorescence of tissue. **D)** A simplified phylogeny depicting orders within the class Chondrichthyes represented by drawings of selected species. Phylogenetic positions of these orders are based on gene sequence data from the 'Chondrichthyan Tree of Life" at sharksrays.org. Note that the positions of some of these clades are still debated but major groups such as Selachii, Holocephali, and Batoidea (Figure I.1) are highly supported (Velez-Zuazo & Agnarsson 2011). Orders portrayed by colored fish contain at least one representative species that exhibited CBD staining within their AoL. The clades represented by black-and-white fish outlines have not yet been examined. Scale bars – A: 500 $\mu$m (inset: 50 $\mu$m); B: 100 $\mu$m.

These initial findings using CBD, though compelling, were not sufficient proof that chitin is being synthesized by the fishes themselves. In fact, it is important to note that

some studies have reported that CBD probes similar to the ones used in this study, although very specific, are not completely specific to chitin. For example, Ujita et al used binding assays with a chitin binding domain from a human chitinase (HCBD), and showed that it bound to chitin, chitobiose, and hyaluronan, suggesting that the domain would bind to any number of molecules containing *N*-acetylglucosamine (GlcNAc) residues (Ujita et al 2003). When the binding domain structure and binding properties of the CBD used in my studies (from chitinase A1 in *Bacillus circulans*) was investigated, the domain did "not bind to chito-oligosaccharides or soluble derivatives of chitin but [did] bind to insoluble or crystalline chitin" (Ikegami et al 2000). This information is particularly relevant and puzzling in the context of my preliminary data because if CBD probes were indeed binding to chitin, then that chitin would need to be soluble to exist as a component of a hydrogel! Therefore, I set out to validate the existence of AoL chitin using multiple methods.

### *1.4.2 Chitinase assays*

I used chitinolytic enzymes (chitinases) on AoL-containing histological sections from the tissues of a few fish species then labeled the slides with CBD and DAPI. With this method, I examined whether or not CBD's specific substrate within the gel could be eliminated by chitinase activity. When chitinases were applied to the sections, I observed the elimination of detectable CBD signals (Figure 1.3A,C) as compared to controls (Figure 1.3B,D). Figures 1.3A and B show serial sections cut from little skate tissue whereas Figure 1.3C and D show serial tissue sections from spotted ratfish. The little skate section (Figure 1.3A) was treated with chitinase from *Streptomyces griseus*, and the spotted ratfish section (Figure 1.3C) was treated with chitinase from *Brugia malayi*. The total elimination of material detectable by CBD in two species of cartilaginous fishes and with chitinases synthesized by two different organisms is strong evidence that chitin is present in AoL gel.

Further, these data serve as evidence that CBD probes are binding specifically to chitin in the AoL gel and not some other polysaccharide.

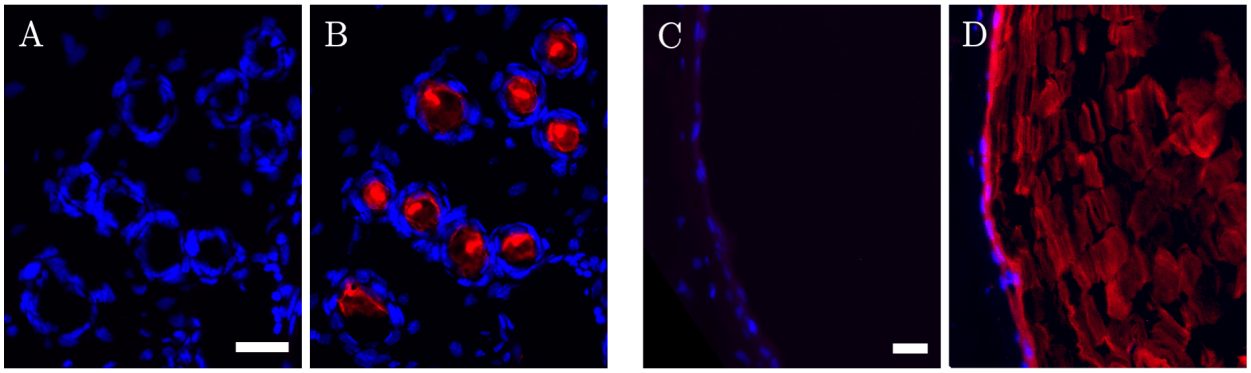


**Figure 1.3** Chitinase treatments using tissue sections from little skate and spotted ratfish. **A)** Paraffin section of tissue from an embryonic little skate (*L. erinacea*) specimen showing nine AoL canals cut in cross section. The section was treated with chitinase from *Streptomyces griseus* (bacterium) before labeling with CBD-Biotin + Streptavidin-546. The lack of red signal in the AoL indicates absence of target material for CBD to bind. Blue signals are from cell nuclei (DAPI). **B)** A section cut serially with that shown A. This section was not treated with chitinase before labeling with CBD-Biotin + Streptavidin-546 and signal was observed very specifically in the AoL gel. **C,D)** Images of serial paraffin tissue sections from an adult spotted ratfish (*H. colliei*) specimen (41 cm total length) showing a single AoL canal cut in cross section. DAPI revealed the curvature of a single AoL canal with the gel-containing lumen on the right side of the images. As with (A,B), the sections were both stained with CBD-546 (red) but one section was first treated with chitinase from *Brugia malayi* (nematode worm) (C) while the other was not (D). CBD signal was observed in the AoL lumen of the control but not the chitinase-digested sample. Scale bars – A,C: 20 $\mu$m.

### *1.4.3 Transcriptomic and genomic searches for chitin synthase genes in little skate*

I had now obtained convincing biological evidence that chitin is a component of AoL gel. However, it was still not clear if chitin was being synthesized by the cells inside the AoL or if it was accumulating from the environment through the open AoL pores. Chitin synthase (CHS) enzymes are critical for chitin synthesis, therefore, to know if chitin was being endogenously produced by the fishes, I needed to study the transcriptional profiles of the cells inside the AoL to determine if they were synthesizing CHS enzymes. I conducted *CHS* gene expression analyses using the little skate (*L. erinacea*) as my model. When I began these experiments in 2015, the little skate was one of the only cartilaginous fishes with a

sequenced genome and by far the most easily obtainable (Wyffels et al 2014). Although the genome was not completely annotated, I used BLAST to search for sequences that aligned with known *CHS* sequences from zebrafish and some invertebrate species, I was able to identify a number of *L. erinacea CHS* (*LeCHS*) fragments. Joyce W Tang, a researcher in the Amemiya lab, generated a pilot transcriptome from adult little skate AoL tissues, which led us to uncover an even longer, albeit still incomplete, *CHS* sequence. Finally, after Bellono et al published transcriptomic profiles of four tissue types (liver, skin, AoL canals, and AoL alveoli) in 2017, I identified two full *LeCHS* sequences (Bellono et al 2017). However, Bellono et al generated their skin transcriptome using tissues that did not contain any AoL pores, so I was not able to get a full picture of spatial *CHS* expression across the entirety of the organs using their published transcriptomic data (Bellono et al 2017)

To understand the spatial distribution of CHS expression throughout the AoL, postdoctoral scholar, Daniel Ocampo Daza and I, in collaboration with QIAGEN, generated transcriptomes using four different tissues: AoL pores, AoL canals, part of the hyoid cluster (an aggregation of alveoli and the distal part of canals), and skin from the pelvic fin. Using the two existing *LeCHS* sequences as query sequences, the new transcriptomes were searched and this time, three CHS genes in *L. erinacea* were discovered! These genes were named, *LeCHS1*, *LeCHS2*, and *LeCHS3*. These sequences were later confirmed using a still unpublished *L. erinacea* genome, so Daniel and I are confident that the little skate has three *CHS* gens. However, evidence from the transcriptomes published in Bellono et al and our transcriptomes suggest that there are two transcript variants of *LeCHS3*.

### *1.4.4 Transcript per millions (TPM) estimations of three LeCHS genes*

Daniel and I compared the spatial expression of *CHS* between AoL and skin tissues, and estimated transcript counts of the three *LeCHS* genes in each tissue-specific transcriptome

using transcript per million (TPM) estimations (Table 1.1). We found that the overall expression of all three *LeCHS* genes was generally quite low across the AoL. *LeCHS1* had the most notable expression, particularly in the AoL pores and canals, with much lower expression levels observed in the pelvic fin skin and alveoli. Although *LeCHS2* and *LeCHS3* are expressed at slightly higher levels in AoL pores as compared to the other three tissues, the TPM values are so low that major comparative conclusions could not be drawn. It is important to note that the dissected alveoli tissue certainly contained pieces of canals, and similarly, the sampled AoL pore tissues would have inevitably contained skin cells, so there would have been unavoidable expression profile crossover between some of the four transcriptomes. However, assuming that the expression profile observed in our pelvic fin skin transcriptome was representative of most non-AoL skin cells, the higher *LeCHS1* TPM count observed in the pore transcriptome, as compared to the TPM count from the pelvic fin skin transcriptome, is likely an indication that the expression is pore-specific.

| | **Pore TPM** | **Canal TPM** | **Alveoli TPM** | **Pelvic Fin TPM** |
|---|---|---|---|---|
| ***LeCHS1*** | 57.1 | 33.8 | 8.1 | 9.5 |
| ***LeCHS2*** | 4.1 | 1.0 | 1.7 | 1.9 |
| ***LeCHS3*** Transcript variant 1 | 3.9 | 0.1 | 0.2 | 1.9 |
| ***LeCHS3*** Transcript variant 2 | 1.3 | 0.2 | 0.5 | 1.2 |

**Table 1.1** Transcripts per million (TPM) of the three *LeCHS* genes within four tissue-specific transcriptomes.

### *1.4.5 In situ hybridization with riboprobes specific to LeCHS1*

I continued investigating *CHS* expression in the AoL of little skates using antisense riboprobes specific to *LeCHS1* for *in situ* hybridization (ISH) on both whole-mount (Figure 1.4A,B) and sectioned tissues (Figure 1.4C-F). The whole-mount ISH patterns using

riboprobes specific to *LeCHS1* indicated expression in the cells of the AoL pores (Figure 1.4A). CBD-546 signal corresponded with the AoL, as expected (Figure 1.4B). The ISH signals in this particular experiment were restricted to the pores, however, I have observed that probe penetration can be variable likely due to the fish's thick skin. I thus used sectioned materials and found *LeCHS1* expression in the epithelial cells lining AoL canal walls at various canal depths (Figure 1.4C,F). Although I began my experiments using sense probes as negative controls, after hybridization I observed clear ISH signals in whole-mount tissues that exhibited the same specific patterns as the antisense probes. I discussed these observations with my collaborators, who suspected that *LeCHS* genes were undergoing some amount of antisense transcription, a phenomenon which is apparently common in these fishes (conversation with Andrew Gillis, Cambridge University). Therefore, for my negative controls, I began using RNA probes specific to genes from planarians (freshwater flatworms) to demonstrate the binding specificity of the *LeCHS1* probes (Figure 1.4E). The co-localization of *LeCHS* expression, as indicated by ISH, and fluorescent CBD signals provided compelling evidence that CBD is indeed binding to chitin, not some other related polysaccharide, and that the cells within the AoL are producing and secreting chitin (Figure 1.4D). Additionally, the distribution of ISH signals on cross sections of AoL at different levels and transverse angles indicated that cells inside the alveoli do not exhibit appreciable *LeCHS1* gene activity (Figure 1.4F). I also performed *in situ* hybridization with whole-mount (Figure 1.4G) and sectioned (Figure 1.4H) tissue from an adult little skate specimen, and observed *LeCHS1* expression in the same patterns as were seen with little skate embryos – signals were apparent in the pore and canal cells but absent from the alveoli.

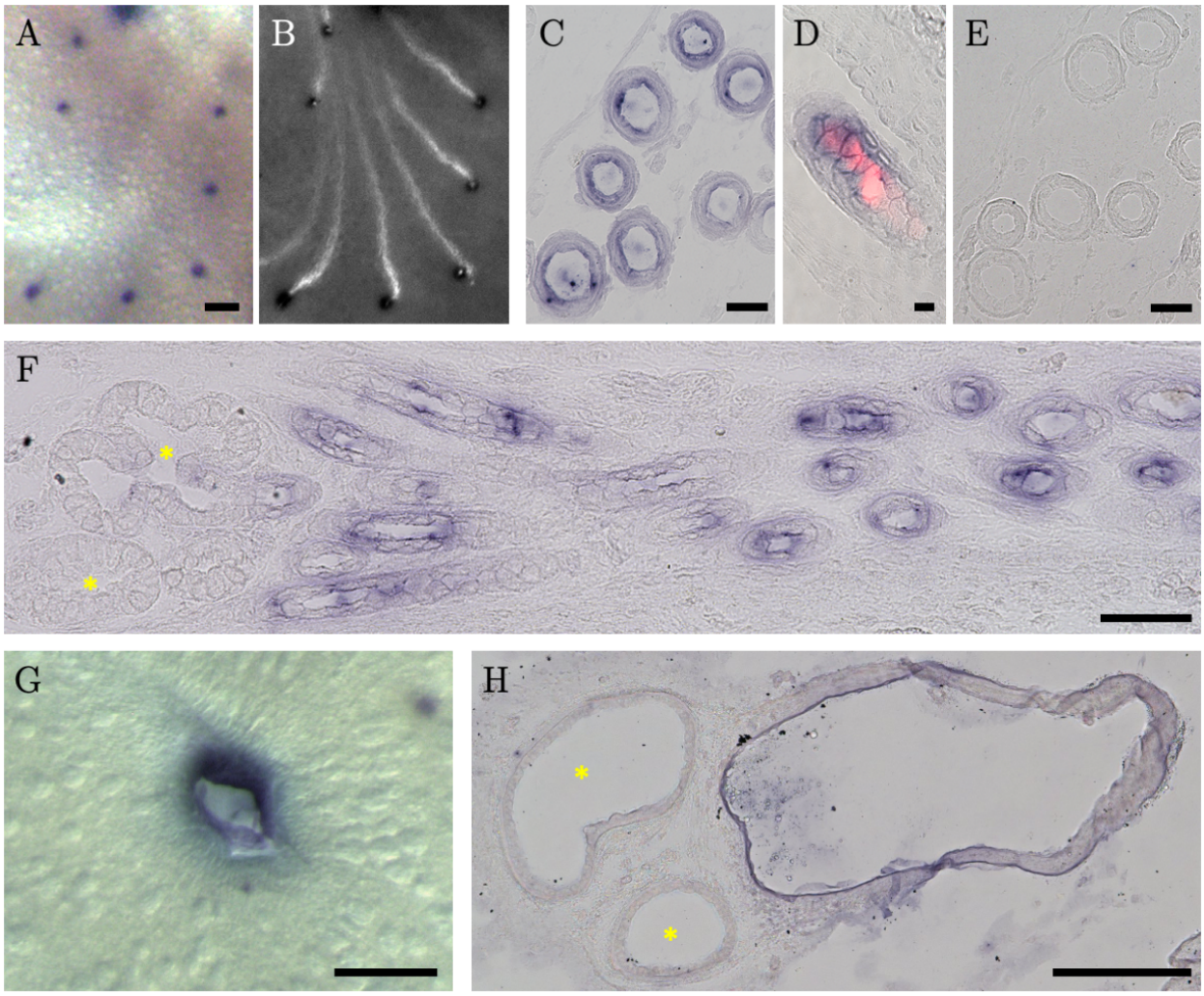


**Figure 1.4** *LeCHS1* expression in AoL pores, canals, and alveoli of little skate specimens. **A,B)** An antisense riboprobe specific to the gene, *LeCHS1* was used for *in situ* hybridization (ISH) on whole-mount tissue from little skate embryos. The riboprobes (purple) localized to regions in the vicinity of the pores of the AoL (A) as made clear by CBD-546 histochemistry (white) of the same tissue specimen (B). **C,D)** ISH with paraffin sections from little skate embryos show *LeCHS1* gene expression in the endothelial cells lining AoL canals cut in cross section (C) and transverse section (D). AoL shown in (C) are each cut at different canal depths demonstrating the widespread expression of *LeCHS* throughout AoL canals. In (D), an image showing fluorescent CBD-546 signals (red) is superimposed on a brightfield image of ISH signals, revealing CBD-labeled gel encased by *LeCHS1*-positive cells lining the AoL canal wall. **E)** Negative control ISH. Paraffin section from little skate embryo was exposed to probe specific to *ChAT* gene from *Schmidtea mediterranea*, and no colorimetric reaction was observed. **F)** ISH of *LeCHS1* riboprobe using section from embryonic little skate. *LeCHS1* expression was observed within the cells that line the AoL canals, however, expression was absent from cells in the alveoli (as indicated by yellow asterisks). **G,H)** *In situ* hybridization with *LeCHS1* probes and little skate tissue from an adult specimen. In (G), an AoL pore from whole-mount tissue exhibits positive *LeCHS1* ISH signals. ISH experiment with a section of tissue containing alveoli from the hyoid cluster of adult skate specimen (H) revealed that, as with embryonic skates, ISH signals were observed in the canal cells but absent from the cells inside the alveoli (as indicated by yellow asterisks). Scale bars – A,F: 50 $\mu$m; C,D,E: 10 $\mu$m; G: 100 $\mu$m; H: 200 $\mu$m.

### *1.4.6 In situ hybridization with riboprobes specific to LeCHS3*

I also synthesized riboprobes specific to a region of the *LeCHS3* gene for *in situ* hybridization. Using whole-mount tissue from little skate embryos, I observed ISH signals in the cells at the AoL pore openings, similar to the patterns seen when using *LeCHS1* probes (Figure 1.5A). Interestingly, I was met with conflicting results when I used ISH with *LeCHS3* riboprobes on skate tissues containing AoL canals. There were barely any observable signals when ISH was performed with sections of tissue containing AoL canals cut in cross section (Figure 1.5B) despite the clear localization of CBD-546 to the interior gel (Figure 1.5C). However, dissected whole-mount embryonic skate tissues told a different story. I sliced through a few AoL right in the middle of the canals and ISH with *LeCHS3* revealed that signals were present in these sliced regions, as shown by the two AoL in Figure 1.5D. The canals had been sliced at different locations along their lengths which indicates that signal is observable at various canal depths. The observed differences between sectioned and whole-mount tissues could be potentially explained by experimental error – perhaps there was variation in probe efficiency when using sectioned vs. whole-mount material with these particular riboprobes. Alternatively, it could be that *LeCHS3* probes were actually binding to transcripts from other *CHS* genes. Because of *CHS* gene sequence similarities, I was suspicious of the specificity of any *LeCHS* probe designed to be complementary to one of the three *LeCHS* genes. When I aligned the gene's amino acid sequences with one another, I found that *LeCHS1* was approximately 46% identical to *LeCHS2*, and 45% identical to *LeCHS3*. Even more remarkably, *LeCHS2* and *LeCHS3* are approximately 90% identical to one another. When I designed the two ISH riboprobes described here, I was careful to make them complementary to ~650bp regions that exhibited the least amount of sequence conservation and avoided the highly conserved glycosyltransferase regions (the active sites of chitin synthesis) of the genes. I did this because, at the amino acid level, the

glycosyltransferase regions were 72% identical between *LeCHS1* and both of the two other genes, and 98% identical between *LeCHS2* and *LeCHS3*! Regardless, even though I chose probe sequences with low conservation, it is still unclear if my *LeCHS3* riboprobes exhibited non-specific binding. It is very likely that *LeCHS3* probes would not have distinguished between the highly similar *LeCHS2* and *LeCHS3* sequences, and I never tried to synthesize a probe specific to *LeCHS2* for that reason.

Even though I couldn't confidently tell if the *LeCHS* riboprobes exhibited some degree of non-specific binding to one or more of the three *LeCHS* genes, my ISH experiments demonstrated that *CHS* genes are being expressed by the cells lining the AoL pores and canals of little skate embryonic and adult specimens. These findings support my hypothesis that the chitin I identified inside the viscous AoL gel is endogenously synthesized by the animals themselves.

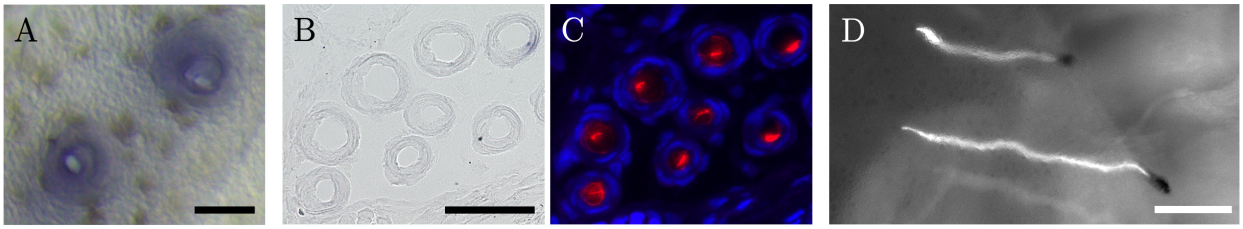


**Figure 1.5** *In situ* hybridization using RNA probe complementary to region of *LeCHS3* sequence. Although riboprobes were designed using the *LeCHS3* sequence, the similarities between the three little skate *CHS* sequences (especially between *LeCHS2* and *LeCHS3*) make it hard to know if the probes bound to LeCHS3 specifically. **A)** ISH with whole-mount tissue from embryonic little skate specimen. The two AoL pores shown here exhibit ISH signals within the cells that line their openings. **B,C)** ISH with tissue section from little skate embryo subsequently labeled with CBD-546. Several AoL are cut in cross section revealing very minimal *LeCHS3* riboprobe signal in the cells that line the canals (B). CBD-546 histochemistry shown in red (C) revealed the presence of chitin in the canal lumens. Blue signals are from cell nuclei (DAPI). **D)** Whole-mount ISH and CBD histochemistry were performed using tissue dissected from a little skate embryo. AoL pores are on the left side of the image and the tissue cut site is visible on the right where the blunt ends of sliced canals are revealed. ISH signals (black) were observed at the sites where canals were sliced, suggesting that *LeCHS3* is expressed in the cells lining AoL canals. These observations contradict the results shown in (B). CBD-546 signal (white) was observed throughout the canals quite prevalently. Scale bars – A,B: 50 $\mu$m; D: 200 $\mu$m.

### *1.4.7 FTIR with chitin extracted from AoL gel*

Although I had already obtained substantial biological evidence of chitin within AoL gel, the findings laid out in this chapter represent the first description of chitin existing as a gel component in nature. This bold claim required an abundance of supportive evidence! Therefore, I decided to chemically extract chitin from spotted ratfish (*Hydrolagus colliei*) gel and analyzed the resulting material using physicochemical methods. I used gel from spotted ratfish for these experiments as I was lucky to get access to dozens of frozen specimens at Moss Landing Marine Laboratory and removed many milliliters worth of gel from their AoL pores. My polysaccharide extraction protocols went through various renditions and were based on well-known methodologies used to isolate chitin from crustacean shells (Arbia et al 2013). I used Fourier transform infrared spectroscopy (FTIR) to analyze the resulting extracted materials and assessed the relative purity of extracted chitin. FTIR uses light to scan a sample of interest and measure the absorption at each wavelength. The resulting data is returned as a spectrum that can be compared to the spectral "fingerprints" of known samples and used to inform the chemical identities of samples such as mine. FTIR is commonly used to determine the allomeric form of chitin – $\alpha$, $\beta$, or $\gamma$– within a sample, as there are some characteristic differences between the allomers (Kaya et al 2017b). After some trial and error, my purest chitin extraction, as evidenced by FTIR, resulted from ratfish gel that was treated with proteinase K, 1 M HCl at 50°C, and several rounds of 1 M NaOH at 50°C, followed by extensive dialysis in water. The FTIR spectrum from extracted gel contained peaks characteristic of two different allomers of chitin: $\alpha$-chitin from shrimp shells and $\beta$-chitin from cuttlefish cuttlebone, which were both also analyzed with FTIR for the sake of comparison (Figure 1.6A). However, the spectrum from extracted AoL gel shared the most similarities with $\beta$-chitin. Additionally, Figure 1.6B shows the FTIR spectrum resulting from commercial chitosan as compared to that from

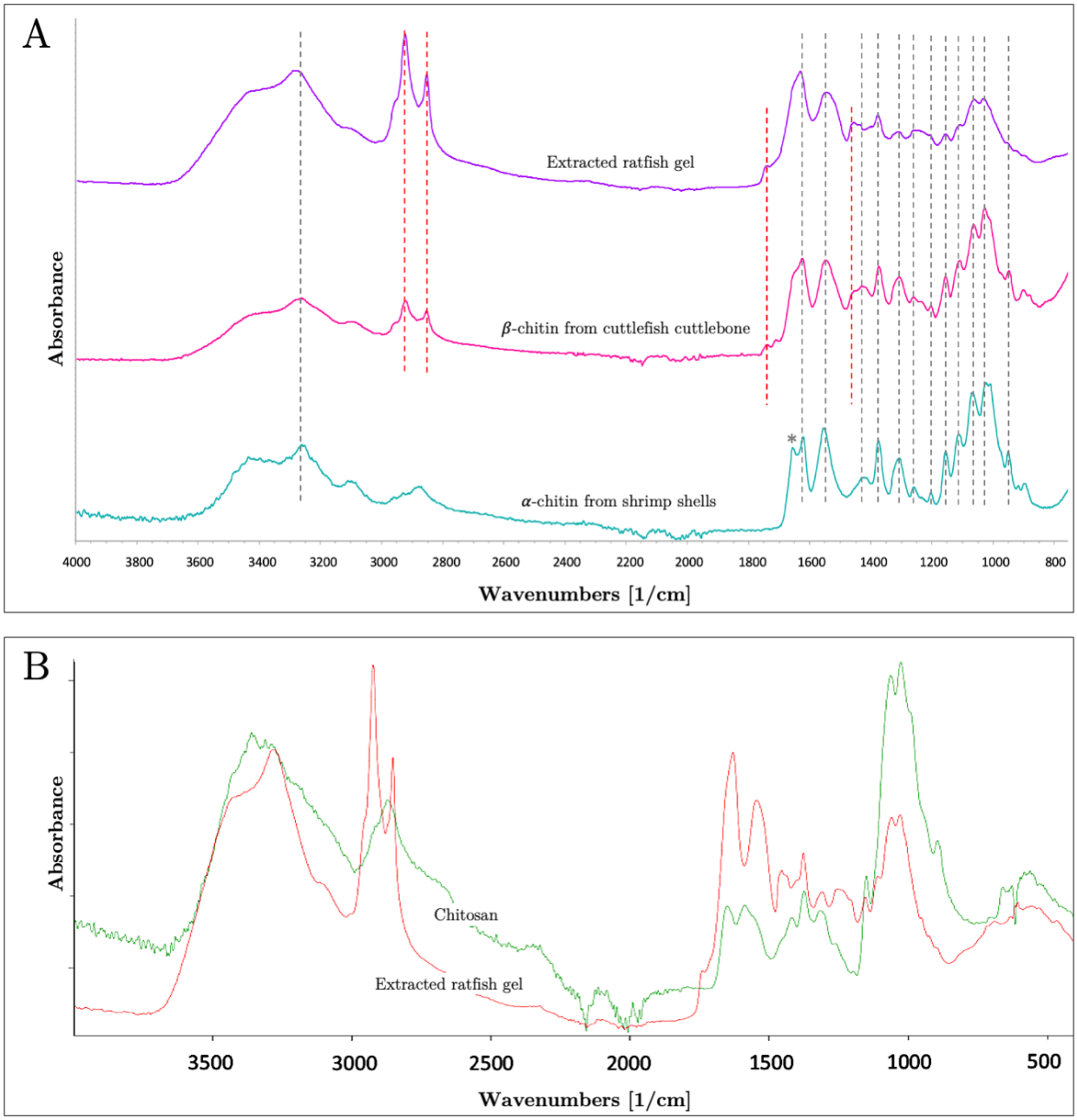


**Figure 1.6** Analyses of chitin extracted from the AoL gel of spotted ratfish (*Hydrolagus colliei*) specimens by Fourier transform infrared spectroscopy (FTIR). **A)** Comparison of FTIR spectra from AoL gel extraction (treatment with Proteinase K, HCl, NaOH, and extensive dialysis against water) (purple), β-chitin obtained from cuttlebone of cuttlefish (pink), and α-chitin from shrimp shells (teal). Black dotted lines indicate shared peaks among all three samples; red dotted lines indicate shared peaks among two of the samples. The * at 1654 $cm^{-1}$ on the shrimp shell chitin plot represents the split amide band that is always observed with α-chitin (Kaya et al 2017a). There are notably more similarities between extracted ratfish gel and β-chitin from cuttlebone, but all three samples shared many of the same peaks. **B)** A comparison of FTIR spectra obtained from commercial chitosan (green) and polysaccharides extracted from AoL gel (red). This comparison reveals that the spectrum from the gel extraction shares many more similarities with chitin samples (A) than with chitosan (B).

extracted gel. This comparison demonstrates that acid and base treatment was not sufficient to deacetylate chitin during the extraction process.

### *1.4.8 Monosaccharide analysis with chitin extracted from AoL gel*

I confirmed that my "best" extraction protocol (described above and shown in purple in Figure 1.6A) yielded a relatively pure chitin solution by comparing its monosaccharide content to that of native ratfish gel. These samples were sent to the GycoAnalytics Core at UC San Diego (UCSD) where analyses were conducted by Biswa Choudhury. Biswa hydrolyzed both samples with HCl as well as a control aliquot of chitin extracted from shrimp shells so that component poly- and oligosaccharides would break into monomers. To analyze the hydrolyzed samples, Biswa used "high-performance anion exchange chromatography with pulsed amperometric detection," or HPAEC-PAD, a method commonly used to separate and identify carbohydrates. Figure 1.7 shows the resulting HPAEC-PAD profiles of control shrimp shell chitin (Figure 1.7A), native spotted ratfish gel (Figure 1.7B) and polysaccharides extracted from spotted ratfish gel (Figure 1.7C). These data demonstrate that spotted ratfish gel contains an abundance of galactosamine ($GalNH_2$) and glucosamine ($GlcNH_2$). Although the observed $GlcNH_2$ can be attributed to the presence of chitin in ratfish AoL gel (the hydrolysis process would have deacetylated *N*-acetylglucosamine monomers), it is not clear if the $GalNH_2$ exists as a monosaccharide in the gel or if it is a component of some other polysaccharide.

After digestion and chemical extraction of the gel, there is a notable reduction in galactosamine, but an abundance of glucosamine remains identifiable. This suggests that chitin (which is the only polysaccharide made entirely of *N*-acetylglucosamine) is the only polysaccharide still present in extracted ratfish gel (Figure 1.7C). It is worth noting that

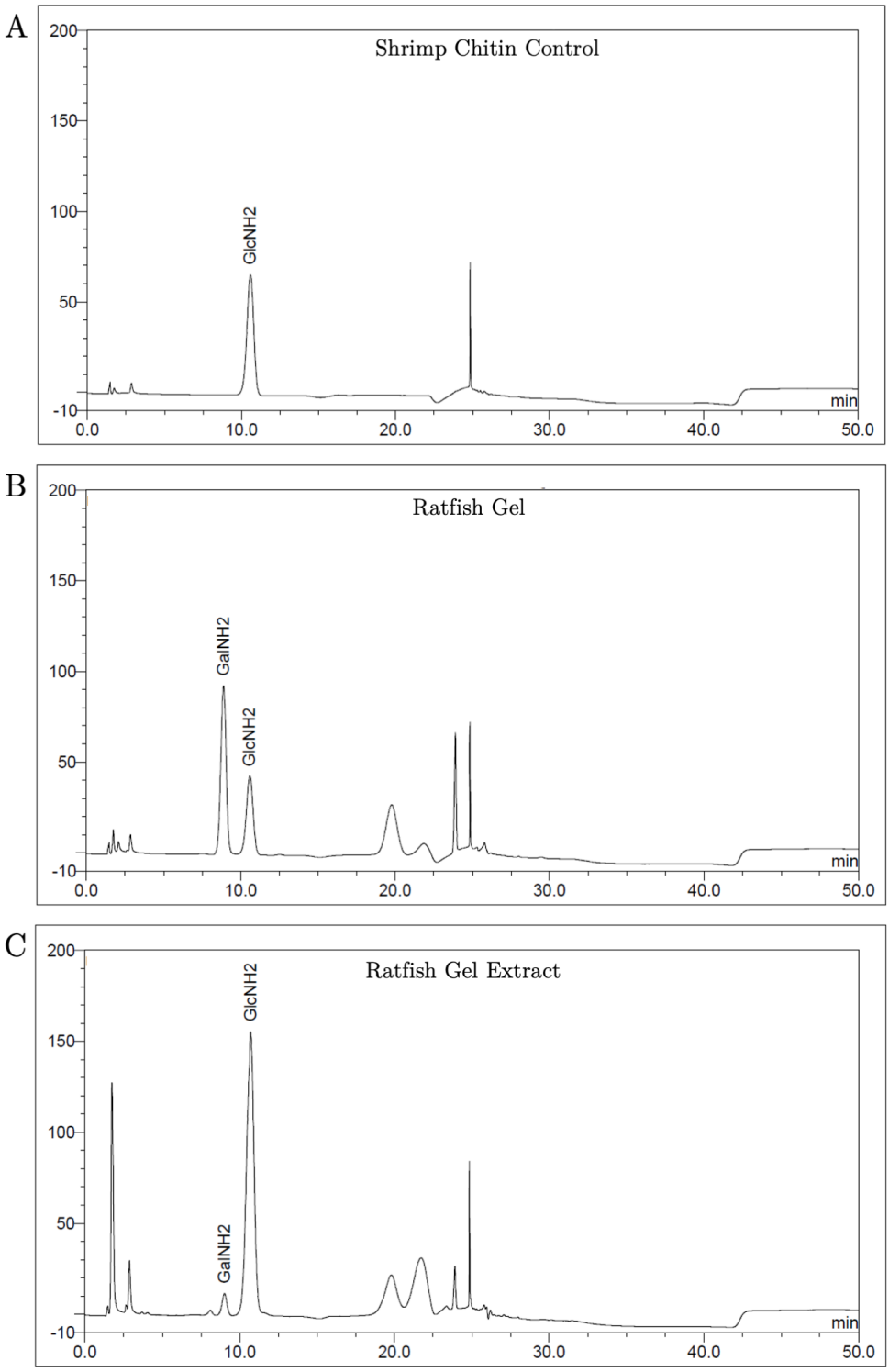


**Figure 1.7** HPAEC-PAD profiles showing the monosaccharide content of shrimp shell chitin, ratfish gel, and extracted ratfish gel after hydrolysis. **A)** Commercial shrimp shell chitin shows an appreciable presence of glucosamine ($GlcNH_2$), indicative of chitin purity. **B)** Ratfish AoL gel contains obvious signals for $GlcNH_2$ and galactosamine ($GalNH_2$). It is unclear if $GalNH_2$ exists as a monosaccharide in native ratfish gel or if it is a component of a larger polymer. **C)** Analysis of ratfish gel extraction shows that the sample experienced a reduction in measurable GalNH2 after treatment but still contains GlcNH2, which suggests chitin was maintained in the sample after digestion + extraction procedure.

despite the absence of galactose in Figure 1.6B, we suspect keratan sulfate, which is made up of N-acetylglucosamine and galactose (Figure I.3), is indeed a component of ratfish gel.

Hassan Khan, a researcher in the Amemiya lab, used an antibody specific to keratan sulfate (MZ15) on sections from spotted ratfish tissue and identified signals in AoL gel (data not shown). The strong acid (6 N HCl) that was used to hydrolyze the samples before analysis with HPAEC-PAD was the optimal treatment for identification of N-acetylglucosamine but may have destroyed galactose molecules in the process (conversation with Biswa Choudhury, UCSD GlycoAnalytics Core). Further analyses are necessary to confirm that galactose is present in native ratfish gel.

### *1.4.9 PAS staining of AoL tissue from little skate*

Substantial biological (histochemistry, chitinase digestion assays, transcriptomics, and *in situ* hybridization) and physicochemical (FTIR & monosaccharide analyses) data suggest that chitin is endogenously synthesized in the AoL of cartilaginous fishes. However, over the course of my studies, the results of one experiment might indicate that AoL chitin is modified in a way that prevents it from reacting with certain reagents. Chitin is known to react with Periodic acid – Schiff (PAS) stain, which turns magenta or red in the presence of free amine groups (Fusaro & Goltz 1960, Krishnamurthy 1999). I treated skate tissue sections with both PAS and Alcian Blue (a stain that reacts with negatively charged acid mucopolysaccharides) and observed that AoL gel was Alcian Blue positive but PAS negative (Figure 1.10). Keratan sulfate, a known component of AoL gel is an acid mucopolysaccharide and would exhibit positive Alcian Blue staining, so it is not surprising that AoL gel in both the canals and alveoli turned blue during this experiment. The absence of PAS positive signals in the AoL of these samples is surprising and may suggest that the amine groups of AoL chitin were bound in a way that prevented a reaction with PAS stain.

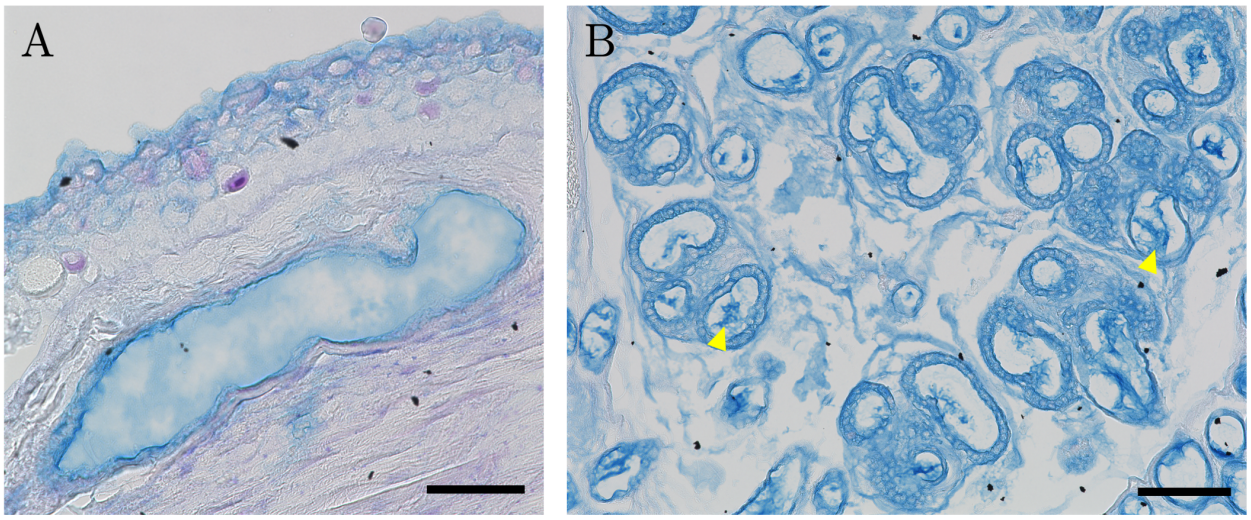


**Figure 1.10** Periodic Acid-Schiff (PAS) and Alcian Blue staining of little skate (*Leucoraja erinacea*) AoL tissues. **A,B)** Paraffin sections of tissues containing a gel-filled AoL canal cut in transverse near the skin surface (A) and many alveoli of the hyoid cluster (B). Tissues are stained with Alcian Blue, which labels acid mucopolysaccharides blue and PAS, which stains mucins, and neutral polysaccharides red or magenta (Fusaro & Goltz 1960). Gel in canals and alveoli (the gel inside some of the alveoli indicted by yellow arrowheads for orientation) are clearly positive for Alcian Blue but are PAS negative. Note that there are some PAS-positive goblet cells (stained magenta) observed in the epidermis of (A). The Alcian Blue positivity can be attributed to the presence of keratan sulfate in AoL gel which is a negatively charged mucopolysaccharide. Scale bars – A: 50 $\mu$m; B: 100 $\mu$m.

### *1.4.10 CBD labeling with tissues from two electroreceptive teleost fishes*

Although the ancestral ampullary system was lost in the neopterygian fishes, two groups of teleost fishes, the mormyrids of Africa and the gymnotiforms of South America, independently evolved electric organs as well as two types of electrosensory organs (tuberous and ampullary) (Lavoue et al 2012). The fishes use their tuberous organs to detect electric discharges generated from their own electric organs or from those of other fish. They use their ampullary organs to detect external electric fields in a similar way that chondrichthyans use ancestral ampullary organs, although teleost ampullary organs are excited by anodal stimuli (Baker et al 2013). Unlike teleost ampullary organs, which exhibit a tube-like, gel-filled morphology similar to ancestral ampullary electroreceptors, tuberous

organs exhibit a number of morphologies but are all plugged with epidermal cells and thereby not open to the environment *via* a pore.

My studies demonstrated that chitin is prevalent in the electrosensory organs of diverse chondrichthyans, however, being very interested in the evolution of vertebrate chitin, I wanted to find out if chitin was synthesized in the gel of electroreceptive teleost fishes. To survey the distribution of chitin in the electrosensory organs of non-chondrichthyan fishes, I used fixed and paraffin sectioned tissue from an African mormyrid (*Gnathonemus petersii*) and a South American gymnotiform (*Apteronotus albifrons*) for CBD histochemistry (Figure 1.9A,D). Mormyrid tissue was dissected from the "schnauzenorgan," a structure extending from the fish's rostrum that is covered in electrosensory organs (Figure 1.9A). CBD-546 histochemistry revealed bright localization of signal to structures that appear to be mormyromasts, a type of tuberous organ (Figure 1.9B) (Hollman et al 2008). The signal was specifically observed in the cells that line the organs and also widespread within the epithelial cells of the skin. Autofluorescence could be examined by imaging the section in the green channel (Figure 1.9C), and a few large cells within the mormyromasts were clearly visible. In my personal communications with Harold Zakon (University of Texas, Austin) he suggested that these autofluorescent structures may be the electrosensory cells, although further experimentation is necessary to know for sure. The mormyromasts, although covered at the very top by an epidermal "plug" of cells, consist of a chamber containing a few electrosensory cells and are filled with a gel-like substance (Baker et al 2013, Jorgensen 2005). This gel was not detectable with CBD-546 (Figure 1.9B) either because it is not chitinous, or perhaps because the gel was lost from the slide during fixation, tissue processing, staining, etc. In my experience, gel from certain cartilaginous fish species readily sloughed off during tissue processing and/or deparaffinization, so that could have easily been the case for the mormyrid as well.

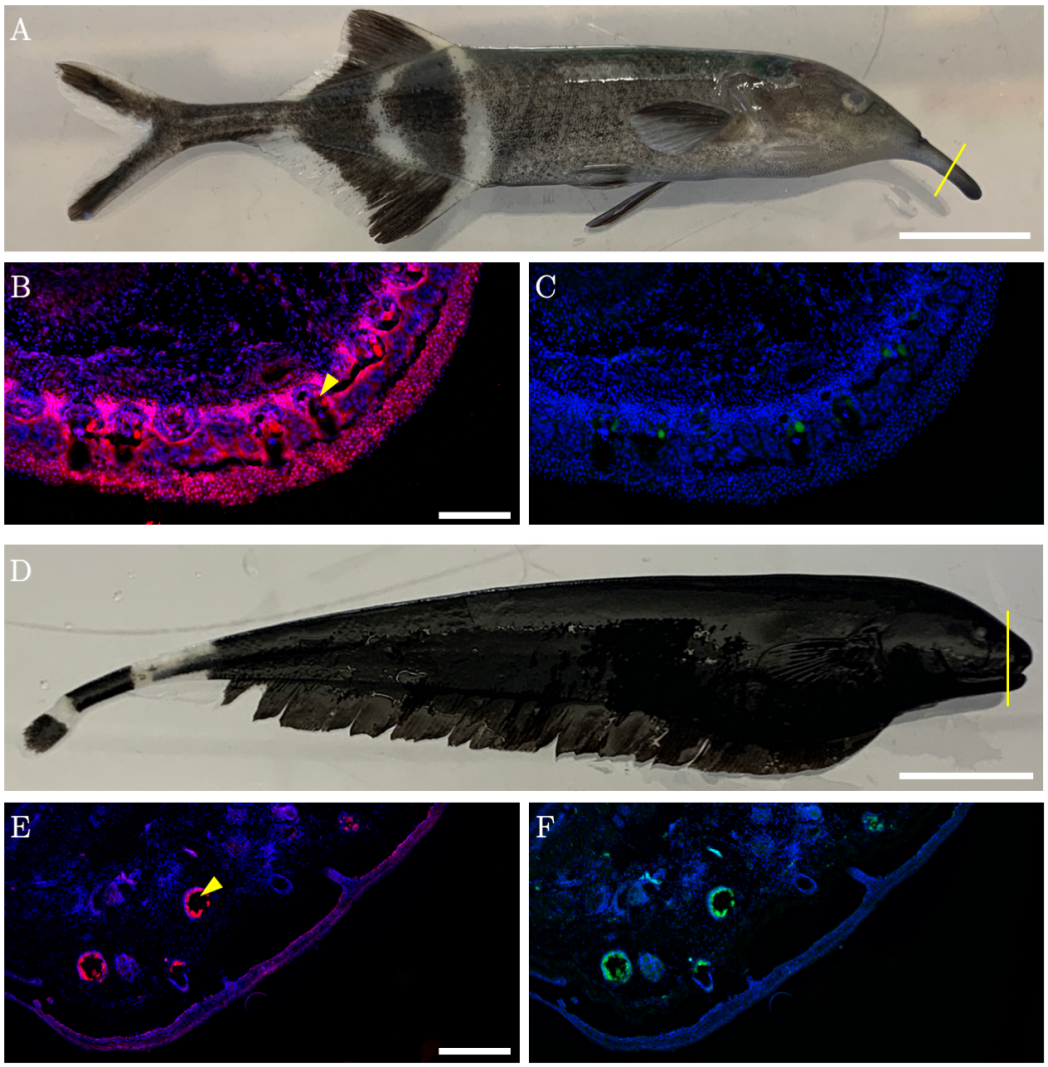


**Figure 1.9** CBD labeling patterns in two teleost fish species. **A)** Image of fixed mormyrid fish, *Gnathonemus petersii*. Yellow line indicates location where tissue was cut and embedded in paraffin for cross sectional analysis. **B,C)** Fluorescence microscopic images of tissue section through what is called the "schnauzenorgan" of the mormyrid fish shown in (A). CBD-Biotin + Streptavidin-546 (red) and the nuclear label, DAPI (blue) were used to label the section. (B) shows CBD signal while (C) shows autofluorescence in the green channel. This section appears to contain numerous tuberous organs called, mormyromasts, one of which is indicated by yellow arrowhead (B), but seemingly no ampullary organs. CBD labeling revealed ample positive staining in the cells within the mormyromasts and in the surrounding skin. There was no obvious staining of gel inside the mormyromasts shown in these sections. This could be because gel was lost during tissue processing, histology, etc, or it could be that gel was present but CBD-negative. Imaging in the green channel revealed that a few cells within the mormyromasts (possibly the electrosensory cells according to Harold Zakon, personal communication) were autofluorescent. **D)** Image of fixed gymnotiform fish, *Apteronotus albifrons*. Yellow line indicates location where tissue was cut and embedded in paraffin for cross sectional analysis. **E,F)** Fluorescent labeling and imaging was performed as in (B,C). The CBD-labeled section shown in these images appears to not include any ampullary organs, but a few tuberous organs are visible subdermally as indicated by yellow arrowhead in (E). These tuberous electroreceptors appeared to contain many autofluorescent cells, as made apparent by imaging in the green channel (F), but no clear labeling within the luminal space where a small volume of gel should exist (Baker et al 2013). There is, however, some positive CBD signals in the fish's skin. Scale bars – A,D: 1 cm; B: 100 $\mu$m; E: 200 $\mu$m.

Colorimetric staining of these sections (with Alcian Blue, for example) might reveal whether or not the gel was present and simply unlabeled with CBD, but sadly I was unable to return to the lab to finish these experiments after our university shut down due to the spread of the novel coronavirus in March 2020.

As for the gymnotiform specimen (Figure 1.9D), I dissected and embedded the snout of an *Apteronotus albifrons* specimen in paraffin wax in an orientation that allowed for sections cut in the middle of the fish's face where both tuberous and ampullary organs are known to be distributed, although the tuberous organs are far more numerous (personal communication with Harold Zakon). The resulting CBD and DAPI-labeled sections revealed what appeared to be a few tuberous organs (Figure 1.9E) that, like the mormyrid, contained many autofluorescent receptor cells (Figure 1.9F). These tuberous organs are surrounded by epidermal cells and therefore have no duct or pore that is open to the environment. It is unclear if gel fills the round lumen that surrounds the electroreceptor cells (Baker et al 2013). No gel was visible (by autofluorescence nor by CBD labeling) in these organs but as with the mormyrid samples, further studies need to be conducted to know if gel was actually present on the slides after processing. Unlike the mormyrid samples, CBD labelling was not readily observed within the cells of the tuberous organs, although the autofluorescence of the electrosensory cells may have prevented the detection of real CBD signals. CBD labeling was, however, specific to cells in the epidermis of the fish, as is now expected from most fish species (Figure 1.9E). I did not rigorously study the CBD-positive cell types within the skin or the tuberous organs of either teleost fish species, so unfortunately these studies will remain descriptive, at best.

## 1.5 Discussion

In this Chapter, I presented multiple lines of evidence suggesting that chitin is synthesized within the AoL of cartilaginous fishes. The findings from CBD histochemistry experiments with diverse chondrichthyan species indicated that chitin is found in the AoL of many species, but I confirmed this claim using ISH and chitinase assays only with little skate (*L. erinacea*) and by physicochemical methods only with spotted ratfish (*H. colliei*). The results obtained by studying these two distantly related species in detail indicate that CBD experiments on their own may be used to infer chitin's presence or absence in the AoL of other chondrichthyan species. More clades need to be sampled to definitively determine if chitin is synthesized in the AoL of all cartilaginous fish orders. However, because I was lucky to sample from diverse clades (and from both subclasses, Holocephali and Elasmobranchii), the most parsimonious hypothesis would suggest that AoL chitin evolved in the ancestors to all cartilaginous fishes, perhaps in the placoderms (King et al 2018). This idea begs the question: do electroreceptive organisms outside the class Chondrichthyes also synthesize chitin in their electrosensory organs?

Chondrichthyan electrosensory organs share homology with those of coelacanths, lungfishes, some amphibians, and basal branching ray-finned fishes including sturgeons, bichirs, and paddlefishes. Although the electrosensory organs of these animals exhibit some morphological variation, they all contain gel of poorly characterized composition. It is still unknown whether or not these fishes synthesize chitin in their ampullary organs. Another group of animals, the neopterygian fishes, lost the ancestral electrosensory system but subsequently developed analogous electrosensory organs. Like the chondrichthyans, many of these organs contain a gel. I attempted to preliminarily examine the spatial distribution of CBD within two teleost species, and although there appeared to be considerable CBD

labeling in the skin of both species, I was not able to sufficiently examine whether or not CBD also labeled the gel inside electrosensory organs.

The CBD probes that I used with tissues both from chondrichthyans and other types of fishes are comprised of chitin binding domains from proteins that interact with chitin. These chitin binding domains are quite specific; however, studies have shown that, in some cases, these domains can bind other kinds of sugars (Ujita et al 2003). When I exposed tissue sections to two different chitinases, I observed the elimination of detectable CBD signals as compared to control sections that had not been treated with enzymes. These results suggest that CBD probes bind specifically to a polysaccharide polymer that is bound and digested by two species of chitinase enzyme. This was evidence that, in the context of AoL gel, CBD probes were binding to chitin and not another sugar.

To strengthen the results of my chitinase assays, I collaborated with two different "sugar labs" (The Complex Carbohydrate Research Center at University of Georgia and the GlycoAnalytics Core at UC San Diego) to analyze the material resulting from chitinase digestions and determine which disaccharide units compose the polysaccharides in question. Chitin is the only known polysaccharide composed entirely of repeating units of *N*-acetylglucosamine (GlcNAc) so the identification of chitobiose, which is composed of dimers of GlcNAc, would have been physical evidence that chitin is a component of AoL gel. Samples of either native gel or polysaccharides extracted from AoL gel were treated with chitinase (from *Streptomyces griseus*) and analyzed with HPAEC-PAD. Unfortunately, although many attempts were made to study the disaccharide content of digested gel samples, each time there was not sufficient detectable material to draw any conclusions.

Although the disaccharide analyses never panned out, by comparing the monosaccharide content of native gel and extracted gel, I learned that my gel extraction procedures yielded a material composed almost entirely of glucosamine. This is what would

be expected of chitin, so this experiment offered compelling chemical evidence of the polysaccharide in AoL gel. Further, the FTIR spectrum of extracted AoL gel shared many characteristic peaks with those from two forms of chitin, especially that of β-chitin extracted from cuttlebones, which further supported the claim that chitin is a gel component and it can be purified using chemical treatments.

In insects and fungi, chitin is synthesized *via* a complex biochemical pathway that involves a number of enzymes (Merzendorfer 2011). The final and limiting step involves CHS enzymes, which transfer GlcNAc molecules onto growing chitin polymers. It is unknown if fishes (or any vertebrates for that matter) utilize a chitin biosynthesis pathway similar to invertebrates and fungi, but because *CHS* expression has already been shown to correlate with chitin in zebrafish, it is fair to assume that its presence alone is indicative of endogenous chitin synthesis (Nakashima et al 2018, Tang et al 2015). Daniel Ocampo Daza and I constructed novel transcriptomic datasets from AoL tissues which provided spatial gene expression information and complemented *in situ* hybridization results. Challenges with suspected cross-reactivity between riboprobes specific to the three *LeCHS* genes of little skates made it difficult to determine their respective spatial expression patterns with ISH. Transcriptomic TPM counts demonstrated that *LeCHS* expression is highest in AoL pores as compared to AoL canals, alveoli, and pelvic fin skin tissue. AoL pore tissue would have inevitably consisted of cells from skin tissue that is not associated with AoL so the increased expression of *LeCHS* in pores as compared to skin is an indication that the expression is AoL specific. Of the three *LeCHS* genes, *LeCHS1* exhibited slightly higher (but still low) expression in the AoL pores as compared to *LeCHS2* and *LeCHS3*. I suspect that AoL gel is continuously synthesized as AoL pores are open to the environment and in contact with surrounding water. Therefore, I do expect that chitin is synthesized in AoL continuously throughout the lifetime of the fishes, but this is strictly speculative. I

performed numerous chitin extraction procedures and polysaccharide analyses over the course of these studies and learned that chitin is seemingly present in very low concentrations in AoL gel, which could explain why *CHS* expression is so low in the organs. I made some attempts to loosely quantify the concentration of chitin in AoL gel using methods described in (Van Dyken et al 2011) but was unsuccessful.

I would be remiss to not address the novelty of my claim that chitin is a component of a hydrogel despite its known water insolubility (Roy et al 2017). I am not aware of any naturally occurring chitin gels – instead chitin is commonly mineralized and associated with rigid structures like arthropod exoskeletons and fungal cell walls. However, a number of studies describe the generation and function of synthetic chitin "nanogels," which are made by dissolving chitin in chemicals such as inorganic solvents or $CaCl_2$ and methanol, or by exposing it to hydrothermal conditions (Nata et al 2012, Tamura et al 2006, Vishnu Priya et al 2016). Synthetic chitin and chitosan (the fully or partially deacetylated form of chitin) nanogels are commonly used as drug carriers and as scaffolds in tissue engineering (Rejinold et al 2012, Shen et al 2015). Worldwide shellfish consumption generates an abundance of chitinous waste, and the non-toxicity and biodegradability of the polysaccharide make it a valuable material for use in biotechnology. To overcome the insolubility and modify the reactivity of chitin, techniques have been developed whereby sulfate groups are attached to chitin molecules by chemical treatment with, among other things, sulfuric acid (Jayakumar et al 2007). Chitin sulfate has been reported as a component of the test from a tunicate species but is otherwise poorly described in the animal kingdom (Anno et al 1974). It is possible that chitin in the AoL of cartilaginous fishes is modified in a way that increases its solubility and reactivity. I observed signatures of sulfate groups in the FTIR spectra from AoL gel and some of my gel extractions, however it is unclear how much of the sulfate signatures can be attributed to the other polysaccharide gel component, keratan sulfate.

There are still many unanswered questions regarding the chemical properties of the chitin synthesized in AoL gel and the mechanism by which newly produced chitin becomes solubilized in a hydrogel material. The results of my experiments using Periodic acid – Schiff stain add emphasis to that point. Significant evidence suggests that chitin is synthesized in the Ampullae of Lorenzini, but PAS staining data might indicate that the chitin produced in AoL gel is of a different form than chitin commonly studied in invertebrates. It is interesting that AoL gel did not also react with PAS staining considering that the free amine groups in molecules like chitin are known to readily react with the stain (Krishnamurthy 1999). It could be that there are such trace amounts of chitin in the AoL that PAS reactivity was hard to observe. It is also possible that AoL chitin is modified by the attachment of a reactive group that prevents chitin's amino groups from being oxidized by periodic acid and exhibiting a color. These PAS experiments support the possibility that chitin may be sulfated, but further testing is necessary to know definitively.

My collaborators have shown that AoL hydrogel is extremely proton-conductive (Josberger et al 2016), and that this property may putatively contribute to the electrosensing mechanism by providing an electrical environment that is markedly more conductive than the surrounding seawater. The role of chitin in this overall scheme is unknown, but by forming a composite material, it may contribute to the gel's space-filling properties and serve as a scaffold for the interaction of proteins and sulfated glycosaminoglycans that are also components of the gel (Doyle 1967, Josberger et al 2016, Zhang et al 2018). I will discuss some continued pursuits to understand AoL gel proton conductivity and the gel's molecular structure in Chapter 3 of this dissertation.

While studying the synthesis and distribution of chitin in AoL gel, I also considered the possibility that chitin is critical for the development and maintenance of tubular AoL morphology. The developmental patterns of chondrichthyan ampullary organs specifically,

however, have not yet been documented. In Chapter 2, I describe my investigations into the detailed development of AoL in little skates and my attempts to disrupt chitin synthesis in order to explore the potential role of chitin in developing AoL.

## 1.6 Acknowledgments

I would like to acknowledge Joyce W Tang who spearheaded a number of early investigations into the distribution of chitin in the AoL of chondrichthyans. Hassan Khan and Mike Rego were also instrumental in some of the early CBD labeling experiments and provided much technical expertise. Daniel Ocampo Daza, a postdoc in the Amemiya lab, led the charge on determining *CHS* sequences from sequenced chondrichthyan species including the three full-length *LeCHS* sequences. Daniel is also responsible for determining the *LeCHS* sequence counts in the four AoL transcriptomes discussed in this chapter. Andrew Gillis and Clare Baker provided ISH protocols and endless advice about little skates during many months of troubleshooting the gene expression experiments. I also want to thank Biswa Choudhury at the UC San Diego GlycoAnalytics core for performing the HPAEC-PAD experiments. Finally, I am grateful to our many sources of animal tissue: Adam Summers, Tsutomu Miyake, Martin Cohn, James Albert, John Field, Thomas Quinn, Jason Cope, Scott Hamilton, Matthew Jew, Joe Sisneros, and the MRC staff at the Marine Biological Laboratory in Woods Hole, MA.

## 1.7 Chapter 1 References

Anno K, Otsuka K, Seno N. 1974. A chitin sulfate-like polysaccharide from the test of the tunicate Halocynthia roretzi. *Biochim Biophys Acta* 362: 215-9

Arbia W, Arbia L, Adour L, Amrane A. 2013. Chitin Extraction from Crustacean Shells Using Biological Methods - A Review. *Food Technol. Biotechnol.* 51: 12-25

Baker CV, Modrell MS, Gillis JA. 2013. The evolution and development of vertebrate lateral line electroreceptors. *J Exp Biol* 216: 2515-22

Bellono NW, Leitch DB, Julius D. 2017. Molecular basis of ancestral vertebrate electroreception. *Nature* 543: 391-96

Bolger AM, Lohse M, Usadel B. 2014. Trimmomatic: a flexible trimmer for Illumina sequence data. *Bioinformatics* 30: 2114-20

Bray NL, Pimentel H, Melsted P, Pachter L. 2016. Near-optimal probabilistic RNA-seq quantification. *Nat Biotechnol* 34: 525-7

Bray RN, Hixon MA. 1978. Night-Shocker - Predatory Behavior of Pacific Electric Ray (Torpedo-Californica). *Science* 200: 333-34

Dishaw LJ, Giacomelli S, Melillo D, Zucchetti I, Haire RN, et al. 2011. A role for variable region-containing chitin-binding proteins (VCBPs) in host gut-bacteria interactions. *Proc Natl Acad Sci U S A* 108: 16747-52

Dishaw LJ, Leigh B, Cannon JP, Liberti A, Mueller MG, et al. 2016. Gut immunity in a protochordate involves a secreted immunoglobulin-type mediator binding host chitin and bacteria. *Nat Commun* 7: 10617

Doyle J. 1967. The 'Lorenzan Sulphates' - A New Group of Vertebrate Mucopolysaccharides. *Biochemical Journal* 103: 325-30

Doyle J. 1968. The Lorenzan Sulphates: A Comparative Study. *Comparative Biochemistry and Physiology* 24: 479-85

Fusaro RM, Goltz RW. 1960. A comparative study of the periodic acid-Schiff and Alcian blue stains. *J Invest Dermatol* 35: 305-7

Grabherr MG, Haas BJ, Yassour M, Levin JZ, Thompson DA, et al. 2011. Full-length transcriptome assembly from RNA-Seq data without a reference genome. *Nat Biotechnol* 29: 644-52

Haas BJ, Papanicolaou A, Yassour M, Grabherr M, Blood PD, et al. 2013. De novo transcript sequence reconstruction from RNA-seq using the Trinity platform for reference generation and analysis. *Nat Protoc* 8: 1494-512

Hollman M, Engelmann J, von der Emde G. 2008. Distribution, density and morphology of electroreceptor organs in mormyrid weakly electric fish: Anatomical investigations of a receptor mosaic. *Journal of Zoology* 276: 149-58

Ikegami T, Okada T, Hashimoto M, Seino S, Watanabe T, Shirakawa M. 2000. Solution structure of the chitin-binding domain of Bacillus circulans WL-12 chitinase A1. *Journal of Biological Chemistry* 275: 13654-61

Jayakumar R, Nwe N, Tokura S, Tamura H. 2007. Sulfated chitin and chitosan as novel biomaterials. *Int J Biol Macromol* 40: 175-81

Jorgensen JM. 2005. Morphology of Electroreceptive sensory organs In *Springer Handbook of Auditory Research - Electrorecption*, ed. T Bullock, C Hopkins, A Popper, R Fay, pp. 47-67: Springer

Josberger EE, Hassanzadeh P, Deng Y, Sohn J, Rego MJ, et al. 2016. Proton Conductivity in ampullae of Lorenzini jelly. *Science Advances* 2: e1600112: 1-6

Kaya M, Mujtaba M, Ehrlich H, Salaberria AM, Baran T, et al. 2017a. On chemistry of gamma-chitin. *Carbohydr Polym* 176: 177-86

Kaya M, Mujtaba M, Ehrlich H, Salaberria AM, Baran T, et al. 2017b. On chemistry of gamma-chitin. *Carbohyd Polym* 176: 177-86

Kempster RM, McCarthy ID, Collin SP. 2012. Phylogenetic and ecological factors influencing the number and distribution of electroreceptors in elasmobranchs. *J Fish Biol* 80: 2055-88

King B, Hu YZ, Long JA. 2018. Electroreception in early vertebrates: survey, evidence and new information. *Palaeontology* 61: 325-58

Krishnamurthy KV. 1999. Procedures for the Cytochemical Localization of Different Cell Wall Substances In *Methods in Cell Wall Cytochemistry*, pp. 53-57: CRC Press

Lavoue S, Miya M, Arnegard ME, Sullivan JP, Hopkins CD, Nishida M. 2012. Comparable ages for the independent origins of electrogenesis in African and South American weakly electric fishes. *PLoS One* 7: e36287

Maduzia LL, Yu E, Zhang Y. 2011. Caenorhabditis elegans galectins LEC-6 and LEC-10 interact with similar glycoconjugates in the intestine. *J Biol Chem* 286: 4371-81

Merzendorfer H. 2011. The cellular basis of chitin synthesis in fungi and insects: common principles and differences. *Eur J Cell Biol* 90: 759-69

Murray RW. 1960. Electrical Sensitivity of the Ampullae of Lorenzini. *Nature*: 957

Murray RW, Potts WTW. 1961. The Composition of the Endolymph, Perilymph, and Other Body Fluids of Elasmobranchs. *Comparative Biochemistry and Physiology* 2: 65-75

Nakashima K, Kimura S, Ogawa Y, Watanabe S, Soma S, et al. 2018. Chitin-based barrier immunity and its loss predated mucus-colonization by indigenous gut microbiota. *Nat Commun* 9: 3402

Nata IF, Wang SS, Wu TM, Lee CK. 2012. beta-Chitin nanofibrils for self-sustaining hydrogels preparation via hydrothermal treatment. *Carbohydr Polym* 90: 1509-14

Newton KC, Gill AB, Kajiura SM. 2019. Electroreception in marine fishes: chondrichthyans. *J Fish Biol* 95: 135-54

Rejinold NS, Nair A, Sabitha M, Chennazhi KP, Tamura H, et al. 2012. Synthesis, characterization and in vitro cytocompatability studies of chitin nanogels for biomedical applications. *Carbohyd Polym* 87: 943-49

Roy JC, Salaun F, Giraud S, Ferri A, Chen G, Guan J. 2017. Solubility of Chitin: Solvents, Solution Behaviors and Their Related Mechanisms In *Solubility of Polysaccharides*, ed. Z Xu: Intech Open

Schroeder A, Mueller O, Stocker S, Salowsky R, Leiber M, et al. 2006. The RIN: an RNA integrity number for assigning integrity values to RNA measurements. *BMC Mol Biol* 7: 3

Selberg J, Jia M, Rolandi M. 2019. Proton conductivity of glycosaminoglycans. *PLoS One* 14: e0202713

Shen X, Shamshina J, Berton P, Gurau G, Rogers RD. 2015. Hydrogels based on cellulose and chitin: Fabrication, properties, and applications. *Green Chemistry* 18: 53-75

Szabo T. 1974. Anatomy of the specialized lateral line organs of electroreception In *Handbook of Sensory Physiology*, ed. A Fessard, pp. 13-58

Szabo T, Enger PS, Kalmijn AJ, Bullock TH. 1972. Microampullary Organs and a Submandibular Sense Organ in Fresh Water Ray, Potamotrygon. *Journal of Comparative Physiology* 79: 15-&

Tamura H, Nagahama H, Tokura S. 2006. Preparation of chitin hydrogel under mild conditions. *Cellulose* 13: 357-64

Tang WJ, Fernandez J, Sohn JJ, Amemiya CT. 2015. Chitin is endogenously produced in vertebrates. *Curr Biol* 25: 897-900

Ujita M, Sakai K, Hamazaki K, Yoneda M, Isomura S, Hara A. 2003. Carbohydrate binding specificity of the recombinant chitin-binding domain of human macrophage chitinase. *Biosci Biotechnol Biochem* 67: 2402-7

Van Dyken SJ, Garcia D, Porter P, Huang X, Quinlan PJ, et al. 2011. Fungal Chitin from Asthma-Associated Home Environments Induces Eosinophilic Lung Infiltration. *J Immunol* 187: 2261-67

Velez-Zuazo X, Agnarsson I. 2011. Shark tales: a molecular species-level phylogeny of sharks (Selachimorpha, Chondrichthyes). *Mol Phylogenet Evol* 58: 207-17

Vishnu Priya M, Sabitha M, Jayakumar R. 2016. Colloidal chitin nanogels: A plethora of applications under one shell. *Carbohydr Polym* 136: 609-17

Wingett SW, Andrews S. 2018. FastQ Screen: A tool for multi-genome mapping and quality control. *F1000Res* 7: 1338

Wyffels J, King BL, Vincent J, Chen C, Wu CH, Polson SW. 2014. SkateBase, an elasmobranch genome project and collection of molecular resources for chondrichthyan fishes. *F1000Res* 3: 191

Zakrzewski AC, Weigert A, Helm C, Adamski M, Adamska M, et al. 2014. Early Divergence, Broad Distribution, and High Diversity of Animal Chitin Synthases. *Genome Biol Evol* 6: 316-25

Zhang C, Zhang B, Lin LL, Zhao S. 2017. Evaluation and comparison of computational tools for RNA-seq isoform quantification. *BMC Genomics* 18: 583

Zhang X, Xia K, Lin L, Zhang F, Yu Y, et al. 2018. Structural and Functional Components of the Skate Sensory Organ Ampullae of Lorenzini. *ACS Chem Biol*

# **Chapter 2:** The Early Development of the Ampullae of Lorenzini and the Distribution of Chitin in Developing Little Skate (*Leucoraja erinacea*) Embryos

## 2.1 Abstract

The electrosensory organs, or Ampullae of Lorenzini (AoL), of cartilaginous fishes, develop from a population of lateral line placodal cells which form small invaginations in the skin surface during embryonic development. The continued development of AoL from these surface invaginations has not been documented. It is also unclear when components of the hydrogel that fills the AoL, including chitin, are synthesized and secreted. I used fluorescent labels to track the early development of the AoL in the little skate, *Leucoraja erinacea*, and identified when chitin is first synthesized in the species as indicated by signals from chitin-binding fluorescent probes. To learn if chitin signals correlated with chitin synthase activity in the early development of the AoL, I then studied the expression of the chitin synthase gene, *LeCHS1* using *in situ* hybridization. In so doing, I discovered a population of chitinous structures found widespread externally across the embryos throughout development. The structures exhibited positive CBD labeling and were consistently bound by *LeCHS1* riboprobes during ISH experiments. Finally, I attempted to perturb chitin synthesis in little skate embryos through the use of two different kinds of chitin synthase-inhibiting drugs, diflubenzuron and nikkomycin Z. I was unable to conclude whether or not chitin synthase inhibition had an impact on AoL development, but I did observe some potential drug treatment effects on chitin synthesis in the AoL and the mysterious blobs.

## 2.2 Introduction

Cartilaginous fishes of the class Chondrichthyes use specialized electrosensory organs known as Ampullae of Lorenzini (also called ampullary organs or "AoL") to detect weak electric fields emitted by prey and mates or earth's electromagnetic field (Newton et al 2019). These organs are numerous and distributed across the fish's body. AoL are tubular in nature, consisting of canals open on one end to the environment and terminating on the other end in a lobed structure (alveolus) that contains specialized electrosensory cells innervated by nerves that project onto the medulla (Figure I.2). Chondrichthyan AoL are filled with a viscous hydrogel made up mostly of water but also consisting of polysaccharides, proteins, and ions of similar identity and concentration to seawater (Doyle 1967, Murray & Potts 1961, Zhang et al 2018). The exact function of AoL gel is unknown and it is also unclear how the interior canal cells secrete the gel contents over the course of a given fish's lifetime. Tubular AoL canals vary in diameter and length depending on the size and age of the fish, species, and anatomic location (Kempster et al 2012). Like other batoids, skates (order Rajiformes) have AoL pores most concentrated near the mouth and rostrum but also distributed on their dorsal and ventral wing surfaces. In skates specifically, although the AoL pores are widespread, the alveoli all terminate at one of four pairs of ampullary clusters (called superficial ophthalmic, buccal, mandibular, and hyoid) found on the left and right sides of the fish (Raschi 1986).

Like other fishes, chondrichthyans possess lateral line organs called neuromasts used to detect mechanical stimuli in their environment. Although there are distinct differences between ampullary and lateral line organs, there are a number of anatomical and functional similarities between them, including their shared use of ribbon synapses, the presence and activity of hair cells, and afferent innervation from fibers of the anterior lateral line nerve (Baker 2019). Ampullary organs evolved in the ancestors to all vertebrates and were lost in

several clades including the neopterygian fishes (Figure 1.8). Some groups of teleost fish secondarily evolved electroreceptive organs that are analogous to the ancestral organs observed in chondrichthyans, so the ancestral ampullary organs can be referred to as "non-teleost electrosensory organs." Although ancestral electrosensory organs were lost in neopterygian fishes, mechanosensory neuromasts were maintained, indicating that ampullary and lateral line development are separable and independent (Modrell et al 2017). In amphibians and some bony fishes, mechanosensory neuromasts are derived from so-called "lateral line placodes," which are composed of ectodermal tissue compartmentalized into regions that will eventually develop into specific anatomic features (Piotrowski & Baker 2014, Wright 1951). To investigate the embryonic origins of ampullary and mechanosensory organs in chondrichthyans, Gillis et al injected dye into cells in the lateral line placodal cells of little skate (*Leucoraja erinacea*) embryos and tracked their fate over development (Gillis et al 2012). This experiment showed that, in little skates, cells from both ampullary organs and neuromasts originate from lateral line placodes and migrate to the eventual location where the organs are then formed (Gillis et al 2012). In another study, transcriptomic analyses using larval paddlefish (*Polyodon spathula*) tissues demonstrated marked transcriptional similarities between ampullary organs and mechanosensory neuromasts (Modrell et al 2017). These findings collectively led researchers to conclude that the electrosensory cells in ampullary organs share common ancestry with lateral line hair cells (Baker & Modrell 2018). Our understanding of the early development and evolution of non-teleost electrosensory organs has expanded greatly over the past decade, especially with the little skate as a model. However, the timing of AoL development, particularly in the context of individual groups of ampullary organs, cell division and movement, and the synthesis of AoL gel has remained largely unexplored. In fact, details on the development of little skates in general has still not been published and researchers currently rely on the ontogeny of the

winter skate (*Leucoraja ocellata*), a closely related species, to stage their little skate embryos (Maxwell et al 2008). Maxwell et al used notable features including the size of the dorsal fins and anal membrane and the shape of the pelvic fins, pectoral fins, mouth and rostrum to make their stage determinations. Some notable anatomical features of little skate embryos are shown in Figure 2.1.

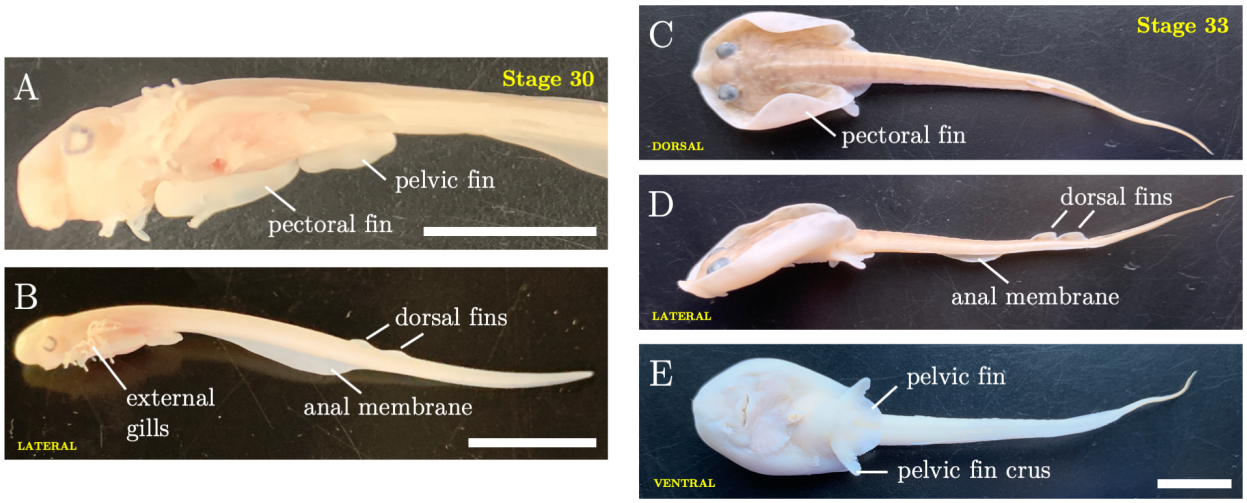


**Figure 2.1** Anatomy of fixed little skate embryos shown at two stages of development. **A,B)** The anterior region (A) and the whole body (B) of an early stage 30 embryo (lateral views). **C-E)** A stage 33 embryo shown in dorsal (C), lateral (D), and ventral (E) views. Note that the pectoral fins are folded up as a result of fixation. As compared to the stage 30 embryo, the anal membrane has reduced in relative size but is still observable. At this stage, the pelvic fins have developed extensions called "crus" that were recently shown to be involved in walking (Jung et al 2018). Scale bars – A: 5 mm; B: 1 cm; E: 1 cm (scale is same for C-E).

In Chapter 1, I presented several lines of evidence suggesting that chitin is a component of the viscous hydrogel found in the lumenal interior of chondrichthyan AoL. I investigated the distribution of chitin in the AoL using various tools including histochemical probes that consist of a chitin binding domain (CBD) attached to a detectable fluorescent marker. Upon discovering chitin in the AoL I became immediately interested in investigating the function of the polysaccharide in AoL gel, especially because chitin had never otherwise been identified as a gel component in a biological material. A number of

hypotheses were put forward that could potentially explain the synthesis of chitin within AoL gel, from antimicrobial interactions to a role in the structural development and maintenance of AoL canals. In the world of animal development, cells can undergo a number of mechanisms to synthesize tubular structures (Baer et al 2009). For example, in vertebrates, epithelial cells roll up forming an invagination that eventually seals up and becomes the neural tube. In the nematode, *Caenorhabiditis elegans*, individual cells of the excretory system develop an open lumen through the inside of their entire length (Chung & Andrew 2008). There has also been evidence of chitin playing a role in tube morphogenesis. Terrestrial arthropods use chitin to develop and maintain the tubular shape of their spiracles – organs used for gas exchange – and when chitin's synthetic pathway is disrupted, spiracles fail to maintain their shape and structure (Devine et al 2005).

To find out if chitin plays a role in AoL development, I had to start by realizing my limitations. Little skate embryos are fertilized internally and harbored in keratinous cases (called "mermaid's purses") that are laid by mature females. The skates are an Atlantic species, are easy to obtain from the Marine Biological Laboratory (MBL) in Massachusetts and can be reared in or out of their egg cases. However, development is already underway when egg cases are laid and the tiny transparent embryos are hard to locate as they reside on top of a comparatively large, opaque, colored yolk. We decided that these factors made injection-based methods using CRIPSR-Cas9 or morpholino knockdowns too challenging to employ. Therefore, I instead tested the impact of chitin synthase-inhibiting drugs on little skate embryos.

Chitin synthase (CHS) enzymes catalyze the final step in a complex biosynthetic pathway to generate chitin by adding monomers of *N*-acetylglucosamine to the growing polysaccharide chain. These enzymes are widespread in the animal kingdom and have only recently begun being characterized in vertebrates. CHS inhibitors disrupt chitin synthesis

in insects through various mechanisms, many still unexplored, and are widely used as pesticides. Diflubenzuron is one of the most common and easily accessible CHS-inhibiting drugs (Merzendorfer 2013). By perturbing cuticular chitin synthesis, the drug has been shown to kill a variety of arthropod species, but it is unknown if diflubenzuron has a similar impact on fish chitin synthases, especially given the possibility that sequence disparities between fish and insect *CHS* genes lead to small differences in protein structure (Zakrzewski et al 2014). It was of particular interest to examine the potential developmental impacts of diflubenzuron exposure because the drug is widely used to kill lice that plague farmed fish and is actively introduced into the environment at an industrial scale (Junquera et al 2019). However, because I was uncertain if diflubenzuron would have an effect on fish chitin synthases, I also experimented with nikkomycin Z, a drug shown to effectively impede chitin synthesis in tunicates, chordate relatives of cartilaginous fishes (Nakashima et al 2018).

To optimize the timing of drug administration, I first studied the distribution of CBD signals in little skate embryos over the course of eleven weeks and observed the onset of AoL development. The time series experiment incidentally illuminated some interesting features of AoL development in skates and also led to some observations about CBD binding in a mysterious set of structures observed widespread along the skate's tail and fins. I also examined the onset of chitin synthase (CHS) expression in little skate embryos to confirm that CBD is binding to chitin in early AoL development.

## 2.3 Methods

### *2.3.1 Biological specimens*

Specimens of live embryonic and adult little skates were obtained from the Marine Resources Center (Marine Biological Laboratory (MBL) – Woods Hole, MA). All animal work was

conducted under approved IACUC protocols: IACUC16-014 (Benaroya Research Institute) and AUP18-0001 (University of California, Merced). Embryonic skates were reared either in Atlantic seawater or in instant ocean "artificial seawater" (#SS15-10) in glass dishes with water exposed to bubbling air stones. Animals were typically kept at 16°C in a wine cooler used as an incubator. Euthanasia was carried out using tricaine methylsulfonate (Western Chemical Inc., #NC0872873) at 1000 mg/L. Embryos were fixed overnight with HA Fixative (70% ethanol, 21% water, 5% glacial acetic acid, and 4% formaldehyde) then stored in methanol at -20°C until used for histochemistry or ISH experiments.

### *2.3.2 Little skate developmental time series*

At the Marine Biological Laboratory in Woods Hole, MA, embryos were laid by several little skate females over the course of one week and collected in a communal holding area where they were left to grow at ~9°C. When the embryos had reached 8-weeks-old, 15 of them were collected and shipped overnight to our lab at UC Merced. Embryos were removed from their egg cases and moved to a large glass dish filled with artificial seawater and placed at ~16°C in a wine cooler with a bubbling air stone. The seal of the cooler was dislodged in one area to allow for air flow. As evaporation occurred, 100-200mL of fresh artificial seawater was added to the dish every few days. A majority of the water was removed and replaced with fresh water twice over the course of the eleven-week-long experiment. Each week, a single embryo was selected, euthanized, then fixed in HA fix overnight before storage in 100% methanol. Only the embryos that appeared to be growing at the same rate were selected each week and, in the end, 4 of the 15 embryos were excluded from the experiment due to inconsistent growth or seemingly poor health.

### *2.3.3 CBD histochemistry*

See sections 1.3.4, 1.3.5, and 1.3.6 for a detailed description of the chitin binding probe, CBD (from *Bacillus circulans*) synthesis and histochemistry. Almost all CBD data shown in this chapter resulted from use of CBD-Biotin + Streptavidin 546. The one exception is the ISH data depicted in Figure 2.6 where CBD-546 was employed.

### *2.3.4 Probe synthesis and in situ hybridization experiments*

See section 1.3.10 for detailed protocol describing probe synthesis (only *LeCHS1* riboprobe was used in this chapter) and for *in situ* hybridization protocol.

### *2.3.5 Imaging*

Stereoscope imaging was done on a Leica M205FA fluorescent stereoscope equipped with a DFC360FX monochrome CCD camera and a DFC425C color CCD camera. 2-photon microscopy was performed in Dr. Joel Spencer's lab (UC Merced) with a custom-built laser-scanning video-rate two-photon microscope. The microscope has two mode-locked tunable lasers (MaiTai and Insight, Spectra-Physics) which are directed through the objective (25X with NA=1.05, Olympus) to excite the sample. Fluorescence emission was detected by two separate photomultiplier tubes through individual bandpass filters for DAPI and CBD-Biotin + Streptavidin 546 (~420-280 nm and 560-610 nm, respectively).

### *2.3.6 Chitin synthase inhibition experiments*

Little skate embryos were placed in 40 mL of either artificial seawater (experiments 3 & 4 with nikkomycin Z) or seawater from the Atlantic Ocean (experiments 1 & 2 with diflubenzuron and experiments 1 & 2 with nikkomycin Z) contained either in 100 mL beakers or deep petri dishes. The volume (40 mL) was selected so as to limit how much

drug needed to be used. Drug was added to the water and swirled to mix before embryos were introduced.

When using diflubenzuron, concentrated solutions were made either in acetone or dimethyl sulfoxide (DMSO) so as to limit the exposure of the embryos to toxic diluents. In experiment 2, 10 mM diflubenzuron was added the seawater to achieve final concentrations of: 1, 30, and 100 $\mu$M. In experiment 3, 20 mM stock concentration of diflubenzuron was prepared and used to generate final concentrations of: 30, 50, 75, 100, 150, and 200 $\mu$M in seawater.

When using nikkomycin Z, we made up a stock concentration of 10 mM in MQ water, which was used to make up the working concentrations described in Table 2.3.

Under almost all circumstances, two embryos were placed in each container and subjected to the treatments. Only in one experiment (experiment 4 using nikkomycin Z) was an air stone placed in the small containers with the embryos. For experiment 2 with nikkomycin Z, a small (<1 cm) tunicate (*Ciona intestinalis*) was introduced to each of the two beakers for the first three days of the experiment. Tunicates were then fixed with HA fix, labeled with CBD and analyzed.

## 2.4 Results

### *2.4.1 Observations of little skate embryos reared nowhere near an ocean…*

Little skate (*Leucoraja erinacea*) embryos, which can be ordered from the Marine Biological Laboratory (MBL) in Massachusetts, are laid by a number of adult females, collected roughly once a week, and reared in batches according to the week they were released. Embryos can be removed from their egg cases and raised in aerated temperature-controlled

artificial seawater seemingly without any negative impacts on development. The yolks of little skate embryos vary in color from pale yellow to deep pink, which according to Andrew Gillis (Cambridge University) supposedly results from the mother's physiology not the health of the embryo (Figure 2.2). Upon opening up little skate egg cases, it also becomes apparent that development proceeds at markedly different rates amongst individual embryos that were all laid during the same week. This observation is depicted in Figure 2.2, which shows a newly arrived batch of 13-week-old embryos (not used for the time series experiment) that were clearly growing at different rates. It is unclear what factors control the observed differences in growth between the embryos, but this phenomenon certainly impacts the reliability of comparative time series studies. To overcome this obstacle, only embryos that appeared to be roughly at the same stage at the start of the time series were selected for study.


**Figure 2.2** Variation in little skate embryo size, stage, and yolk color. Embryos had just arrived from the Marine Biological Laboratory after developing for 13 weeks at ~9°C. Note the very apparent difference in both yolk color and developmental stage when comparing, for example, the two embryos marked with black asterisks. Scale bar – 1 cm.

### *2.4.2 Time series of AoL development in little skates & the onset of chitin synthesis*

A batch of 8-week-old embryos were shipped to my lab where they were removed from their egg cases and development was left to proceed in artificial seawater at 16°C. One embryo was fixed each week and examined to determine its developmental stage. Currently, little skates are staged based on a staging guide developed for the winter skate (*Leucoraja ocellata*) which delineates stage progressions based on the developmental changes of several anatomic features (Maxwell et al 2008). Using Maxwell et al's guide, I determined the stage of each little skate embryo collected every week of the time series experiment and listed my determinations in Table 2.1 (Maxwell et al 2008). Notably, despite significant growth and a number of external anatomic changes, stage 30 lasted a relatively long time (approximately 4 weeks) as compared to the other stages.

| **Weeks Since Embryo Release** | 8 | 9 | 10 | 11 | 12 | 13 | 14 | 15 | 16 | 17 | 18 |
|---|---|---|---|---|---|---|---|---|---|---|---|
| **Approximate Stage** | 24 | 25 | 27 | 28 | 29 | 30 | 30 | 30 | 30 | 31 | 31 |

**Table 2.1** Estimated stage of individual little skate embryo during each week of development from 8-18 weeks at 16°C.

To document the initial patterns of AoL development and the onset of chitin synthesis, skate embryos from the time series were labeled with two fluorescent histochemical reagents, the chitin label, CBD and nuclear label, DAPI. DAPI labeling, as revealed with fluorescence microscopy, was used to study the anatomy of the embryos from the time series and identify the appearance of AoL (Figure 2.3). While imaging the distribution of signals from both fluorescent probes, I learned that the first AoL appear on the ventral surface below the mouth in two "patches" mirrored on the left and right sides

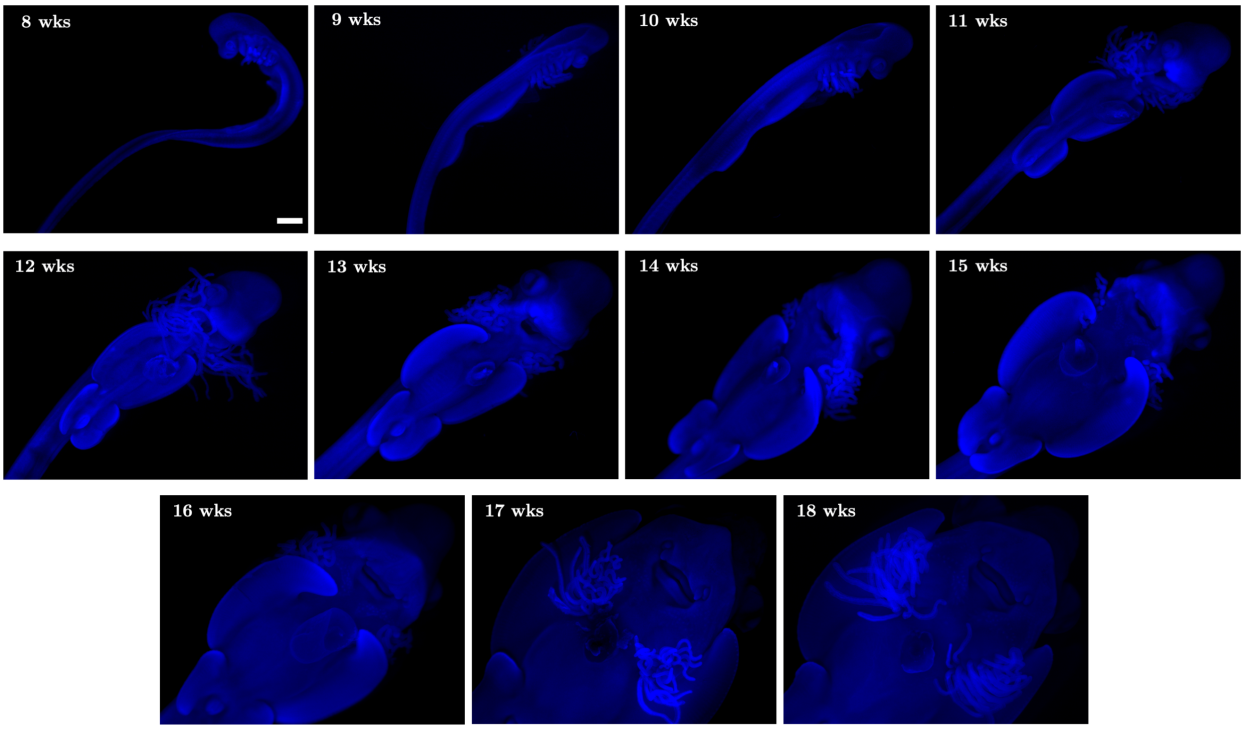


**Figure 2.3** Weekly development of little skate embryos at 16°C. Nuclear label (DAPI, blue) shows embryonic outlines and external structures. Embryos fixed at weeks 8-10 were imaged on their sides and a ventral view is shown of 11-18-week-old embryos. Scale bar – 1mm (scale is same for all images).

when the skate is at stage 30 and approximately 13 weeks old (Figure 2.4A). There was no apparent CBD labeling at this time in development. After another week, individual AoL could be resolved within the patches and became clearer as time went on (Figure 2.4B,C). By week 16, more AoL had developed and were widely distributed around the mouth but still no CBD signal was detectable in the organs (Figure 2.4D,E). By week 17, when the embryo had progressed to stage 31, CBD signal was first observed in the ventral AoL (Figure 2.4F). On the dorsal side of the embryos, two clusters of AoL just posterior to the spiracles on the left and right side became apparent in the 14-week-old embryo (stage 30) (Figure 2.4G). CBD signal was prevalent in the organs from the time they were first observed which suggests that the dorsal AoL are the first to synthesize chitin during little skate development (Figure 2.4H,I).

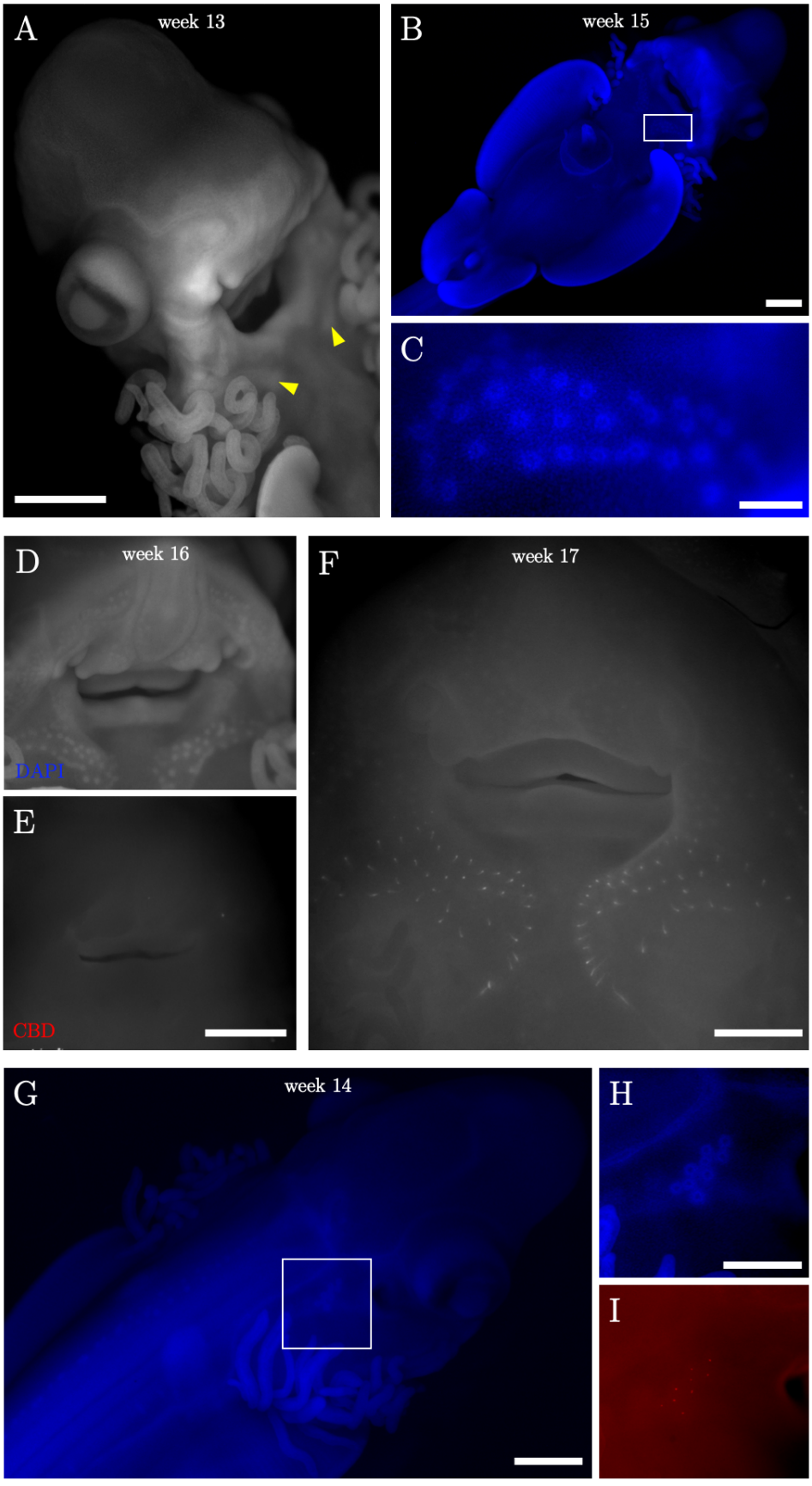
A
week 13
B
week 15
C
D
week 16
DAPI
E
CBD
F
week 17
G
week 14
H
I

**Figure 2.4** The appearance of AoL and onset of chitin synthesis in developing little skates. **A)** Fluorescence microscopy reveals the outline of a 13-week-old embryo labeled with the nuclear stain, DAPI (no pseudocolor). Two cell-dense patches are observed under the mouth where AoL are developing (yellow arrowheads). Individual AoL are not quite distinguishable at this stage. **B,C)** By 15 weeks, the two patches under the mouth are even more apparent (B) and individual donut-shaped AoL are clearly resolved with DAPI (C). White box shown in (B) indicates rough location of (C). No positive CBD signal was observed at this stage. **D,E)** Anterior ventral view of embryo at week 16 showing DAPI (D) and CBD (E) signals. At this point in development, although more AoL pores have appeared above and to the side of the mouth, CBD signal is still absent from the AoL. **F)** Anterior ventral view of 17-week-old embryo labeled with CBD-Biotin + Streptavidin-546 (no pseudocolor). CBD signals are observed for the first time in the AoL of the skate's ventral surface. **G)** DAPI (blue) signals revealed AoL on the dorsal surface of the 14-week-old skate on either side of the head behind the spiracles. White box indicates area shown in H and I. **H,I)** Dorsal AoL on 14-week-old embryo labeled with DAPI (H) and CBD-Biotin + Streptavidin 546 (I). Unlike the ventral AoL, CBD signal was prevalent in the dorsal organs at this time point. Scale bars – A,B,E-G: 1mm; C: 200 $\mu$m; H: 500 $\mu$m.

### *2.4.3 Discovery of cellular "caps" over AoL mid-development*

After the 18$^{th}$ week of development at 16°C, I did not track the growth or distribution of individual AoL populations specifically but did make some interesting observations about AoL development in some of the later embryonic stages. Gillis et al showed that AoL development begins with shallow invaginations in the skin surface, so it was presumed that the centers of the cell-dense donut-shaped organs, which were shown to contain CBD-positive signal (Figure 2.4F,I), are (or soon will be) the gel-filled canal lumens open to the environment *via* a pore in the skin (Gillis et al 2012). However, during the time series experiment at 16°C, between 16 and 18 weeks of little skate development there was an interesting change in the shape of the AoL below the mouth (Figure 2.5A,B). When imaging whole-mount skate embryos, I observed that the donut-shapes had, within two weeks, given rise to ovoid morphologies that seemed to lack observable pore openings (Figure 2.5B). Using 2-photon microscopy in collaboration with Dr. Joel Spencer at UC Merced, we imaged CBD- and DAPI-labeled tissues from the anterior ventral surface of little skates at stage 32 (Figure 2.5C) and stage 34 (Figure 2.5E) and observed a similar phenomenon. Optical cross sections were taken through the tissues, starting subdermally and moving towards the skin surface. Unexpectedly, the proximal "pore" ends of the stage 32 embryo's AoL were covered

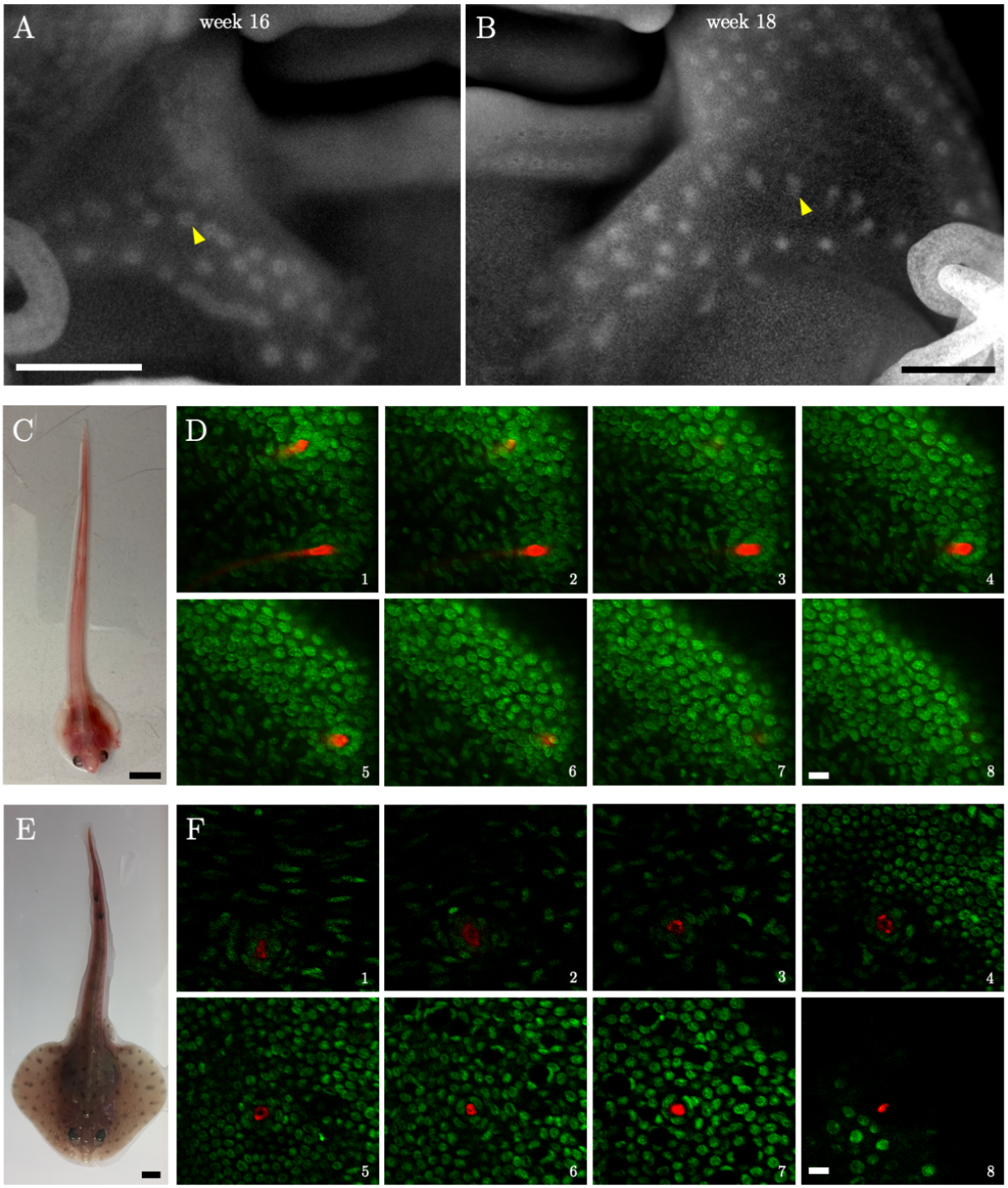


**Figure 2.5** Demonstration of cellular "caps" over AoL in late stage development of little skate embryos. **A)** Left side of ventral surface of 16-week-old little skate embryo (from time series experiment at 16°C) imaged under fluorescence with a stereomicroscope (mouth is in upper right). Yellow arrowhead points to one of many donut-shaped ampullary organs (as made visible by DAPI, no pseudocolor) developing in region below the skate's bottom lip. Note that this same pattern is mirrored on the right side of the embryo. **B)** An embryo from the same time series experiment fixed 18 weeks after being released from adult female skate, labeled with DAPI and imaged with fluorescent stereomicroscopy. Here, the right

side of the ventral surface is shown with the mouth occupying the upper left side of the image. With DAPI highlighting cellular density, AoL in the same area as those specified in (A) can be observed, however, the donut shape has seemingly been replaced by an ovoid morphology (yellow arrowhead points to one of such structures). There is no apparent pore opening in these AoL suggesting that the initial invagination that creates AoL becomes covered by a cellular cap later in development. **C)** Stage 32 little skate embryo used in (D) pre-fixation. **D)** AoL from the ventral surface of a stage 32 embryo labeled with DAPI (green) and CBD-Biotin + Streptavidin 546 (red) and imaged with 2-photon microscopy. At this stage, AoL have lengthened extensively as compared to those shown in (B). Here, the 8 images portray z-stack optical sections at 5 $\mu$m increments from depth up to the surface, effectively showing cross sections through two AoL near the skin surface. Between frame 2 and 3, one of the AoL, as made visible by internal CBD staining (red), is covered by cell nuclei (green). This same phenomenon is observed with a second AoL in frames 6-8. **E)** Stage 34 little skate embryo used in (F) pre-fixation. **F)** A single AoL from the ventral surface of a stage 34 embryo imaged with 2-photon microscopy. Same methodology was used here as in (D) with DAPI-labeled cell nuclei shown in green and the interior gel labeled with CBD (red) with 5 $\mu$m optical sections from depth up to the surface of the tissue. Images reveal subdermal cross sections through the ampullary organ. In the last image (8), CBD is still observed at the skin surface indicating that the cellular "cap" over the AoL pore is absent. Scale bars – A,B: 500 $\mu$m; C,E: 5mm; D,F: 20 $\mu$m.

by cellular caps and not open to the environment (Figure 2.5D). This was true for all AoL observed on the skate's ventral surface, but it was hard to tell which specific populations of ventral AoL were being imaged at any given time. Inspection of the AoL on the embryo's dorsal side was not carried out, so we don't know if cellular caps cover all of the organs at stage 32. When optical sections were taken through the ventral surface of a CBD and DAPI-labeled stage 34 embryo, there were no observable cellular caps and the AoL were open to the environment through the characteristic pores observed in all adult chondrichthyans (Figure 2.5F).

### *2.4.4 In situ hybridization with LeCHS1 riboprobes in stage 30 little skate embryo*

CBD serves as a useful AoL marker as it very distinctly illuminates the interior of individual AoL organs. Evidence laid out in Chapter 1 indicated that CBD is indeed binding to the chitinous component of AoL gel. However, the gene expression data described in Chapter 1 did not address whether or not chitin synthase activity corresponds with the initial appearance of detectable chitin in developing chondrichthyan embryos. To explore this, I used *in situ* hybridization (ISH) with riboprobes specific to the chitin synthase gene,

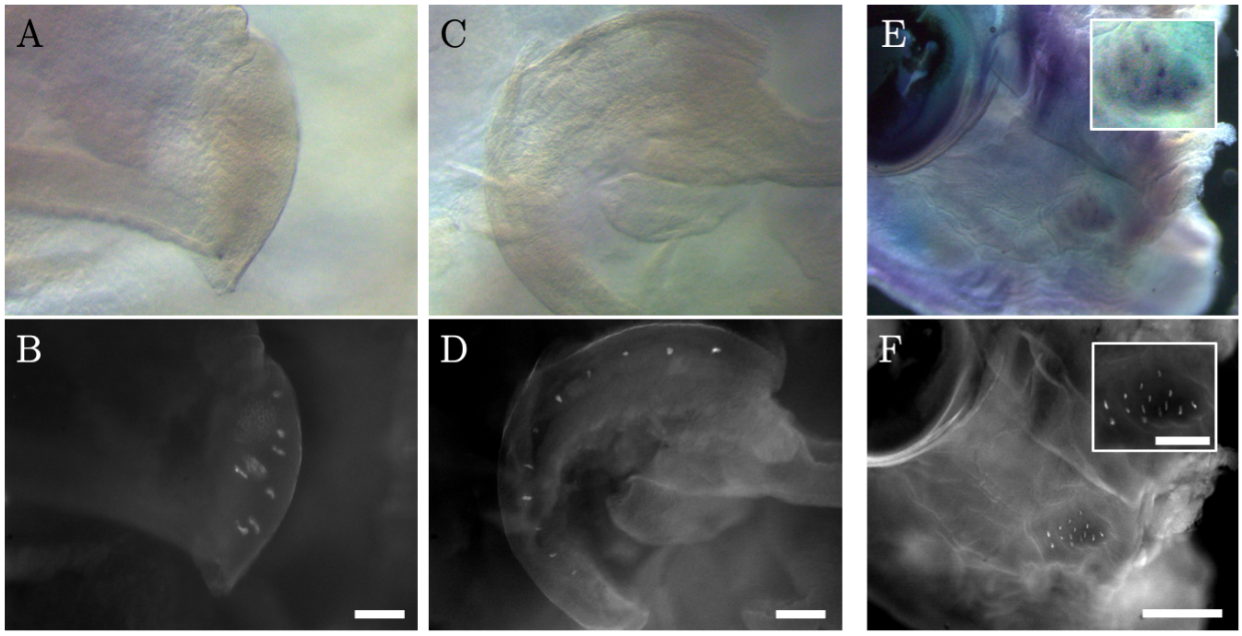


**Figure 2.6** *In situ* hybridization (ISH) using *LeCHS1* riboprobes with a stage 30 little skate embryo. All images obtained using stereomicroscopy (A,C,E: brightfield; B,D,F: fluorescence). **A)** ISH signals (antisense probe) on the edge of the upper lip of embryo. There is arguably some very faint purple signal along the edge of the lip. **B)** The same region as shown in (A) with noticeable CBD-546 signal (white). **C,D)** Image of little skate nostril hybridized shows no obvious signs of positive ISH signals from antisense probe (C) despite the clear presence of CBD-positive areas (D). **E)** Image shows a piece of tissue taken from the same little skate embryo shown in images A-D. This tissue was used for ISH with *LeCHS1* sense probes. Positive signals were observed in a cluster posterior to the eye, likely due to probe binding to antisense RNA molecules. Inset shows close-up detail of region with positive ISH signals. **F)** Same tissue as that shown in (E) but under fluorescence. CBD-546 signal (white) was observed in exact same pattern as ISH signals providing evidence that there is a correspondence between ISH signal from sense probe and CBD. Inset shows detail of CBD-positive region. Scale bars – B,D: 100 $\mu$m; F: 500 $\mu$m; F(inset): 200 $\mu$m.

*LeCHS1* and tissue from the anterior end of a stage 30 embryo. In Chapter 1, I showed that *LeCHS1* is the most highly expressed of the three *CHS* genes in the AoL of little skates so I suspected that the most reliable results would be obtained using riboprobes specific to *LeCHS1*. Only a small piece of tissue from the rostrum was used for this experiment so spatial information was reasonably limited, and ISH signals were extremely faint on the upper lip (Figure 2.6A). When the piece of tissue was labeled with CBD-546, signals were observed in the same region of the upper lip where faint ISH signals had been seen (Figure 2.6B) but also along the edge of the nostril (Figure 2.6D) where ISH signals were not at all

obvious (Figure 2.6C). As noted in Chapter 1, sense probes were initially used as negative controls for my ISH experiments. However, due to the likelihood of antisense transcription, when *LeCHS1* sense probes were employed, the ISH signals localized to the same areas that exhibited positive binding with antisense probes, including the AoL. In this experiment, there was marked expression of *LeCHS1* in AoL detected by sense probes on the dorsal side of the embryo in a cluster near the eye (Figure 2.6E). These newly developing AoL also exhibited positive CBD labeling (Figure 2.6F).

### *2.4.5 Discovery of chitinous structures widely dispersed on skin of little skate embryos*

Over the course of my studies, I stained embryonic skate specimens with CBD many times and I consistently observed signal localization to a mysterious and widely distributed set of structures on the animal's skin surface. I have referred to these structures simply as "blobs" and am still unsure of their detailed anatomy and function. CBD signals first became apparent in the blobs between 8 and 9 weeks in the time series experiment described earlier in the chapter and were observed widespread along the embryo's tail in two rows on the dorsal surface and one row along the animal's ventral side (Figure 2.7A,B). When the anal membrane and dorsal fins developed between 9 and 10 weeks, CBD-positive blobs lined their peripheral edges on both sides (Figure 2.7C,D). By the time the embryos reached 12 weeks (at 16°C), the edges of the pelvic and pectoral fins had also become lined with the structures. There were no obvious morphological differences between those located on the fins and those observed in other regions (i.e. the anal membrane or tail) (Figure 2.7E). When I performed ISH experiments using probes specific to *LeCHS1* and imaged with brightfield microscopy, I observed very dark ISH signals in the blobs (Figure 2.7F). Embryos with newly developing AoL (e.g. stage 30) exhibited faint *LeCHS1* ISH signals in their AoL

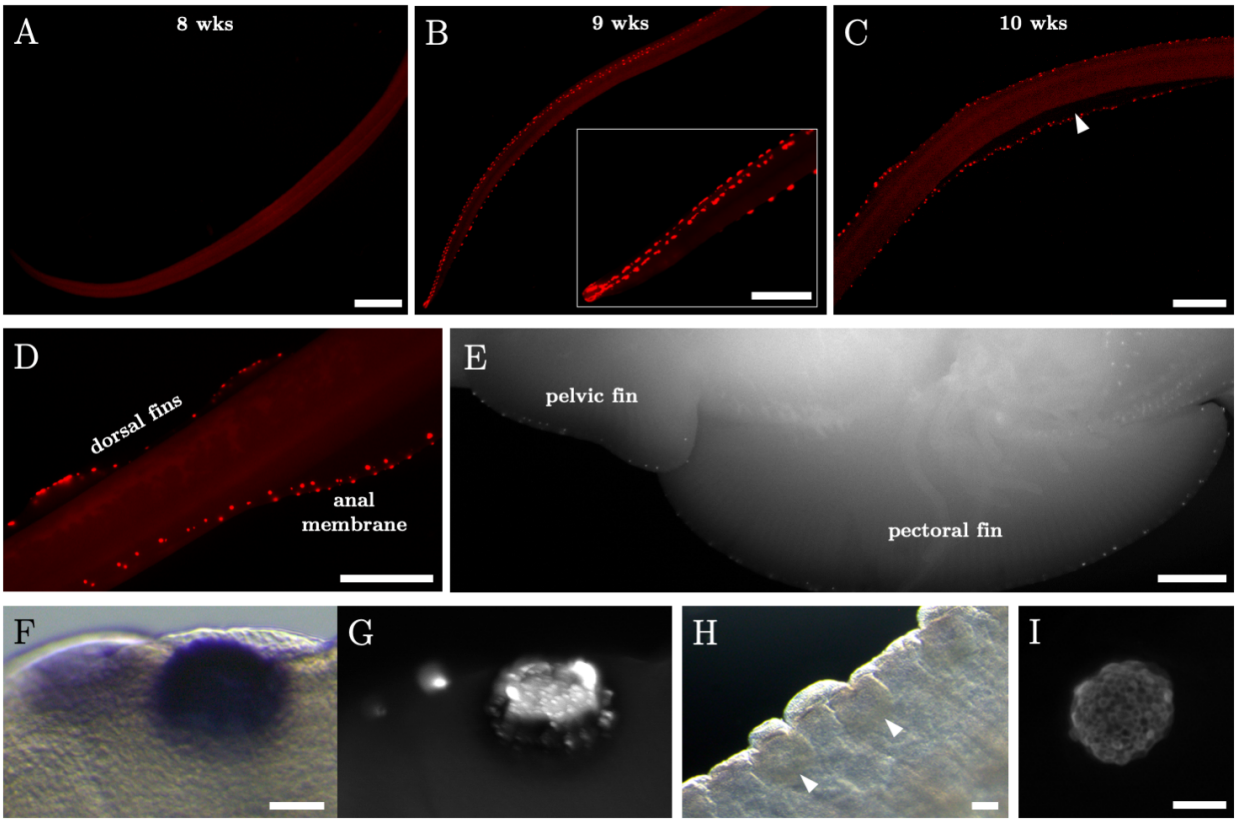


**Figure 2.7** CBD and CHS-positive labeling in mysterious globular structures ("blobs") of little skates. **A)** Tail of 8-week-old embryo from time series experiment shown labeled with CBD-Biotin + Streptavidin 546 and imaged under fluorescent light (pseudocolored red). The faint red hue of the tissue is due to autofluorescence – no obvious labeling with CBD is observed at this stage. **B)** One week later, 9 weeks after egg case was laid, an array of CBD-positive structures (red) can be observed along the embryo's tail on both the dorsal and ventral sides. The inset shows close-up image of embryo's tail tip. **C)** Image of the newly developed anal membrane (white arrowhead) and dorsal fins of 10-week-old embryo from the time series experiment labeled with CBD-Biotin +Streptavidin 546 (red) and imaged with fluorescence microscopy. The anal membrane and dorsal fins were absent from 9-week-old embryo, so they had seemingly developed over the course of the 9$^{\text{th}}$ week of development at 16°C. The peripheral edge of the anal membrane and dorsal fins were covered with CBD-positive structures similar in anatomy to those observed on the tail. **D)** Close-up image of CBD-positive structures (red) on anal membrane and dorsal fins of 13-week-old embryo from time series experiment. **E)** Ventral view of pelvic and pectoral fins from 17-week-old embryo showing the distribution of CBD-positive structures (bright white spots) lining the edges of both fins. Embryo outline is visible by autofluorescence. **F,G)** Embryonic tissue from a stage 31 embryo was treated by *in situ* hybridization (ISH) with antisense riboprobe specific to *LeCHS1* gene (F) and stained with CBD-Biotin + Streptavidin 546 (G). Tissue was visualized using both brightfield (F) and fluorescence (G) microscopy. ISH signal (purple) and CBD (white) localized to the peripheral blobs indicating that chitin is prevalent in these structures. **H)** ISH using tissue from another part of the embryo and hybridized to riboprobes specific to a planarian gene, *ChAT*. This probe serves as a negative control showing that the blobs (two of which indicated by white arrowheads) were not bound by non-specific probe. **I)** Close-up image of an individual CBD-positive blob (white) from the anal membrane of an early stage 30 embryo under fluorescence. Magnification reveals complex morphology seemingly composed of many round units. Scale bars – A,C-E: 1 mm; B (inset): 500 $\mu$m; F,I: 50 $\mu$m; H: 100 $\mu$m.

while the blobs labeled quite conspicuously, indicating that the structures were actively expressing chitin synthase. When the same tissue that was used with ISH was stained with CBD-Biotin + Streptavidin 546, fluorescent signals localized specifically in the blobs (Figure 2.7G). Further, when planarian ChAT probes were used as negative controls (as in Chapter 1), like the AoL, the structures exhibited no detectable purple signal (Figure 2.7H). The structures could be imaged at high magnification and CBD staining revealed complex, organized patterns (Figure 2.7I).

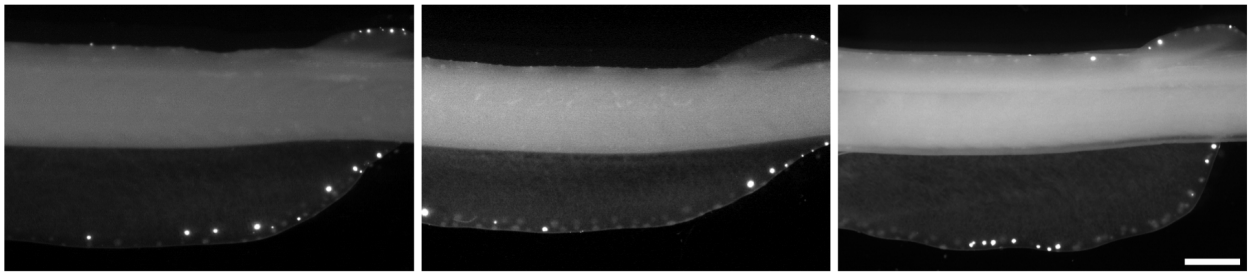

**Figure 2.8** Variability in distribution of mysterious blobs across the anal membrane and dorsal fins of three little skate embryos. Images show whole-mount tissue pieces cut from three different embryos, labeled with CBD-Biotin + Streptavidin 546 (white) and imaged with fluorescent stereomicroscopy. Embryos were at stage 31 when imaged, and they all appeared to be healthy before fixation. Scale bar – 1 mm.

Interestingly, as I compared more embryos over the course of my developmental studies, I learned that there was marked variability in the distribution of the mysterious blobs across the anal membrane, dorsal fins, and tail (Figure 2.8). They were seemingly always found peripherally on the anal membrane of the skates, but the little structures were inconsistently spaced. A neuronal staining assay did not indicate any semblance of innervation near the structures (data not shown), suggesting that the blobs do not perform a sensory function, although this requires a more exhaustive functional analysis.

### *2.4.6 Treatment with chitin synthase inhibitors*

As noted earlier, I initially began studying the onset of chitin synthesis in the AoL of little skates so that I could treat embryos with chitin synthase-inhibiting drugs, determine if chitin is eliminated from the organs, and observe any subsequent phenotypic changes associated with the perturbation. I tested the efficacy of the chitin synthase inhibitor, diflubenzuron, a reasonably cheap and accessible drug that is actively used to kill unwanted arthropods by disrupting chitin synthesis (Merzendorfer 2013). Because there are no published studies that describe the dose at which diflubenzuron blocks chitin synthase activity in fishes (or any chordate for that matter), I used various dosages of drug on little skate embryos and imaged the resulting CBD binding patterns. Only two of my experimental attempts at determining practical diflubenzuron dosage are worth mentioning and are described in Table 2.2. In experiment 1, the volume of acetone required to provide

| Exp. | Stage at start | Stage at end | # of Embryos per Treatment | Diluent | Length of exp. | Water changes | Dosages | Notes | Analysis | Results |
|---|---|---|---|---|---|---|---|---|---|---|
| **1** | 31 | 32 | 2 (for 30 $\mu$M) & 1 (for all other doses) | Acetone | 3 wks | Every 7 days | 1, 30, 100 $\mu$M drug + no-drug control + vehicle (acetone) control | Vehicle control embryos were very unhealthy and euthanized in middle of experiment. Some white precipitate observed. | Sectioned & whole-mount tissue labeled w/ CBD | No differences in CBD labeling patterns (sections). Potential faint reduction in CBD signal observed in drug dosed embryos (whole-mount) |
| **2** | 29 | 31 | 1 | DMSO | 3 wks | Every 3 days | 30, 50, 75, 100, 150, 200 $\mu$M drug + no-drug control + vehicle (DMSO) control | Significant amount of white precipitate in beakers after every water change. | Whole-mount tissue labeled w/ CBD | Diluent did not seem to impact development on its own. All embryos exhibited comparable CBD staining – drug had no apparent effect. |

**Table 2.2** Experimental set up and results from two separate diflubenzuron treatments.

a 100 $\mu$M dosage of diflubenzuron was lethal to the embryo on its own, making the resulting phenotype of the 100 $\mu$M diflubenzuron-dosed embryo unreliable. The embryo exposed to

30 $\mu$M, however, appeared to show a very faint reduction of CBD signal in some AoL as compared to the no-drug control embryo (Figure 2.9A,B). However, based on what I learned from the embryonic time series, the AoL of this embryo would have already begun synthesizing CHS and chitin before drug was administered, making the results harder to interpret. In experiment 2, DMSO seemed to have less of an impact on embryo health, although the appearance of white precipitate throughout the experiment was seemingly a result of drug insolubility and rendered the whole experiment unreliable.

| Exp. | Stage at start | Stage at end | # of Embryos per Treatment | Length of exp. | Water changes | Dosages | Notes | Analysis | Results |
|---|---|---|---|---|---|---|---|---|---|
| **1** | 31 | 32 | 2 (for 30 $\mu$M) & 1 (for all other doses) | 3 weeks | Every 7 days | 1, 10, 30 $\mu$M drug + no-drug control | Yolks of 30 $\mu$M-dosed embryos looked a little unhealthy at the end but embryonic growth seemed normal. | Sectioned & whole-mount tissue labeled w/ CBD | No differences in CBD labeling patterns (sections). Potential faint reduction in CBD signal observed in 30 $\mu$M-dosed embryo (whole-mount). |
| **2** | 30 | 30 | 2 | 5 days | Every 3 days | 50 $\mu$M drug + no-drug control | Small tunicate (*Ciona*) in each beaker with skates. Fish were very unhealthy after only 5 days. | Whole-mount tissue labeled w/ CBD | All animals (drug-dosed and controls) were so unhealthy that results were not reliable. Tunicate results were inconclusive. |
| **3** | 29 | 30 | 2 | 2 weeks | Every 3 days | 50 $\mu$M drug + no-drug control | Obvious differences in growth rates of the embryos over time, independent of drug treatment. Drug dosed embryos looked unhealthier than controls. | Whole-mount tissue labeled w/ CBD | One of the two drug-dosed embryos was so unhealthy that its anal membrane had degraded, and the other embryo had no visible "blobs." None of the embryos had developed AoL by the end of experiment. |
| **4** | 30 (early & late stage) | 30 & 31 | 2 | 8 days | Every 3 days | 50 $\mu$M drug + no-drug control | Drug-exposed embryos exhibited signs of poor health after 6 days in treatment, by the 8$^{th}$ day they were so unhealthy that euthanasia was necessary. | Whole-mount tissue labeled w/ CBD | No obvious differences in CBD labeling between wild type and drug-treated embryos, despite the apparent differences in health at the end. |

**Table 2.3** Experimental set up and results from four separate nikkomycin Z treatments.

I also employed the drug, nikkomycin Z, which has been shown to inhibit chitin synthesis in tunicates, chordate relatives of fishes such as skates (Nakashima et al 2018). I surmised that treatment with nikkomycin Z would have less of an impact on embryo heath because, unlike diflubenzuron, it is soluble in water so I wouldn't have to worry about the impacts

of a potentially toxic diluent. Unfortunately, nikkomycin Z is much more expensive than diflubenzuron so I was limited by the number of water changes that I could practically perform and the number of doses that could be tested. The results of four separate experiments performed with nikkomycin Z are reported in Table 2.3.

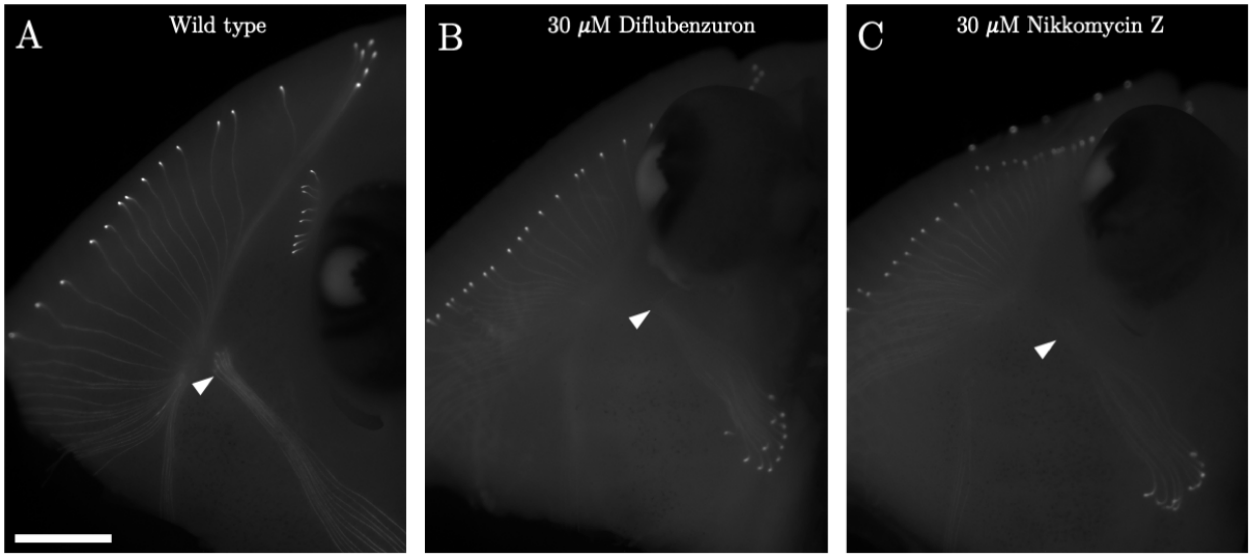


**Figure 2.9** CBD labeling patterns of untreated and CHS inhibitor-treated little skate embryos. These images show results from Experiment 1 using either diflubenzuron or nikkomycin Z (experimental details found in Tables 2.2 & 2.3). Stage 32 embryos (dorsal anterior shown here for all three) were fixed after drug experiments and treated with CBD-Biotin + Streptavidin 546. Images were taken using fluorescent stereoscope and the same exposure was used for all three images to allow for accurate comparisons. AoL canals exhibited CBD signal (white) with the brightest signals observed at the pore-end of the canals. Signals taper off as canals plunge into tissue. White arrowheads show some AoL that exhibit reduction in CBD binding from pore to alveolus. **A)** Control embryo from drug dosage experiment - animal was exposed only to seawater and no CHS inhibiting drug. Note that even though CBD signal tapers off from pore to alveolus, signal is still detectable all the way to the alveolar ends of the canals. **B)** Embryo exposed to 30 $\mu$M diflubenzuron for three weeks. As compared to (A), CBD signal fades from pore to alveolus. **C)** A similar pattern was observed in the embryo treated with 30 $\mu$M nikkomycin Z for three weeks. Qualitatively, the distribution and brightness of CBD signals were comparable between the two embryos exposed to different drugs. Scale bar – 1 mm.

In my first experiment with nikkomycin Z (which was actually performed in tandem with experiment 1 using diflubenzuron) the embryos were at stage 31 when they were introduced to drug, so their AoL had surely already begun developing and chitin synthase activity was presumably already underway. Regardless, treatment with 30 $\mu$M nikkomycin

Z, like diflubenzuron, led to a reduction in detectable CBD signals in the distal canal regions of the AoL as compared to a control (Figure 2.9A,C).

The results of experiments 2 and 3 with nikkomycin Z revealed that outside factors were influencing embryonic health. Some of the variables that I suspected could be possibly impacting the health of the embryos were salinity changes associated with evaporation, pathogens from Atlantic Ocean seawater, anoxic conditions due to sealing of incubator, and temperature fluctuations caused by gaps created in the incubator door seals. Interestingly, the control embryos were healthier than the 50 $\mu$M drug-dosed embryos in experiment 3 and there were observable defects in areas like the anal membrane where CBD and *LeCHS1* riboprobe signals are present in blobs under normal conditions (data not shown). This could have indicated that chitin synthase inhibition had occurred, but the embryos had not yet developed AoL by the time they were euthanized.

Finally, in my 4$^{th}$ experiment with nikkomycin Z, I once again exposed two embryos to either regular seawater (controls) or 50 $\mu$M nikkomycin Z in seawater. One of the two embryos in each treatment was at late stage 30 and the other was early in stage 30. Because of this, I was already suspicious that at least one of the two embryos in both treatments would have already begun synthesizing chitin in their AoL before drug was introduced. All four embryos appeared healthy until the fifth day of the experiment. However, on the sixth day, both drug-treated embryos had developed strange splotchy coloration in their yolks and were far less active. By the 8$^{th}$ day of the experiment, the yolks of the drug-treated embryos were falling apart and the poor, pale little embryos were barely moving. The control embryos looked relatively normal despite some faint red pigmentation that had appeared on their yolks, but I ended the experiment due to the poor health of the drug-dosed embryos. CBD labeling revealed that both of the older embryos (which were approximately stage 31 at the end of the experiment), one treated with drug and the other not, exhibited normal

AoL distributions, very similar to the images of the 16 and 17-week-old embryos in Figures 2.3 and 2.4. The AoL of both embryos labeled clearly with CBD. At the end of the experiment, the younger embryos in each of the two treatments had just begun developing AoL, as made clear by DAPI. CBD signals were very faint in the dorsal AoL of the drug-treated embryo and absent from those of the control embryo. The results of this experiment indicated that chitin synthesis was not inhibited in the embryos (potentially because it had not been given enough time to work) even though the drug-exposed animals exhibited poor health as compared to the controls. In all four embryos, the anal membranes maintained a "normal" morphology throughout the experiment and CBD-positive blobs were widespread.

## 2.5 Discussion

Over the course of 11 weeks, I used histochemical reagents to track the growth of little skate embryos and determined that AoL first develop in stage 30. AoL on the ventral surface appeared to develop and expand for a few weeks before chitin is synthesized (as evidenced by CBD labeling) while those on the dorsal surface started synthesizing chitin from the time that they were first noticeable. It is important to note that although I documented the appearance and distribution of AoL at specific weeks of development, the rate of stage progression observed each week is entirely dependent on factors such as embryonic health and water temperature. Therefore, my observations about the timing of the onset of AoL development cannot necessarily be expected in all circumstances and reflect the specific conditions of the experiment.

Using *in situ* hybridization (ISH), I showed that the expression of *LeCHS1* also became detectable during stage 30 although the most evident colorimetric reaction was observed by the binding of *LeCHS1* sense probes to alleged transcripts resulting from antisense transcription. Further testing is necessary to confirm that antisense transcription

of *LeCHS1* is occurring in the cells of the AoL. It is puzzling that some regions of the little skate embryo were clearly labeled with CBD, and in patterns characteristic of AoL, but did not appear to hybridize with *LeCHS1* riboprobes (Figure 2.6A-D). A number of variables could have interfered with probe hybridization. Alternatively, perhaps *LeCHS1* expression was so low at stage 30 that the colorimetric reaction was not dark enough to be visible in these particular tissues. It would be informative to examine the expression of *LeCHS2* and *LeCHS3* in stage 30 little skate embryos as perhaps one or both of those genes are expressed at this stage and responsible for synthesizing the chitin that is clearly labeled by CBD.

While observing whole-mount stage 31 embryos labeled with the nuclear stain, DAPI, I noticed that populations of AoL located near the mouth appeared to have undergone a morphological change. Whereas the AoL looked to be donut-shaped in the 16-week-old, stage 30 embryo, with a central dark spot seemingly representative of the early developing canal lumen, some of the ventral AoL in the stage 31 embryo were now ovoid and seemingly enclosed entirely by DAPI-positive cells. Work by Gillis et al showed that AoL first develop as small, shallow invaginations in the skin surface (Gillis et al 2012). I suspect that the donut-shaped cell-dense early AoL observed in the stage 30 embryos are open to the environment *via* a central pore, however, I did not examine the embryos shown in Figures 2.3 and 2.4 in cross section so I cannot say definitively. I did observe the AoL on the ventral surface of a stage 32 little skate embryo with optical sectioning and confirmed that they were indeed closed off to the environment by a cellular "cap." These caps were absent from the ventral AoL of stage 34 embryos and the pores were open to the environment, as made visible by CBD staining. Detailed analyses documenting the initial development of AoL are necessary to determine if all AoL start out open to the environment and if they all close those openings soon after. As of now, the functional significance of AoL pore closure during early development is curious and hard to explain. It is not surprising,

however, that the AoL were shown to be open to the environment by stage 34 (pre-hatching) when the AoL are likely fully functional.

It is still unclear when exactly the electrosensory system of little skate embryos, or any batoids for that matter, become functional. However, some studies have shown that cartilaginous fishes are electroreceptive before they hatch. During late development (timing dependent on the species) small holes open up in the corners of the embryo's egg cases and allow seawater to enter. Embryos will wiggle their tails to help bring in water and aerate their egg cases. Amazingly, several species of embryonic chondrichthyans have been shown to cease aeration and stop moving for several seconds when predators approach (a behavior known as a "freeze response"), indicating that they are able to detect the danger (Kempster et al 2013, Peters & Evers 1985, Sisneros et al 1998). Studies have shown that freeze response behaviors can be induced in embryos by exposing them to electric fields, indicating that their electrosensory systems are functional and employed for predator detection. Sisneros et al determined that the afferent neurons of AoL from clearnose skate (*Raja eglanteria*) embryos respond most readily at a particular frequency range (1-2 Hz) and the animals exhibited reliable freeze response behaviors when exposed to the "peak frequency" range that they are most sensitive to (Sisneros et al 1998). Before experimentation, the embryos used by Sisneros et al were cultured until they were 8-11 weeks old (reared at 20°C), and from the images provided in the paper, they look to have been stage 33-34 based on the winter skate staging guide (Maxwell et al 2008, Sisneros et al 1998). Given that I observed AoL pores "uncapped" and open to the environment in a stage 34 little skate embryo, it seems reasonable to presume that AoL pore opening precedes, or at least corresponds with, the onset of electroreceptive abilities in little skates.

Over the course of several weeks, I observed remarkable differences in growth rate between embryos. In some cases, the embryos arrived from MBL already at disparate stages

in development. In other cases, certain embryos would seem to suddenly enter rapid growth spurts while others would stop growing entirely, despite otherwise appearing healthy and normal. A caveat that became evident over the course of my study on little skate development was the growth rate variability between individuals. It is certainly possible that using a wine cooler as an incubator led to harmful variations or limits in temperature and oxygen availability and perhaps a temperature-controlled room would have allowed for more consistent embryonic growth patterns. Although I determined the stage at which AoL first develop in little skate embryos (stage 30), there is marked growth and change that occurs over the course of the stage. Based on the descriptions by Maxwell et al, the skate I used for ISH was at stage 30 of development, however, it is likely that its AoL had just begun to develop, chitin synthesis was starting, and ISH signals were thereby faint or non-existent. It would therefore be useful to study the ISH patterns of embryos at several different "phases" of stage 30 to confirm that *LeCHS1* expression consistently coincides with CBD detection.

From the first time that I used CBD with both whole-mount and paraffin sections of skate tissue, I observed the presence of bright and consistent signal in a set of structures that I refer to as "blobs." The structures are observed in a linear pattern straight along the dorsal surface, along the ventral and dorsal sides of the tail, rimming the anal membrane and dorsal fins, and eventually the pectoral and pelvic fins later in development. CBD staining showed that these structures synthesize chitin early in development, weeks before AoL appear, and were first observed when the embryos had reached stage 25 (week 9 of the time series experiment at 16°C). In a 1992 study of chondrichthyan scales, Raschi & Tabit describe a set of organs called free neuromasts (or pit organs) that are similar in distribution and morphology to the mysterious blobs (Raschi & Tabit 1992). However, pit organs have been well documented in shark species where they were shown to exist in close association

with scales – a relationship that was not at all obvious in the context of skate blobs (Peach & Marshall 2000). The electron micrograph images that Peach & Marshall show in their studies of pit organs from rays are also very dissimilar from the rounded volcano-like morphology of skate blobs (Peach & Marshall 2000, Peach & Marshall 2009).

The "vesicles of Savi," first described in the mid-1800s on the ventral surfaces of Torpedo rays, are another category of mechanosensory structures that could account for the skate blobs (Garman 1892). However, a study of lateral line morphology stated that vesicles of Savi were absent from clearnose skates (*Raja eglanteria*), the only skate species analyzed in the paper (Maruska 2001). Despite our lab's interest in the mysterious structures, I did not perform any exhaustive functional analyses to determine whether or not the blobs are lateral line related, but their anatomic locations would argue against this idea. Skate tissue was exposed to silver stain in order to visualize the lateral line neurons that innervate the AoL, but the blobs did not seem to exhibit positive nerve staining (data not shown). This preliminary data also argues against a potential mechanosensory function of the blobs. However, to know definitively, it would be interesting to find out if blobs are positive for Parvalbumin3 (Pv3), a marker used to identify hair cells (Gillis et al 2012, Modrell et al 2011). My current suspicion is that the blobs are glandular in nature, potentially secreting chitin as a component of the skin's mucus. Previous work from our lab showed that chitin is produced in the skin of zebrafish, salmon, and salamanders and we suspect that chitin is found on the skin of most fish species (Tang et al 2015).

I made many attempts to perturb chitin synthesis in skate embryos through the use of CHS-inhibiting drugs. One chitin synthase inhibitor that I employed was diflubenzuron, one of several drugs commonly employed on cattle farms to kill flies and on fish farms to kill salmon lice (*Lepeophtheirus salmonis*), pests that plagues many fisheries across the world (Junquera et al 2019). Diflubenzuron, also called "Dimilin" was discovered in the

1970s and belongs to a category of compounds called benzoylphenyl ureas. Although we don't fully understand the complete mechanism by which chitin synthesis is inhibited by diflubenzuron in arthropods, there has been some evidence that in *Drosophila*, diflubenzuron impacts a protein transporter that may carry *N*-acetylglucosamine molecules to sites of chitin synthesis (Matsumura 2010). Still, given the phylogenetic distance between arthropods and chondrichthyans, it is unclear if I should have expected the drug to impact chitin synthesis in little skate embryos. Diflubenzuron is introduced to the food of farmed Atlantic salmon as a method to control the spread of salmon lice to both the farmed fish and wild species occupying the same habitat (Olsvik et al 2013). When diflubenzuron is added to fish food, a significant amount of the drug collects in the surrounding sediment as uneaten food or feces dropped from the fish enclosures where it can then be consumed or taken up by wild organisms (Selvik et al 2002). A study by Olsvik et al showed that the concentrations of diflubenzuron measured in the environment surrounding salmon farms had no impact on the life expectancy or health of Atlantic cod, when ingested (*Gadus morhua*) (Olsvik et al 2013). Despite this, the impacts of CHS-inhibiting drugs on wild and farmed fishes alike must be reassessed in light of our discovery that chitin is synthesized by vertebrates (Tang et al 2015).

The biggest hurdle that I encountered when using diflubenzuron was its low solubility in water at ~.08 mg/L (Extoxnet 1993). In both of my experiments with diflubenzuron, I attempted to make stock solutions that were as concentrated as possible to limit the potential harmful impacts of the diluent, all the while trying to keep the maximum dosages below a final concentration of .08 mg/L in seawater. I tried both acetone and DMSO as diluents and in both cases observed the generation of significant amounts of white precipitate in the seawater. To achieve a 100 $\mu$M dose of diflubenzuron, the amount of acetone that needed to be used had a negative effect on the health of the embryo.

Comparatively, DMSO did not appear to have an impact on embryonic health even at a concentration of 1%. I observed precipitate in all of the beakers (i.e. all of the concentrations) containing diflubenzuron dissolved in DMSO. However, precipitate did not seem to be a problem when I exposed a stage 31 embryo to a 30 $\mu$M dose of diflubenzuron dissolved in acetone. Interestingly, the embryo exposed to this treatment was the only one that exhibited a potential reduction in CBD labeling as compared to the control.

A recent study demonstrated that nikkomycin Z (at a concentration of 30 $\mu$M) will disrupt the production of the chitinous barrier membrane produced in the gut of *Ciona intestinalis*, a solitary tunicate species (Nakashima et al 2018). So far, nikkomycin Z is the only drug shown to inhibit CHS in a chordate, which made it an attractive candidate to use on little skates. Unlike diflubenzuron, nikkomycin Z is soluble in water, so I was able to eliminate the unfavorable variables of diluent controls that had existed with diflubenzuron treatments. However, nikkomycin Z is very expensive, so I was only able to test the efficacy of a few drug concentrations, had to limit the reaction volume and thereby the number of embryos exposed to each treatment at a given time, and the number of times that water could be changed over the course of the experiments. It was certainly a limitation that I only had up to two embryos per treatment, especially because, as noted earlier, there is such variation in the growth rates of embryos from the same "batch." There were a number of other challenges associated with the nikkomycin Z experiments. In the second experiment with the drug, the health of all four embryos (2 controls and two drug-exposed embryos) deteriorated after only a few days. I suspect that the deterioration may have been associated with the introduction of tunicates to the water but was never able to determine this for sure.

In my first and third experiments with nikkomycin Z, the embryos were either too old (experiment 1) or too young (experiment 3) to draw any definitive conclusions. I was

hesitantly encouraged by the results of experiment 1 with nikkomycin Z, because, like experiment 1 with diflubenzuron, I observed reduced binding of CBD to the distal regions of AoL as compared to wildtype (no drug exposure). Given that AoL growth and chitin synthesis appears to progress from the skin surface "down" into the tissue until alveoli eventually reach their final destination, it makes sense that the distal portions of the AoL were impacted by chitin synthase-inhibiting drugs and not the proximal pore-region where chitin had likely already been synthesized before drug was introduced. However, as with the diflubenzuron experiment, it is hard to know if nikkomycin Z had a repeatable effect because only one embryo underwent treatment. The embryos were estimated to be at stage 31 when the experiment began, so they had likely already been synthesizing chitin for some time and CHS-inhibiting drugs would have no influence on chitin that already existed within the AoL. I don't have a quantitative understanding of how often AoL hydrogel is turned over, but I expected that there would be some amount of chitin present in the embryos, regardless of the drug's efficacy.

Despite my many efforts, CHS enzyme activity was not reliably inhibited in developing AoL, so it is still unclear if chitin is critical for the structural development and/or maintenance of the tubular organs. When it comes to AoL development in little skates and chondrichthyans in general, there are still many stones left unturned as my study did not address the cellular processes involved in the generation of the AoL from stage 31 up until hatching. Among many other things, we still don't know how cells divide to form the various populations observed in mature AoL, how the outer collagenous tubes of the AoL are produced, or how the organs find a path through surrounding tissue to the sites where their alveoli eventually congregate as a cluster.

## 2.6 Acknowledgments

I want to thank Andrew Gillis for extensive advice about rearing little skate embryos and for practical help with my methods, particularly when designing the drug treatment experiments. Thank you to Clare Baker for her comments on the identity of the mysterious "blobs." Thanks to Joel Spencer for performing the 2-photon microscopy experiments and to Nastaran Abbasizadeh and Negar Tehrani for providing advice on image analysis.

## 2.7 Chapter 2 References

Baer MM, Chanut-Delalande H, Affolter M. 2009. Cellular and Molecular Mechanisms Underlying the Formation of Biological Tubes. *Curr Top Dev Biol.* 89: 137-62

Baker C. 2019. The Development and Evolution of Lateral Line Electroreceptors: Insights from Comparative Molecular Approaches In *Electroreception: Fundamental Insights from Comparative Approaches*, ed. BA Carlson, JA Sisneros, AN Popper, RR Fay. Switzerland: Springer Nature

Baker CVH, Modrell MS. 2018. Insights into Electroreceptor Development and Evolution from Molecular Comparisons with Hair Cells. *Integr Comp Biol* 58: 329-40

Chung S, Andrew DJ. 2008. The formation of epithelial tubes. *J Cell Sci* 121: 3501-4

Devine WP, Lubarsky B, Shaw K, Luschnig S, Messina L, Krasnow MA. 2005. Requirement for chitin biosynthesis in epithelial tube morphogenesis. *PNAS* 102: 17014-19

Doyle J. 1967. The 'Lorenzan Sulphates' - A New Group of Vertebrate Mucopolysaccharides. *Biochemical Journal* 103: 325-30

Extoxnet. 1993. Pesticide Information Profile: Diflubenzuron. http://pmep.cce.cornell.edu/profiles/extoxnet/dienochlor-glyphosate/diflubenzuron-ext.html

Garman S. 1892. The Vesicles of Savi. *Science* 19: 128

Gillis JA, Modrell MS, Northcutt RG, Catania KC, Luer CA, Baker CV. 2012. Electrosensory ampullary organs are derived from lateral line placodes in cartilaginous fishes. *Development* 139: 3142-6

Jung H, Baek M, D'Elia KP, Boisvert C, Currie PD, et al. 2018. The Ancient Origins of Neural Substrates for Land Walking. *Cell* 172: 667-82 e15

Junquera P, Hosking B, Gameiro M, Macdonald A. 2019. Benzoylphenyl ureas as veterinary antiparasitics. An overview and outlook with emphasis on efficacy, usage and resistance. *Parasite* 26

Kempster RM, Hart NS, Collin SP. 2013. Survival of the Stillest: Predator Avoidance in Shark Embryos. *PLOS One* 8: 1-6

Kempster RM, McCarthy ID, Collin SP. 2012. Phylogenetic and ecological factors influencing the number and distribution of electroreceptors in elasmobranchs. *J Fish Biol* 80: 2055-88

Maruska KP. 2001. Morphology of the mechanosensory lateral line system in elasmobranch fishes: ecological and behavioral considerations. *Environmental Biology of Fishes* 60: 47-75

Matsumura F. 2010. Studies on the action mechanism of benzoylurea insecticides to inhibit the process of chitin synthesis in insects: A review on the status of research activities in the past, the present and the future prospects. *Pesticide Biochemistry and Physiology* 97: 133-39

Maxwell EE, Frobisch NB, Heppleston AC. 2008. Variability and conservation in late chondrichthyan development: ontogeny of the winter skate (Leucoraja ocellata). *Anat Rec (Hoboken)* 291: 1079-87

Merzendorfer H. 2013. Chitin synthesis inhibitors: old molecules and new developments. *Insect Sci* 20: 121-38

Modrell MS, Bemis WE, Northcutt RG, Davis MC, Baker CV. 2011. Electrosensory ampullary organs are derived from lateral line placodes in bony fishes. *Nat Commun* 2: 496

Modrell MS, Lyne M, Carr AR, Zakon HH, Buckley D, et al. 2017. Insights into electrosensory organ development, physiology and evolution from a lateral line-enriched transcriptome. *Elife* 6

Murray RW, Potts WTW. 1961. The Composition of the Endolymph, Perilymph, and Other Body Fluids of Elasmobranchs. *Comparative Biochemistry and Physiology* 2: 65-75

Nakashima K, Kimura S, Ogawa Y, Watanabe S, Soma S, et al. 2018. Chitin-based barrier immunity and its loss predated mucus-colonization by indigenous gut microbiota. *Nat Commun* 9: 3402

Newton KC, Gill AB, Kajiura SM. 2019. Electroreception in marine fishes: chondrichthyans. *J Fish Biol* 95: 135-54

Olsvik PA, Samuelsen OB, Erdal A, Holmelid B, Lunestad BT. 2013. Toxicological assessment of the anti-salmon lice drug diflubenzuron on Atlantic cod Gadus morhua. *Dis Aquat Organ* 105: 27-43

Peach MB, Marshall NJ. 2000. The pit organs of elasmobranchs: a review. *Philos Trans R Soc Lond B Biol Sci* 355: 1131-4

Peach MB, Marshall NJ. 2009. The comparative morphology of pit organs in elasmobranchs. *J Morphol* 270: 688-701

Peters RC, Evers HP. 1985. Frequency Selectivity in the Ampullary System of an Elasmobranch Fish (Scyliorhinus canicula). *J Exp Biol* 118: 99-109

Piotrowski T, Baker CV. 2014. The development of lateral line placodes: taking a broader view. *Dev Biol* 389: 68-81

Raschi W. 1986. A Morphological Analysis of the Ampullae of Lorenzini in Selected Skates (Pisces, Rajoidei). *Journal of Morphology* 189: 225-47

Raschi W, Tabit C. 1992. Functional aspects of placoid scales: A review and update. *Marine and Freshwater Research* 43: 123-47

Selvik A, Hansen PK, Ervik A, Samuelsen OB. 2002. The stability and persistence of diflubenzuron in marine sediments studied under laboratory conditions and the dispersion to the sediment under a fish farm following medication. *Sci Total Environ* 285: 237-45

Sisneros JA, Tricas TC, Luer CA. 1998. Response properties and biological function of the skate electrosensory system during ontogeny. *J Comp Physiol A* 183: 87-99

Tang WJ, Fernandez J, Sohn JJ, Amemiya CT. 2015. Chitin is endogenously produced in vertebrates. *Curr Biol* 25: 897-900

Wright MR. 1951. The lateral line system of sense organs. *Q Rev Biol* 26: 264-80

Zakrzewski AC, Weigert A, Helm C, Adamski M, Adamska M, et al. 2014. Early Divergence, Broad Distribution, and High Diversity of Animal Chitin Synthases. *Genome Biology and Evolution* 6: 316-25

Zhang X, Xia K, Lin L, Zhang F, Yu Y, et al. 2018. Structural and Functional Components of the Skate Sensory Organ Ampullae of Lorenzini. *ACS Chem Biol*

# **Chapter 3:** Structural Discoveries About the Hydrogel Inside Ampullae of Lorenzini of Spotted Ratfish (*Hydrolagus colliei*)

## 3.1 Abstract

The Ampullae of Lorenzini (AoL) of cartilaginous fishes are sensory organs used to detect environmental electric fields. The proximal ends of the organs open as pores in the skin that lead into gel-filled tubular canals and terminate in a rounded structure filled with highly specialized electrosensory cells. The thick hydrogel that fills the organs is composed of proteins and polysaccharides – the identity of which have only just begun being characterized. I recently collected evidence using histochemistry, enzymatic digestions, *in situ* hybridization, and chemical assays suggesting that chitin is present in AoL gel. The gel is also known to contain the glycosaminoglycan, keratan sulfate, a molecule that is suspected to confer the gel's known proton conductive capabilities. Attempts have been made to sequence the gel's protein components, but cellular contamination make interpretation of proteomic datasets challenging. Further, it is still unclear how the gel's components are structurally arranged and how the structure influences overall function. Here I present the first microscopic descriptions and x-ray scattering data from AoL gel). The results suggest that AoL gel is colloidal in nature and composed of spherical globules ~10-100 nm in size. I investigated the structural influence of the gel's protein components specifically by digesting gel with proteolytic enzymes and analyzing the resulting material again using microscopy and x-ray scattering analyses. In so doing, I explored the effects of protein removal both on proton conductivity and crystallization. The findings described here lay the groundwork for more detailed studies into the specific interactions of molecules inside AoL gel at the nanoscale.

## 3.2 Introduction

Electroreception, the ability of some animals to detect electric fields, is widespread amongst vertebrates. Some of the most well-studied electroreceptive animals are rays, skates, sharks, and chimaeras – cartilaginous fishes of the class Chondrichthyes. These fishes use their electrosensory organs to detect low frequency electric fields (~1-8 Hz) from biological sources such as prey or mates and even to navigate using earth's geomagnetic field (Collin & Whitehead 2004, Kalmijn 1974, Tricas et al 1995). The electrosensory organs, called ampullae of Lorenzini (AoL), are observable externally as small pores (< 1 mm) open to the surrounding environment. In sharks and chimaeras (including the spotted ratfish (*Hydrolagus colliei*) shown in Figure 3.1A), pores are most concentrated on the snout and around the mouth whereas in skates and rays, they are more widespread across the ventral and dorsal surfaces of the animals. AoL pores lead into tubular collagenous canals of varying length and diameter depending on the species and anatomic location. The canals are lined on the inside by two layers of squamous epithelial cells that have been imaged and documented in several species using scanning electron microscopy (SEM) (Gauthier et al 2018, Waltman 1966, Wueringer et al 2008). At the distal end of each canal is a bulbous alveolus containing specialized electrosensory hair cells that synapse with neurons that project to principal cells in the electrosensory hindbrain (Bodznick & Northcutt 1980). Importantly, the whole organs are filled with a stiff hydrogel that can be squeezed out of the pores and studied (Figure 3.1B). The sensory capabilities of the AoL have been studied in detail over the past several decades, however the process by which signals move from the environment through the organs and how the gel is involved in the process remains a subject of debate (Newton et al 2019).

Research in the 1960s showed that AoL gel is approximately 95% water containing $Na^+$, $K^+$, $Cl^-$, and urea (Murray & Potts 1961). The same research showed that AoL gel is roughly 5% hypertonic to seawater. A few years later, Doyle determined that AoL gel is composed of "mucopolysaccharides," having measured the relative abundances of hexosamines, sulphates, and other chemical groups (Doyle 1967). Doyle compared the chemical composition of AoL gel extracted from various cartilaginous fish species and learned that there was remarkable variation in the ratio between galactosamine and glucosamine in the gel of different species (Doyle 1968). Since then, a few studies have attempted to uncover the complete molecular makeup of AoL gel with a focus on the polysaccharide and protein components (How & Jones 1969, How et al 1970, Zhang et al 2018). It has been proposed that keratan sulfate, a proton conductive glycosaminoglycan, is a component of AoL gel (Josberger et al 2016, Selberg et al 2019, Zhang et al 2018). The polysaccharide, keratan sulfate should not be confused with the similarly named protein, keratin! Although admittance data has shown that AoL gel is a poor electrical conductor, gel extracted from three cartilaginous fish species demonstrated extremely high proton conductivity (higher than that of any other reported biological material) and it has been suggested that keratan sulfate is responsible for conferring the substance's proton conductive properties (Brown et al 2005, Josberger et al 2016). Zhang et al carefully studied the keratan sulfate component of the gel, determining that it has a molecular weight of 20-30 KDa (Zhang et al 2018). They report that keratan sulfate is the only glycosaminoglycan (GAG) in AoL gel, and that the gel is thereby the purest keratan sulfate source yet discovered (Zhang et al 2018). The authors used a strong anion exchange membrane to isolate GAGs from AoL gel and they did not address the possibility that AoL gel may contain other polysaccharides that would not have bound to the membrane. Strong anion exchange membranes consist of immobilized positively charged ligands that strongly bind anions but

not neutral molecules, such as chitin. In Chapter 1, I presented evidence suggesting that chitin is another polysaccharide component of the gel. This finding is quite novel, so it is still not understood how chitin, keratan sulfate, and proteins interact to form a stiff gel.


**Figure 3.1** Introduction to spotted ratfish (*Hydrolagus colliei*) anatomy and AoL gel removal. **A)** Picture of a spotted ratfish held by Molly. White box indicates the location shown in (B). **B)** An image that shows gel being squeezed from the AoL pores of an expired ratfish specimen. Thumb (in purple glove) applies pressure to the canals between the eye (right) and mouth (left). Gel is pink in color due to blood and cellular contaminant resulting from freeze-thaw process.

There has been little advancement in our knowledge of which specific proteins make up the AoL gel of cartilaginous fishes. Zhang et al recently generated a proteome from the AoL gel of a big skate (*Raja binoculata*) and identified a number of potential proteins that may contribute to the gel's structure (Zhang et al 2018). However, there is an inevitable accumulation of cellular contamination during the gel extraction process, and this makes interpretation of proteomic datasets challenging. Although Zhang et al proposed a molecular model of the structure of AoL gel based on their proteomic findings, there has still been no specific structural evidence detailing how the molecular components of AoL gel are arranged (Zhang et al 2018).

While I was studying chitin in the AoL of cartilaginous fishes (as detailed in Chapters 1 & 2), it became clear that I would not fully understand the function nor the synthesis of chitin in the context of the electrosensory organs if I didn't know how it was structurally arranged in the material. However, given how little we know about the gel's molecular components and how they are arranged in general, I started by studying the structural patterns of native gel as a whole and then analyzed the changes associated with removing one macromolecular component – proteins.

Here, I provide the first structural description of gel extracted from spotted ratfish (*Hydrolagus colliei*) specimens (Figure 3.1A). In collaboration with researchers from the Physics and Materials Sciences departments at UC Merced, ratfish gel was imaged with fluorescence microscopy, scanning electron microscopy (SEM), and atomic force microscopy (AFM) to develop an understanding of its molecular structure. These studies revealed that native gel is seemingly composed of globular structures roughly 10-100 nm in diameter, however it was unclear what effects desiccation may have had on their observed size. Therefore, to reduce the potential artefacts of desiccation, gel was subjected to supercritical drying before SEM imaging revealed a typical porous aerogel-like structure composed once again, of globules (~10-100 nm). To examine the influence of proteins on gel structure specifically, I imaged samples of proteinase K-digested gel using the same methods. Microscopy revealed a number of artefacts likely associated with desiccation, so I also used small angle scattering (SAXS) and powder x-ray diffraction (XRD) to compare the scattering properties of particular components extracted from the gel. Protein removal also allowed for an examination of the crystallization properties of chitin extracted from ratfish gel. Ever interested in gel function, I also collaborated with Marco Rolandi's group at UC Santa Cruz where we compared the proton conductivity of ratfish gel and proteinase K-digested gel and learned that proteins do not have a direct role in the gel's conductivity –

in fact they appear to dampen it. Finally, in an effort to characterize the proteins in the AoL gel, I worked with researchers at the University of Washington's Genome Science department and generated proteomes using gel from little skate, *Leucoraja erinacea*, and spotted ratfish, *Hydrolagus colliei*. These proteomes were annotated using various transcriptomic and genomic datasets and revealed, as expected, a presumed abundance of cellular contamination but also a few interesting candidate gel component proteins.

## 3.3 Methods

### *3.3.1 Biological specimens*

One adult spotted ratfish (*Hydrolagus colliei*) specimen was captured by Thomas Quinn (University of Washington) on a research cruise in Puget Sound, and brought to the Benaroya Research Institute for processing. Animal was euthanized using tricaine methylsulfonate (Western Chemical Inc., #NC0872873) at 1000 mg/L under approved IACUC protocol: IACUC16-014 (Benaroya Research Institute). Tissue from this animal was fixed with HA fixative (70% ethanol, 21% water, 5% glacial acetic acid, and 4% formaldehyde) then used for paraffin sectioning and histochemistry experiments with CBD. Additional expired and frozen spotted ratfish were obtained from Jason Cope (NOAA), Scott Hamilton (Moss Landing Marine Labs, MLML) and Matthew Jew (MLML). These specimens were dethawed in a refrigerator overnight then AoL gel was removed by applying pressure to the AoL pores, placed in tubes, and stored at -80°C until use.

### *3.3.2 Paraffin sections*

Wax sections of formalin-fixed spotted ratfish tissues were prepared using standard processing, embedding and microtomy protocols.

### *3.3.3 Histochemistry with chitin binding probes (CBD)*

See sections 1.3.4, 1.3.5, and 1.3.6 for detailed description of chitin binding (CBD) probe (from *Bacillus circulans*) synthesis and histochemistry. CBD conjugated to Alexa-546 was used for the experiments shown in Figure 3.2. For the gel staining experiment shown in Figure 3.2B & C, ~50 $\mu$L of gel was added to a centrifuge tube. CBD-546 was added to the gel tube and let sit at 4°C overnight (in foil). The next day, gel was still organized into a stiff glob, so it was pulled out of tube with a pipet tip and placed on a depression slide. 1X PBS was gently washed over the glob then DAPI was added on top of it and incubated for 30 minutes. Washing was challenging due to the possibility that gel would wash away or become diluted in solution. Gel was moved to a slide and squeezed underneath a coverslip before imaging with fluorescent microscopy.

### *3.3.4 Gel digestion with proteinase K & Analysis by SDS PAGE*

The proteinase K digest used for ultracentrifugation and synchrotron (shown in Figures 3.8 & 3.9) was prepared as follows: equal volumes of ratfish gel and 1X PBS were vortexed vigorously. Proteinase K was added to a final concentration of 0.1 $\mu$g/$\mu$L and incubated at 50°C for one hour. It was then dialyzed with 3.5 KDa dialysis tubing in 2 L of water for 5 hours.

The proteinase K digests imaged with SEM & AFM (shown in Figure 3.6 & 3.7) were prepared either by digesting with equal parts water and gel or equal parts buffer (0.1 M Tris + 0.05 M EDTA + 0.1% SDS) and gel. Proteinase K was added to a final concentration of 40 $\mu$g/$\mu$L and incubated for one hour at 50°C. Some aliquots of the digests were added to dialysis tubing with MWCO of either 3.5 KDa (Fisher #21-152-10) or 12-14 KDa (Fisher #21-152-15), dialyzed overnight in 5 L of water at 4°C, then stored at -20°C until use. Digested samples that were used for supercritical drying were moved to fresh 3.5 KDa

dialysis tubing and submerged in 200 proof ethanol overnight before treatment with supercritical $CO_2$.

The proteinase K digest data shown in Figure 3.11D was prepared as follows: An equal volume of gel and proteinase K buffer (see above recipe) were combined and proteinase K was added to a final concentration of 40 $\mu$g/$\mu$L. The solution was incubated at 50°C for an hour, then the heat was turned up to 60°C for 30 min to denature enzymes. The resulting solution was dialyzed overnight in 5 L of water with 12-14 KDa dialysis tubing. Lastly, the sample was sonicated on the continuous setting on ice for 20 minutes.

The proteinase K digest used for XRD (Figure 3.12) was prepared the same way as the sample used in Figure 3.11D, except no sonication was used. To prepare for XRD analysis, 200 $\mu$L aliquots of digested sample were dropped in dozens of layers on the XRD sample holder and heat dried at 62°C over the course of several days.

For SDS PAGE, 30 $\mu$L of gel sample was combined with 10 $\mu$L of reducing buffer and incubated at 95°C for 5 minutes. 1X running buffer was prepared and 1% SDS added. Samples were loaded into precast gels (Sigma #PCG2001-10EA) along with marker (Lonza ProSieve Color Protein Marker #BMA50550). I ran gels at 50 V for 20 minutes, then at 100 V for 50 minutes. Gels were removed from cases and rinsed with DI water. Coomassie Brilliant Blue stain (Fisher #501035935) was poured over gel and incubated for ~24 hours (Figure 3.5C) or for 5 hours (Figure 3.5B). Destain was then added to gel and swirled for 2 hours (Figure 3.5C) or overnight (Figure 3.5B) before pictures were taken.

### *3.3.5 Ultracentrifugation of ratfish gel*

Several milliliters of ratfish gel were dialyzed overnight in 3.5 KDa dialysis tubing in 5 L of water at 4°C to remove salts. A thick-walled polycarbonate lidless centrifuge tube was filled

with dialyzed ratfish gel (~500 $\mu$l) then spun at approximately 300,000-400,000 x g for 16 hours at 4°C with a TLA-120.1 Beckman Coulter rotor in an Optima Max-XP ultracentrifuge. After centrifugation there was a layer of transparent supernatant (majority of material), a thick white pellet and a smaller dark red pellet observed in the tube (see Figure 3.8B). Each of the layers were put into separate capillary tubes for analysis.

A sample of Proteinase K-digested gel was put into a centrifuge tube and also spun at approximately 300,000-400,000g for 16 hours. There was an abundance of clear supernatant, a dark red pellet similar to that of the non-dialyzed gel was observed at the bottom of the tube and a faint yellow, cloudy material was loosely on top of it (Figure 3.8B). All three of these materials were also moved to individual capillary tubes for analysis (although it was challenging to recover all of the yellowish material from the bottom of the tube as it readily dispersed into the supernatant when perturbed).

### *3.3.6 Synchrotron x-ray experiments*

Ultracentrifugation methods are described in Section 3.3.5. Proteinase digestion is described in Section 3.3.4. Samples were placed in glass capillaries along with some water and spun very gently with a centrifuge to push sample to the bottom of the tube.

Small angle x-ray scattering (SAXS) experiments were carried out by Alauna Wheeler and Dr Linda Hirst (of UC Merced Physics Department) at Lawrence Berkeley National Laboratory's (LBNL) Advanced Light Source (ALS) on beamline 7.3.3. Synchrotron radiation provides a high intensity, collimated x-ray beam, ideal for studying poorly ordered, dilute isotropic aqueous materials such as biological gels.

Previously prepared gels were inserted into 1.5 mm quartz x-ray capillaries (Charles Supper Inc.) by gentle centrifugation and mounted in the beam path in a transmission

configuration. Capillaries were mounted in a motorized translation stage, allowing precise control of capillary position in a plane perpendicular to the beam direction. A water filled capillary was included to obtain scattering data for the water background of the gels. A capillary containing silver behenate was included for beam center calibration and determining the sample to detector distance which was 3529.37 mm.

To perform the scattering experiments, we used an approximately 300 $\mu$m (H) x 700 $\mu$m (W) beam at 10 keV and exposed the gels for 2.0 seconds per capillary at several different positions along the capillary, to obtain the most intense scattering pattern for analysis. The scattering patterns were recorded on a Pilatus 2M detector for later analysis. The pixel size of the detector was 172 $\mu m^2$.

Data analysis was performed using the Nika and Irena macros in Igor Pro by WaveMetrics. The scattering patterns showed rings of uniform intensity (no significant alignment was observed) and were radially integrated to obtain 1D intensity plots as a function of q, the scattering vector. To perform the integration, we selected wedges on the scattering pattern image at various azimuthal angles and angular widths to check the scattering data for anisotropy and to find the smoothest graph. The intensity plots shown were taken from the integration of a wedge at an azimuthal angle of 60 degrees with an angular width of 20 degrees. The Igor wave arithmetic tool was used to subtract the water background.

### *3.3.7 Supercritical drying*

Gel samples were placed in 3.5 KDa dialysis tubing, sealed on both ends using dialysis clamps, and left in 200 proof ethanol for several hours (in most cases, overnight). Dialysis tubing became very stiff and little liquid remained inside after ethanol incubation. Often, white precipitate was observed coating the inside of the tube. Dialysis clamps were replaced with twist-ties before being introduced to the supercritical drying system. Supercritical

drying was performed with a Denton Vacuum, Inc supercritical drying system. The chamber was flushed with liquid $CO_2$ until no ethanol smell was observed in the effluent followed by a 2-hour soak in pressurized liquid $CO_2$ to allow exchange of ethanol inside the dialysis tubing. Phase change to supercritical $CO_2$ was achieved by heating the chamber to ~50 Celsius (reaching pressure of ~1400 psi). Final drying was achieved by reducing sample chamber pressure allowing the supercritical $CO_2$ to transition to the gas phase. Samples were stored under vacuum until imaging.

### *3.3.8 Polysaccharide extraction from ratfish gel*

See Section 1.3.13 for polysaccharide extraction protocol. I made several adjustments to my extraction protocols over the course of our studies, but the most effective strategy to isolate chitin from the other gel materials (as evidenced by the FTIR and monosaccharide analyses shown in Chapter 1) involved the use of Proteinase K, NaOH, and HCl treatments.

### *3.3.9 Scanning Electron Microscopy (SEM)*

For SEM images shown in Figure 3.3 & 3.6, gel samples were dropped directly onto aluminum stub and ambiently dried. Aluminum stubs were often visibly scratched so deep divots were often very apparent during imaging. No gold coating was used. For supercritically dried samples, a piece of double-sided carbon tape was stuck onto aluminum stubs then pressed onto the inside of the dialysis tubing containing supercritically dried samples. Chitin extracted gel samples were prepared in several different ways. In some cases, gel extract was dropped on a petri dish, scraped up and affixed to an aluminum stub using double-sided carbon tape (SEM). Other times, gel extract was dropped and ambiently dried on a freshly cleaved piece of mica which was then attached to an aluminum stub with double-sided carbon tape. Scanning electron microscopy was performed with the Zeiss Gemini500 FEG-SEM at the Imaging and Microscopy Facility of University of California,

Merced. Ambiently dried particles were adhered to conductive carbon tape. Beam landing energy of 500 eV and secondary electron detection were used.

### *3.3.10 Atomic Force Microscopy (AFM)*

For atomic force microscopy (AFM), samples were dropped directly onto freshly cleaved sheets of mica and either dried ambiently or with heat at 62°C. Atomic Force Microscopy (AFM) was performed using a Veeco Innova instrument in tapping mode. Probes with a spring constant of 40 N/m (Tap300Al-G, Budget Sensors) were used to image air-dried samples drop-cast on freshly cleaved mica to obtain topographical, amplitude and phase images of crystals formed on the surface in air. Images were collected at a scan rate of 1 line per second at room temperature.

### *3.3.11 Fluorescence microscopy*

Image shown in Figure 3.2A was taken using a Leica DMR upright epifluorescent microscope equipped with a SPOT RT Slider cooled 1.4 megapixel color/monochrome CCD camera and an Insight 4 megapixel color CCD camera (Diagnostic Instruments). Images shown in Figure 3.2B,C were taken on a Leica DMP fluorescence microscope with a Qimaging Retiga Exi CCD camera.

### *3.3.12 Proton conductivity*

Samples of dialyzed gel and proteinase-K treated dialyzed gel were brought to UC Santa Cruz where analyses were performed by Manping Jia and Marco Rolandi.

### *3.3.13 XRD*

In collaboration with Matthew Robinson, a PANalytical X'Pert PRO Theta/Theta Powder X-ray Diffraction system equipped with a cobalt x-ray source was used at UC Merced to

perform powder x-ray diffraction analyses with ratfish AoL gel samples. Diffractometer beam focusing elements were selected to balance minimizing low angle scattering while maximizing diffracted signal from the weakly diffracting organic crystals. As such, the configuration was: 0.04 radian soller slits (on both tube and detector side), 2° divergence slit, 10 mm beam mask, 4° anti-scatter slit, 6.6 mm receiving slit, and active length of 2.122 degrees on the X'cellerator detector. A slower scan speed (0.425 degrees 2-theta/second) than is necessary for highly crystalline materials was used to allow for best resolution of weak peaks and maximization of signal:noise. Specimens were scanned over a 2-theta range of 5-90 degrees (native ratfish gel) or 5-40 degress (ratfish gel extract and proteinase K digest). The specimen was rotated at the instruments maximum speed of 2 revolutions per second to ensure complete sampling or crystallites within the specimen. An iron foil filter was inserted into the x-ray beam path to eliminate cobalt k-beta radiation. The native gel sample was prepared by drying three layers (approximately 1 mL each time) of dialyzed (3.5 KDa) ratfish gel at 37°C on sample holder. A dark brown flake was formed. Sample preparation for digested and extracted gel material is described in sections 3.3.4 and 3.3.8.

### *3.3.14 Proteomics*

Little skate (*Leucoraja erinacea*) and spotted ratfish (*Hydrolagus colliei*) gel was extracted from freshly expired fishes and sent to Richard Johnson and Mike MacCoss (University of Washington, Genome Sciences) for proteomic analyses. Detailed methods of proteome preparation and annotation are described in a recent manuscript (Johnson et al 2020). The ratfish proteome was annotated using the genome of elephant shark (*Callorhincus milii*) and the little skate genome was annotated by Postdoc Daniel Ocampo Daza using an unpublished little skate genome. The little skate proteomic data was then merged with

transcriptomic datasets from three types of AoL tissue (pore, canal, and alveoli + canals) as well as non-AoL skin tissues that Daniel and I prepared (described in Chapter 1).

## 3.4 Results

| Method | Sample Type | Rationale | Results |
|---|---|---|---|
| **Atomic Force Microscopy (AFM)** | Native ratfish gel | Method is used to gather information about the surface topography of a dried sample. By comparing native and proteinase-digested gel samples with this method, the structural elements composing AoL gel were imaged and I learned whether or not the observed structure was maintained after removal of proteins. | Aggregated spherical globules were observed (with a size of ~ 100 nm). |
| | Proteinase K-digested ratfish gel | | Spherical globules were still consistently observed. |
| **Scanning Electron Microscopy (SEM)** | Native ratfish gel | Images with a notable depth of field are generated using dried samples under vacuum. I used SEM to confirm and complement my structural findings with AFM. | Aggregated spherical globules were observed (with a size of ~ 100 nm). |
| | Proteinase K-digested ratfish gel | | Results varied – sometimes globules, other times fibers. |
| **Supercritical Drying + SEM** | Native ratfish gel | Method was employed to overcome the potential effects of desiccation on the gel samples (which may have influenced AFM/SEM data). Supercritical $CO_2$ replaces spaces inside the sample that are naturally occupied by water so when $CO_2$ is removed, the gel structure is maintained as a porous network. | A porous material containing spherical globules was revealed |
| | Proteinase K-digested ratfish gel | | A repeatable artefact was observed. Similar results have been published for supercritically dried chitosan. |
| **Small Angle X-Ray Scattering (SAXS)** | Native ratfish gel | Information about size and/or spacing of objects in a hydrated sample is acquired with this method. In collaboration with UC Merced physicists, we used this method to get information about the size of the structure of aqueous gel samples. Signals are only observed if there are abundant objects in the same lengthscale. I ultracentrifuged gel to concentrate the non-water components. | Two peaks were observed. One corresponds to objects ~10-100 nm in size (globules). The other could be due to cellular debris. |
| | Proteinase K-digested ratfish gel | | No peaks observed indicating that polymer network was disrupted. |
| **Proton Conductivity** | Native ratfish gel | Gel is known to exhibit high proton conductivity. In collaboration with electrical Engineers at UC Santa Cruz, we wanted to learn if gel exhibited the same level of proton conductivity after proteins had been enzymatically removed. | Conductivity of 2.4 mS/cm |
| | Proteinase K-digested ratfish gel | | Conductivity of 11.9 mS/cm |
| **Powder X-Ray Diffraction (XRD)** | Native ratfish gel | Method used to characterize dried crystalline materials. We were curious if chitinous AoL gel samples would exhibit same scattering patterns as commercial chitin extracted from shrimp shells. Used gel samples with varying degrees of chitin purity to study the crystallinity of the material. | All three samples displayed characteristic features of "amorphous" chitin. |
| | Proteinase K-digested ratfish gel | | |
| | Chitin extracted from ratfish gel | | |
| **Proteomics** | Gel from little skate (*Leucoraja erinacea*) | Little is known about which proteins contribute to gel composition and structure. Synthesized two proteomes to investigate the gel's protein components in more detail. | Compared proteome to little skate transcriptomes and identified a few candidate gel component proteins. |
| | Gel from spotted ratfish (*Hydrolagus colliei*) | | Homologous matching algorithm was employed. Still hard to tell which proteins are gel components and which result from cells. |

**Table 3.1** Description of techniques used in this chapter, the rationale behind their use, and brief summary of results.

### *3.4.1 CBD histochemistry with fixed and unfixed gel samples*

When AoL contained in spotted ratfish tissue sections were labeled with a chitin binding histochemical reagent called, CBD-546 and the nuclear marker, DAPI and imaged with fluorescent microscopy, the AoL gel was organized in consistent patterns (Figure 3.2A). The gel, which had been exposed to fixative when ratfish tissue was processed, was arranged in little packets that reflected the shape and size of the canal cells (Figure 3.2A). It is still

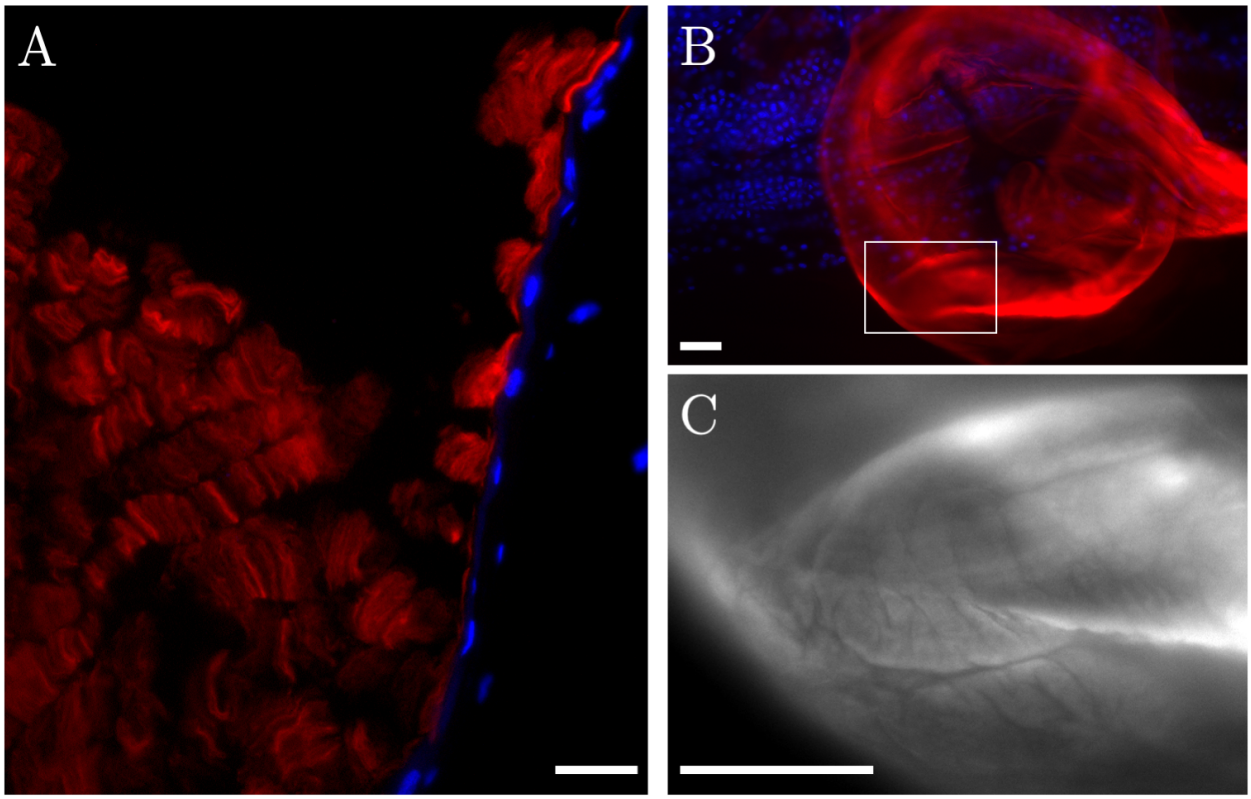


**Figure 3.2** Fluorescent microscopy images of fixed and unfixed spotted ratfish (*Hydrolagus colliei*) AoL gel. **A)** Paraffin tissue section from snout of adult ratfish specimen (TL: 41 cm) showing the edge of one AoL canal with canal lumen shown on the left side of the image. DAPI signals (blue) show the nuclei of cells lining the canal wall. CBD-546 signals (red) label the chitinous gel inside the canal. The image gives the impression that chitinous "packets" are being extruded from the canal cells. **B)** Unfixed ratfish gel smeared on glass slide and labeled with CBD-546 and DAPI. DAPI reveals a large number of cells that were apparently extruded into the gel from the canals or skin surface when gel was removed from fish. CBD-546 stained gel was concentrated in a few spots across the slide displaying fluidity and folding patterns. White box indicates rough location of image shown in (C). **C)** Close-up view of one portion of the gel shown in (B). Gel labeled with CBD-546 but no pseudocolor was added here. Fine folding patterns were readily observed at this magnification. Scale bars – A: 20 $\mu$m; B,C: 50 $\mu$m.

unclear how gel components are synthesized, but these observed patterns suggest that chitin is secreted by the squamous epithelial cells lining the inside of the AoL canals. Similar patterns have been observed in at least three other cartilaginous fishes (data not shown). However, it is unclear if fixation affected the arrangement of CBD-labeled materials. To overcome this, I labeled raw unfixed ratfish gel with CBD-546, spread it on a slide and imaged by fluorescence microscopy. The images revealed an abundance of cells and several gel dense areas where a finer structure was observed (Figure 3.2B,C). At this magnification, it appeared that the gel was composed of many fine, folded sheets of material. Admittedly, I was unsure what to take away from these images. I suspected that the patterns seen in Figure 3.2A (and also shown with fixed tissues from other species shown in Figure 1.1G-J) were representative of how chitinous material is excreted into the canal lumens. However, it was still unclear at this point how these chitinous packets organize into the folded patterns observed with unfixed gel. Therefore, I looked more closely at native gel to resolve finer structures.

### *3.4.2 AFM & SEM imaging using ambiently dried native AoL gel*

In collaboration with Dr. Linda Hirst (UC Merced, Physics) and Matt Robinson (UC Merced, Materials Science), I turned to AFM and SEM to image the gel at much higher magnifications. However, these experiments focused on the overall molecular gel structure, not on any one component. First, dilute ratfish gel was deposited on mica and imaged with AFM. Abundant spherical globules were observed at various locations across the mica surface (Figure 3.3A-C). These globular structures were often piled up on top of one another (lower right corner of Figure 3.3A) and in some cases, appeared to combine to form large aggregates. An average globule had a diameter of approximately 100 nm, while many of the large aggregates were several hundred nanometers in diameters. The observed shape of the

globules gave the impression that most of them were buried in some kind of mat. When smaller scan areas were used, rope-like objects could also be seen weaving in between the globules. In Figure 3.3, there are two types of images generated from the same run with AFM: one is an amplitude image (Figure 3.3B), which shows how the AFM tip deflected when it encountered an object on the mica surface, and the other is a height image (Figure 3.3C), which uses color to represent the height of features on the image, with lighter spots representing "hills" and darker spots representing "valleys." I didn't know what to expect at first, so I was surprised by the consistent distribution of the round globules observed with AFM. To understand whether or not they were simply AFM artefacts, I next examined gel samples with SEM to see if the same patterns were prevalent.

Gel that had been directly deposited on an aluminum stub was imaged with SEM and there were no consistent features observed at first. Therefore, knowing that AoL gel is made mostly of water, ultracentrifugation was used to concentrate the gel components. Ultracentrifugation yielded a dark red pellet (which I assumed contains blood), a dense whitish pellet, and a clear supernatant. When the white pellet was smeared across a piece of mica then attached to a stub, SEM revealed dense aggregated material in dispersed mounds (Figure 3.3D). At higher magnification, the surface was coated in globules of similar shape and size to those observed with AFM – approximately 100 nm in diameter (Figure 3.3E). Based on the shape of the observed globules that were observed with both microscopic methods, these initial observations led us to suspect that AoL gel is colloidal in nature and composed of spherical particles. However, it is critical to address the known impacts of drying effects, which have been shown to reduce the natural porosity of gel materials (Buchtova & Budtova 2016, Ganesan et al 2016). Both AFM and SEM revealed densely packed globules when desiccated gel was imaged, however the shape and certainly the scale of the objects observed had to be interpreted cautiously.

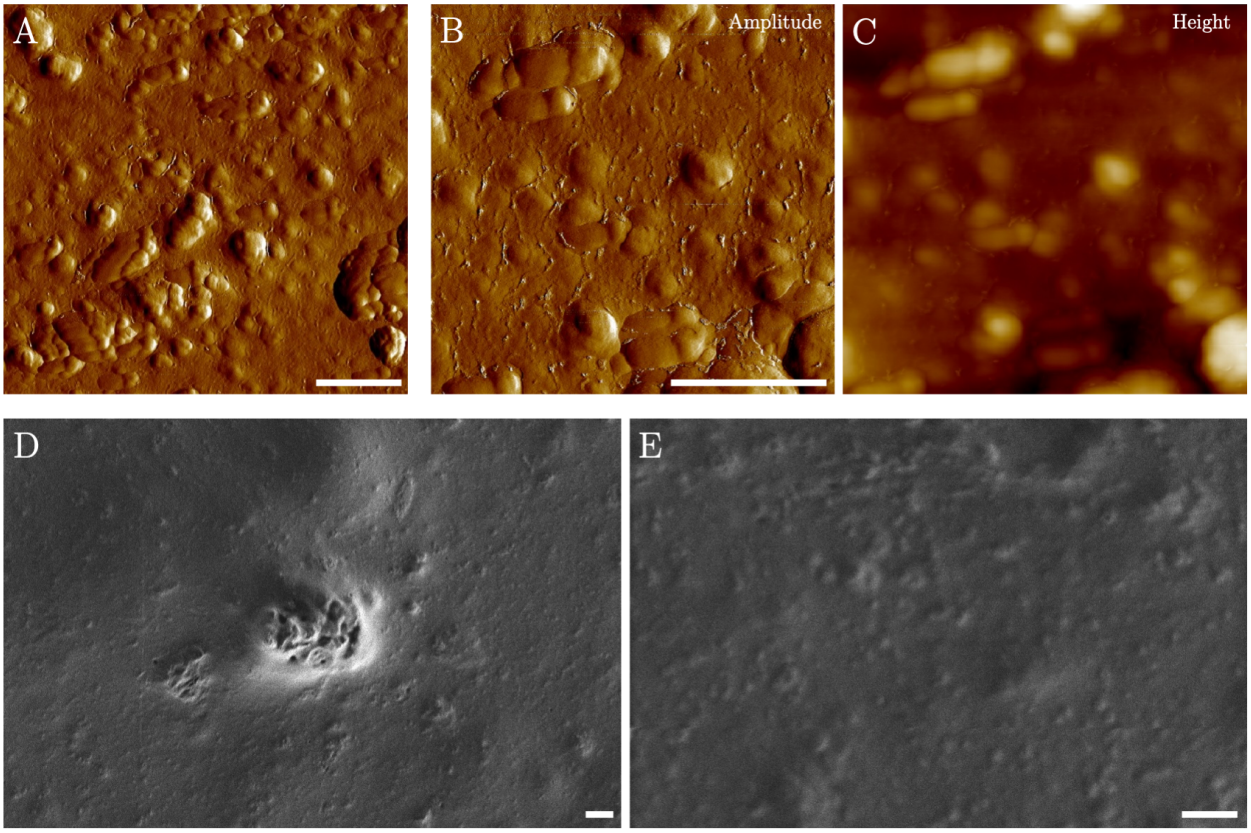


**Figure 3.3** Ratfish gel with AFM and SEM. **A-C)** Ratfish gel was diluted 1/20 in water, dropped on a freshly cleaved mica sheet, air dried and imaged with AFM. Globular structures were observed widespread across the surface (A) and close examination revealed rope-like objects winding in between the globules, made apparent both with amplitude (B) and height (C). **D,E)** A white pellet resulting from ultracentrifugation of ratfish gel was dragged across a freshly cleaved piece of mica then imaged with SEM. There were a number of relatively large lumpy features spread across the surface of the stub (center of D), but the majority of the surface appeared to be covered in a mat of material. At higher magnification, the surface of the mat appeared to be composed of globules comparable in size to those observed with AFM. Scale bars – A,B,E: 500 nm; D: 1 $\mu$m.

### *3.4.3 SEM imaging with supercritically dried native gel*

To overcome the inevitable effects of desiccation on gel structure, samples of ratfish gel were supercritically dried and imaged with SEM. The gel samples were first placed in dialysis tubing and exposed to ethanol for several hours before placement in a supercritical dryer where ethanol was exchanged with supercritical $CO_2$. After approximately two hours,

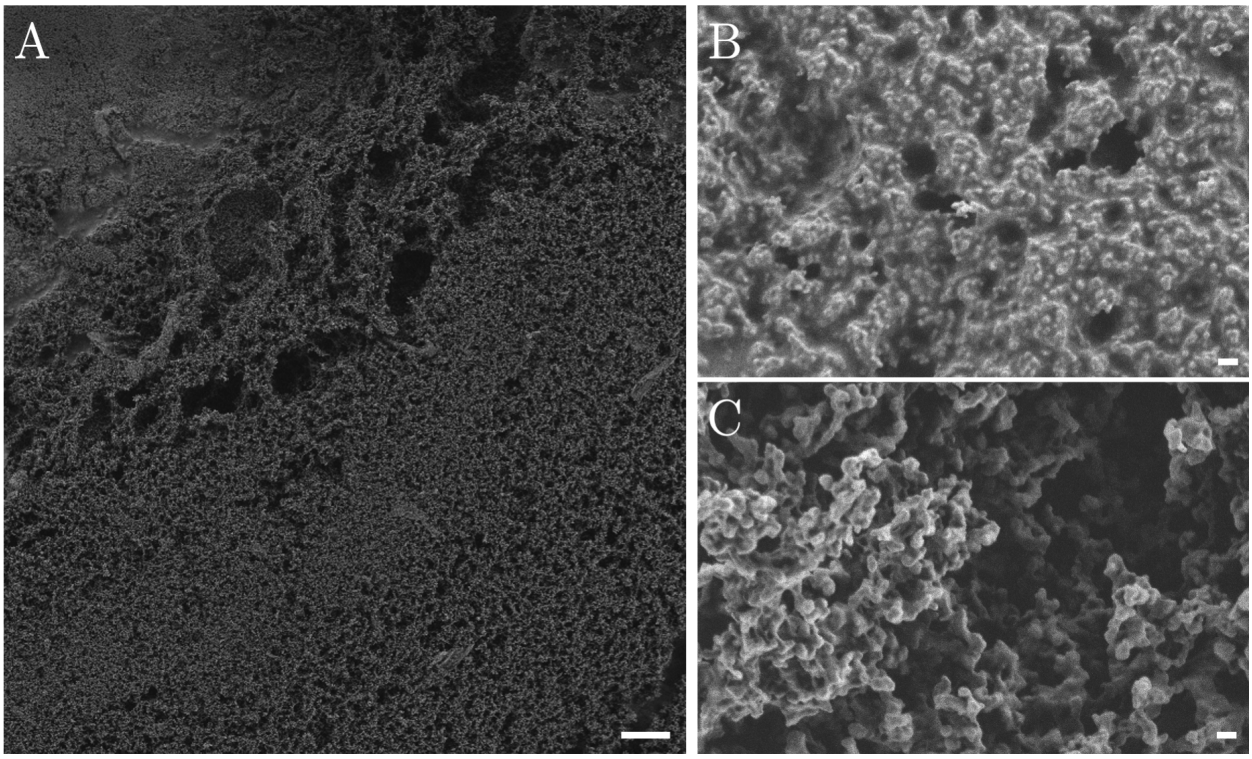


**Figure 3.4** SEM images of supercritically dried ratfish AoL gel. **A)** Low magnification demonstration of the texture of supercritically dried AoL gel. **B,C)** High magnification images of AoL gel in two different areas of the sample. There was some variability in the texture and order of the structures. In a few areas, the structure appeared dense and tightly packed (B), but the majority of the material demonstrated marked porosity (C), as is typical of aerogels (Ganesan et al 2018). Scale bars – A: 10 $\mu$m; B,C: 200 nm.

there was a resulting white powdery precipitate adhered to the dialysis tubing. Some of this white material was stuck on carbon tape and mounted on an aluminum stub for imaging. SEM revealed a fine porous network similar in form to published images of so-called aerogels (Figure 3.4)(Ganesan et al 2018, Quignard et al 2008). An aerogel can be produced when hydrogel is dried in a manner that allows for the maintenance of the original form, such as by supercritical drying (Quignard et al 2008, Sahin et al 2017). Given this, the SEM images of supercritically dried gel are surely more representative of aqueous gel structure than those images of ambiently dried gel. Close examination of the supercritically dried gel structure revealed various structural arrangements, some densely packed and solid (Figure 3.4B), but

most porous and loose (Figure 3.4C). In all cases, the gel structure appeared to consist of globular elements that were on average 100-200 nm in diameter. These findings corroborated the proposition that AoL gel is colloidal and composed of aggregating spherical objects.

### *3.4.4 Proteinase K-treated AoL gel analyzed by SDS PAGE & AFM imaging*

Knowing that ratfish gel contains both polysaccharides and proteins, I was curious if I could learn about the composition of the observed globules by removing one of the macromolecular components and imaging the resulting structure. I was particularly interested in finding out if the globules were composed of chitin, but because I was unable to develop an effective method to label and study the chitinous component alone, I focused on studying carbohydrates in AoL gel, in general. To do this, I treated samples of dialyzed ratfish gel with proteinase K to remove contaminating proteins. I experimented with a few digestion protocols, initially, I admit, without much thought. I varied the incubation solution (water vs buffer) and after some of the digestions, I dialyzed the solution to remove remaining proteins. Regardless, in all cases, I observed a gel to liquid transition during digestion (Figure 3.5A). SDS PAGE showed that these methods demonstrated variable protein-removing efficacies (Figure 3.5B,C). For example, when I digested samples with buffer instead of water, the efficacy of protein digestion was slightly improved as evidenced by a small change in number of bands on the gel. Not surprisingly, when I dialyzed the sample after digestion, and as I increased the molecular weight cut-off (MWCO) of the tubing, a large majority of remaining small peptides were removed (Figure 3.5B,C). Regardless of the digestion solution, SDS PAGE revealed that proteinase K was highly effective at digesting AoL gel proteins into smaller peptide units <11 KDa. In all cases, when digested gel was imaged with AFM, globules similar to those observed with undigested gel were observed

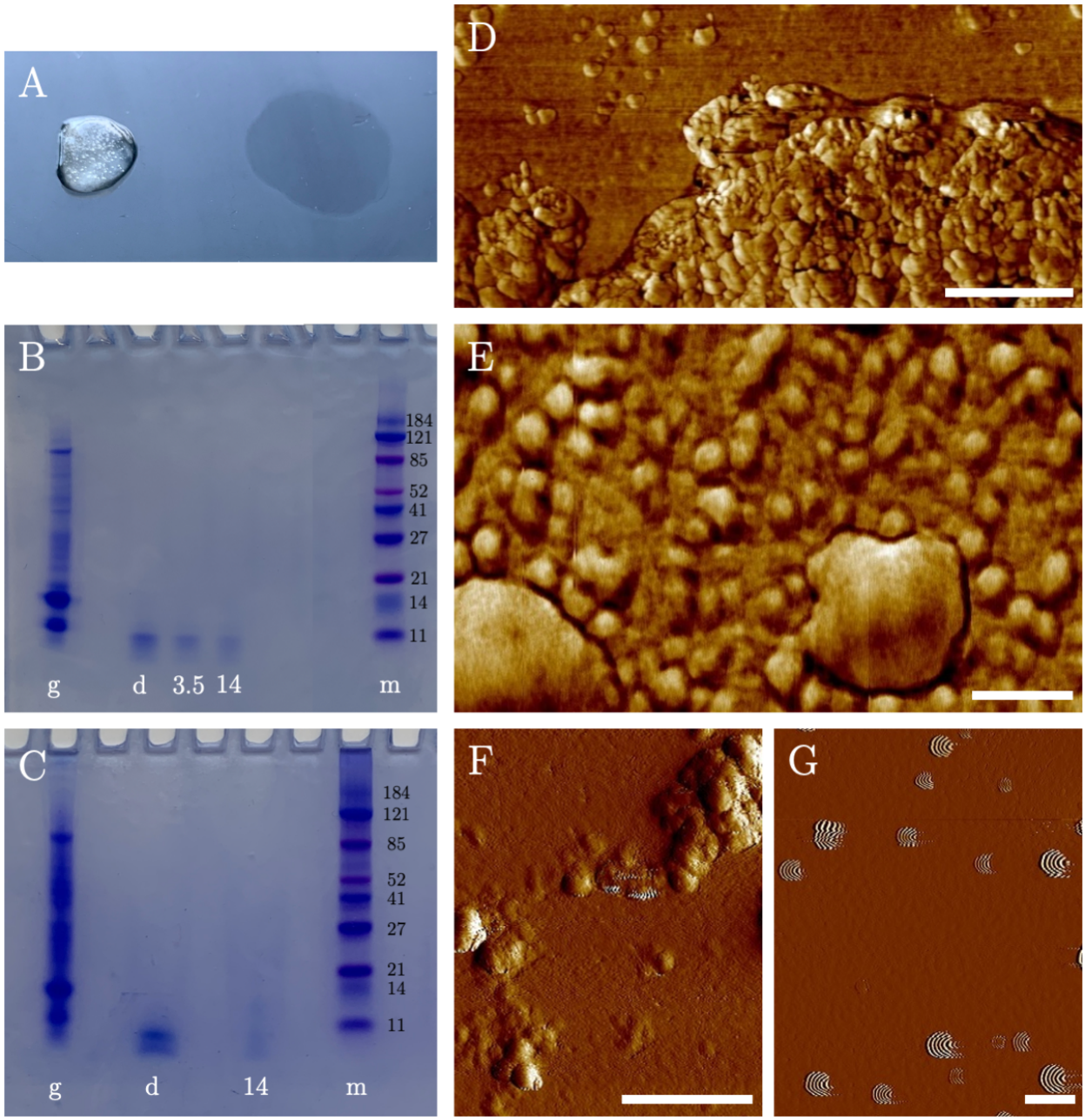


**Figure 3.5** Analysis of proteinase K-digested with ratfish gel by SDS PAGE and AFM. **A)** Image showing a fresh aliquot of ratfish gel (left) next to a drop of proteinase K-treated ratfish gel (right), which demonstrates the remarkable reduction in material stiffness following protein digestion. **B)** Image of a polyacrylamide gel (PAG) stained with Coomassie Blue. The lanes contain native ratfish gel (g), gel digested with proteinase K in water (d), digested gel that had been dialyzed overnight in 3.5 KDa dialysis tubing (3.5), digested gel that had been dialyzed overnight in 12-14 KDa dialysis tubing (14), and a marker (m). MWCO in KDa are shown in black next to the marker. This gel shows that ratfish AoL gel contains proteins of many sizes and digestion in water is effective at breaking the large proteins into smaller peptides that are <11 KDa. Dialysis is effective at removing most but not all of the remaining small proteins/amino acids and is more effective the larger the MWCO. **C)** Image of another PAG showing again, ratfish gel (g), proteinase K-digested gel, but this time digested in buffer (d), digested gel that had been dialyzed in tubing with 12-14 KDa (14), and the same type of marker (m) as shown in (B). When comparing these results to those shown in (B), this gel shows that there is a slight improvement in digestion efficacy when buffer is used instead of water and also that there is a dramatic reduction in

leftover small peptides after dialysis with 12-14 KDa tubing. **D)** AFM image (phase) showing a sample of ratfish gel that had been digested with proteinase K (in water), not dialyzed, diluted 1/20 in water, and dropped onto a freshly cleaved mica sheet to ambiently dry. We observed globules across the surface and in this particular area, we observed what looked like the edge of an aggregate of globules. **E)** This AFM image (phase) is from the same sample as shown in (D) but here the globules appeared to be slightly more diffuse. Like those globules observed in the non-digested gel samples (Figure 3.3), the majority of the globules were ~100 nm in diameter, however there were globules that were much larger, several hundred nm in diameter, and it is unclear if these structures were conglomerations of smaller globules that had joined together, or separate entities entirely. **F)** An AFM image (amplitude) showing a sample of ratfish gel that had been digested with proteinase K in water, dialyzed in tubing with 12-14 KDa, then dropped and ambiently dried on freshly cleaved mica. Here, very little protein remained and yet globules were still observed in aggregates. **G)** AFM image (amplitude) showing ratfish gel digested with proteinase K in buffer and dialyzed in 12-14 KDa tubing before it was dropped on mica. Globules (which were generally a couple hundred nm in diameter) were observed, however, they seemed to induce a repeatable artefact when in contact with the tip. This artefact occurred even when a fresh sample was prepared. Objects like those shown here were seemingly widespread as we observed similar patterns consistently when tip was moved to various sites across the mica surface. Scale bars – D,F,G: 1 $\mu$m; E: 200 nm.

(Figure 3.5D-G). Aggregates of globules were present in all of the samples that had been digested in water, although there were marked differences in the size and shape of the aggregations (Figure 3.5D-F). Interestingly, when I imaged gel that had been digested in buffer and dialyzed with 12-14 KDa tubing, which was in theory the most "protein-free" of all of the samples, I observed a consistent artefact that appeared to result from interactions of globular objects a few hundred nanometers in diameter (Figure 3.5G). These data all together suggest that globules exist in the absence/reduction of protein. I did not observe the same rope-like objects that were seen with untreated gel (Figure 3.3A-C). Also, the shapes of the globules were arguably more distinct than those observed when imaging the native gel. However, as with all the images in Figure 3.3, these AFM results must be interpreted cautiously as desiccation likely had an impact.

### *3.4.5 SEM imaging with proteinase K-treated AoL gel*

Proteinase K-digested gel was also imaged with SEM highly variable patterns were observed (Figure 3.6). In almost all cases, the samples presented as mats composed of varying fine structures. Although globules were not consistently observed the way they were with AFM,

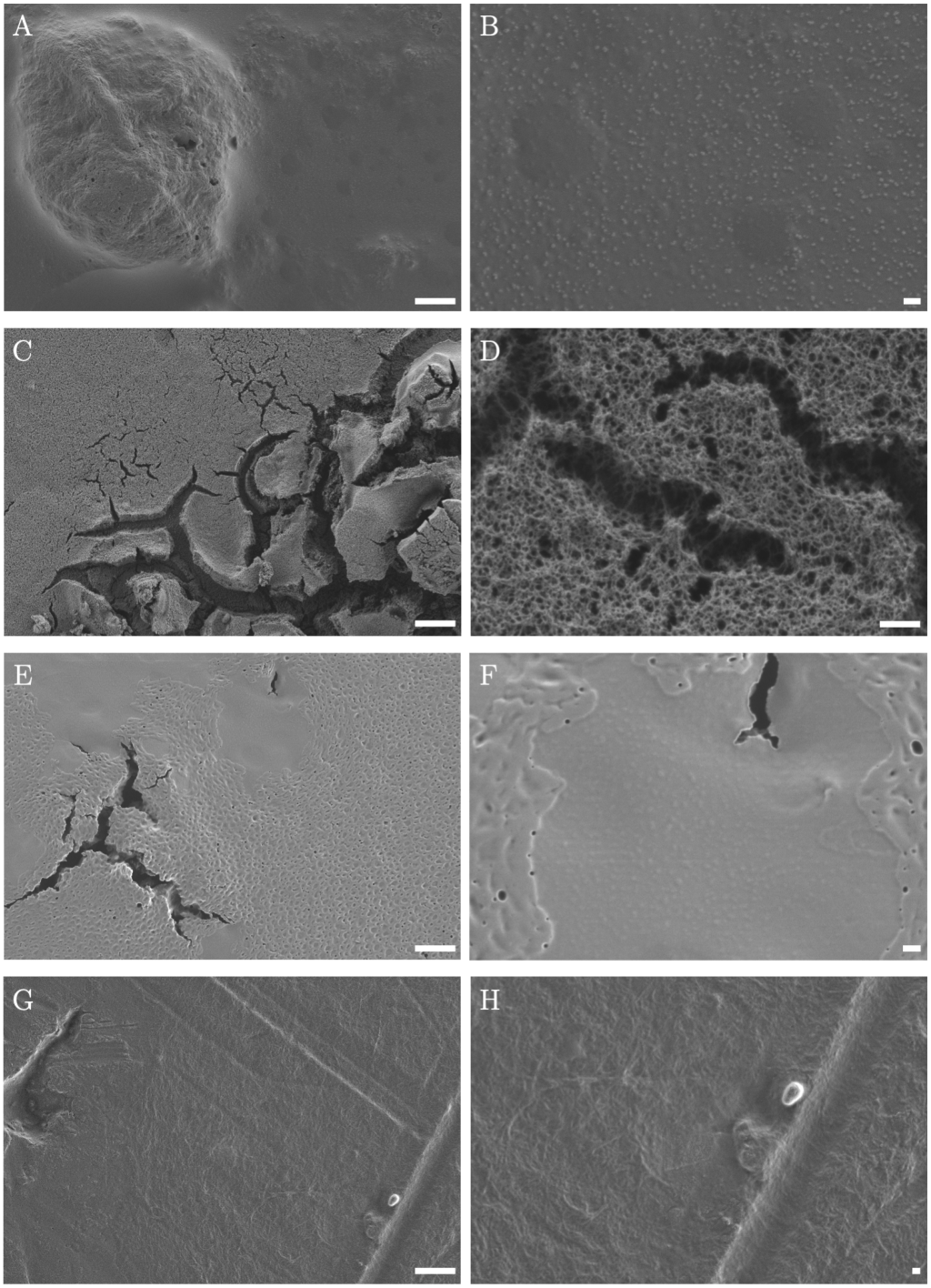


**Figure 3.6** SEM images of proteinase K-digested ratfish gel. Various digestion methods employed, and multiple patterns observed but all samples were ambiently dried on aluminum stubs before imaging. All images in the first column were imaged at a lower magnification and all images in the second column show select regions from the first column images at higher magnification to display details. These images demonstrate the broad structural diversity observed with the gel material. **A,B)** Ratfish gel digested with proteinase K in water and diluted by ½ with water. No dialysis was performed after digestion. Globular objects were observed at high magnification (approximate diameter <100 nm). **C,D)** Images of gel digested with proteinase K in water and dialyzed with 3.5 KDa tubing. A very delicate, porous material was observed across the surface of the stub. **E-H)** Gel digested with proteinase K in buffer and dialyzed with 12-14 KDa tubing. One

sample was diluted ½ in water (E,F) and the other was diluted by 1/20 (G,H). In (E) we see what appears to be a mat of material – the depth of which was made clear by deep cracks observed across the whole stub surface. In this region, the surface of the mat exhibited a repetitive pattern consisting of many small divots. In some areas, the surface appeared to consist of globules (F) similar in shape and size to those observed in (B). In the center of the 1/20 dilute sample shown in (G,H), encrusting fibrous material was observed. The fibers were localized the center of the stub as the material thickened and the texture changed as we scanned toward the edge of our sample droplet. Scale bars – A,C,E,G: 2 $\mu$m; B,D,F,H: 200 nm.

there were some samples that exhibited globular textures (Figure 3.6 A,B,E,F) and others that, in certain areas, appeared to be composed of fibrous material (Figure 3.6 C,D,G,H). When protein and minerals are removed from crab shells, chitin nanofibers are readily observed (Ifuku & Saimoto 2012). It is possible that after I digested away proteins in the gel, some of the endogenous chitin assembled into fibers *de novo*, or perhaps fibers that had always been present became exposed and visible, but I wasn't able to test this. Although there were a few repeatable patterns observed in the various proteinase K digestions imaged with SEM (i.e. globules and fibers), the majority of the samples exhibited a lot of variability. Therefore, like with the untreated gel, I tried supercritically drying our proteinase-digested samples and examined the resulting material with SEM.

### *3.4.6 SEM imaging with supercritically dried proteinase K-digested gel*

To investigate the influence of proteins on AoL gel structure and understand what effect dialysis had on the results, I supercritically dried three samples that had all been digested with proteinase K in buffer. Then, one aliquot of digested gel was left undialyzed, while another was dialyzed with 3.5 KDa tubing and the last was dialyzed with 12-14 KDa tubing. As with the non-digested gel, these samples were incubated in ethanol before exposure to supercritical $CO_2$. Some interesting differences between the three samples were observed (Figure 3.7). There were spherical structures in all three samples that were unlike the globules observed in the other samples up to this point as they were very smooth and had

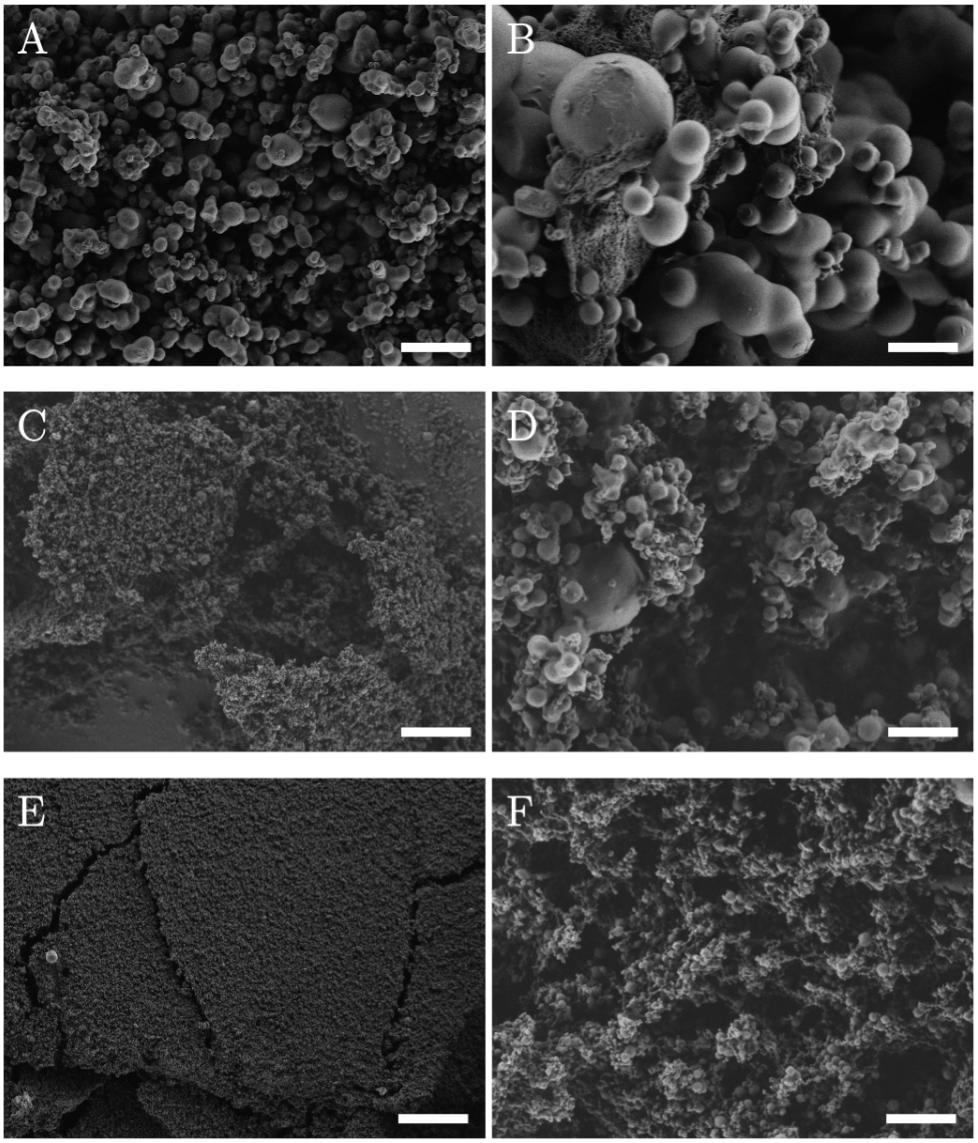


**Figure 3.7** Supercritically dried samples of proteinase K-digested gel imaged with SEM. Images in the first column were all taken at the same (relatively) low magnification and the second column consists of higher magnification images with more detail. **A,B)** Proteinase K-treated gel (in buffer) that had not been dialyzed. It is important to note that because this sample was not dialyzed, it was still diluted in buffer before it was exposed to ethanol and supercritically dried (which would have influenced the pH). The majority of the sample was composed of spherical particles of variable size with an average diameter of either 1 or 4 $\mu$m. A small amount of the material was porous and web-like (B) and wrapped around the spheres. **C,D)** Proteinase K-treated sample dialyzed with 3.5KDa tubing. Here, spherical particles were observed but were much smaller than those shown in (A & B), with an average size of 200-400 nm. **E,F)** Proteinase K-treated sample dialyzed with 12-14 KDa tubing. Once again, spherical particles were observed, but these were even smaller than those in the 3.5 KDa dialyzed sample, with an average size of 100 nm. Scale bars – A,C,E: 10 $\mu$m; B,D,F: 1 $\mu$m.

remarkably defined curved surfaces – in fact, they resembled "Dippin' Dots" ice cream! The spherical structures were present in all three samples; however, their average size was

markedly smaller in the samples that had been dialyzed. Further, the sample that had been dialyzed with 12-14 KDa tubing contained smaller spheres than the sample that was dialyzed with 3.5 KDa tubing (Figure 3.7). In the non-dialyzed sample, the spherical particles were quite variable in size but could be roughly sorted into those with an average diameter of ~1 $\mu$m, and those with an average diameter of ~4 $\mu$m (Figure 3.7 A,B). In contrast, the 3.5 KDa dialyzed sample contained spheres that were mostly 200-400 nm in size (Figure 3.7 C,D), while the spheres in the 12-14 KDa dialyzed sample were mostly 100 nm (Figure 3.7 E,F). Because spherical objects were not observed with supercritically dried non-digested gel, I suspect that these spherical objects are produced by the supercritical drying process itself, and only generated when the carbohydrate component of the gel is unbound by protein.

### *3.4.7 SAXS comparison between native and proteinase K-digested AoL gel*

Of all the data reported so far, the images of supercritically dried gel samples were, in theory, the best representation of the gel's aqueous structure. However, the supercritically dried, proteinase K-digested samples exhibited some interesting artefacts which made images of the native and digested samples impossible to compare. Further, although I had collected compelling microscopic evidence of globules inside both native gel and proteinase K-digested gel, I was still not certain what these structures "looked like" in an aqueous solution. To get a better understanding of the differences between aqueous native gel and proteinase K-treated gel, I collaborated with Dr. Linda Hirst and Alauna Wheeler in the Physics department at UC Merced to study the small angle x-ray scattering (SAXS) of gel samples using the synchrotron at UC Berkeley's Advanced Light Source (ALS). To perform SAXS, an aqueous sample of interest is placed in a glass capillary tube positioned inside the synchrotron and illuminated by an x-ray beam. The patterns generated by x-rays scattering

from the material are collected and displayed on a plot that provides information about the size and structure of the molecular components within a sample (Kikhney & Svergun 2015). SAXS analyses are ideal for studying poorly ordered dilute aqueous materials like AoL gel. Knowing that AoL gel is approximately 95% water, I subjected proteinase K-digested and non-digested ratfish gel to ultracentrifugation to separate the water and concentrate the remaining gel components. (Murray & Potts 1961). As mentioned earlier, ultracentrifugation of untreated ratfish gel results in three layers: a clear supernatant, a thick whitish pellet, and a small dark red pellet. Each of these three layers were placed into separate capillary tubes for analysis with SAXS (Figure 3.8A). For this experiment, I used gel that was digested with proteinase K in PBS and dialyzed with 3.5 KDa tubing after digestion. When digested gel was centrifuged overnight, I obtained supernatant and a red pellet both similar in appearance to those observed with untreated gel, but in lieu of a dense white pellet, there was a cloudy layer of diffuse material loosely floating above the densely packed red pellet (Figure 3.8B). The three fractions were separated into individual capillary tubes for analysis, although it was challenging to ensure that all of the loose cloudy layer was collected and separated from the supernatant. I already suspected that the white pellet contained some, if not all, of the chitinous and proteinaceous material of interest, especially after SEM imaging of the white pellet from non-digested gel looked to contain globules (Figure 3.3D,E). Given this, I figured that carbohydrates and remnant proteins would localize to the loose cloudy fraction after centrifugation of the digested sample.

The scattering from a sample of water was subtracted from both the white pellet (non-digested gel) and yellow cloud (digested gel) plots and the resulting curves are shown in Figure 2.8C. Because water had been subtracted, the curves reflect the scattering from polymers existing in the gel material. After water was subtracted from the cloudy layer of

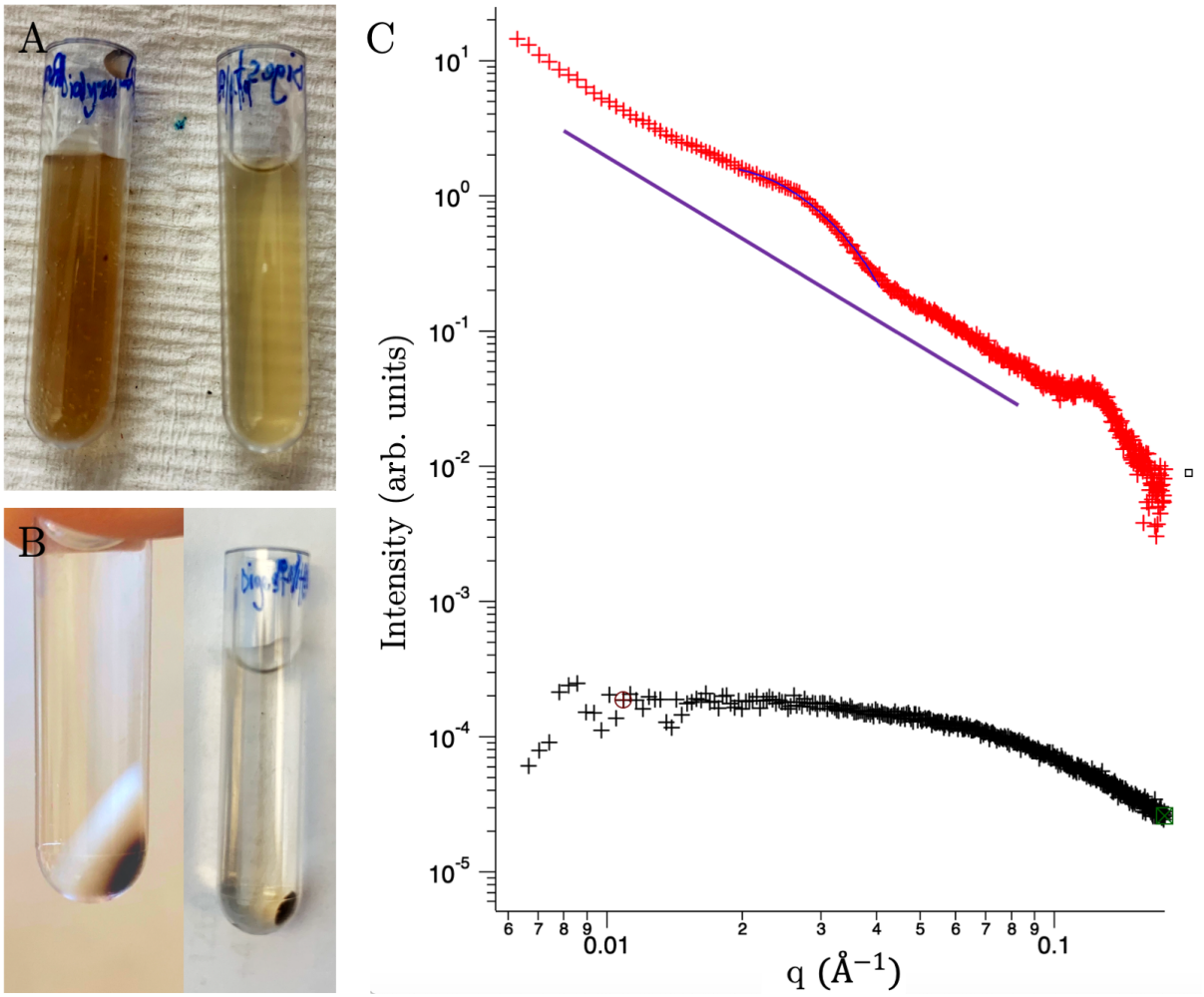


**Figure 3.8** Small angle x-ray scattering (SAXS) of fraction resulting from ultracentrifugation of ratfish gel. **A)** Image showing two centrifuge tubes containing non-digested ratfish gel (left) and proteinase K-treated gel (right) before ultracentrifugation. **B)** Image of the same tubes shown in (A) after ultracentrifugation overnight at 300,000-400,000xg. Centrifugation of untreated ratfish gel (left) yielded clear supernatant, a thick white pellet, and a small dark red pellet, whereas centrifugation of digested gel (right) yielded supernatant, a dark red pellet, and a faint yellow cloudy material. **C)** SAXS results from the white pellet resulting from centrifugation of untreated ratfish gel (red) and the light cloudy material resulting from centrifugation of digested gel (black). Scattering intensity is plotted as a function of the scattering vector, $q$. The purple line has a slope of -2 which is the approximate slope of the scattering pattern generated from the white pellet (red plot).

the digested sample, the resulting curve was relatively flat with a shallow slope and no obvious peaks (Figure 3.8C, black curve). This suggests that the polymers remaining in the gel after digestion are likely dilute, of varying lengths, and without organization. In contrast, the slope of the curve resulting from the non-digested gel pellet, is close to -2 (see purple

line with slope of -2 in Figure 3.8C). That the slope of the white pellet's curve has this magnitude suggests that it behaves as an ideal polymer chain. An ideal polymer chain is freely jointed and self-avoiding, with characteristic scattering described by the Debye function,

$$S(q) \propto 1/q^{v}$$

where $v$ is exactly equal to 2. For a self-avoiding chain, the value of $v$ can be slightly higher as the chain effectively swells. Figure 3.8C demonstrates that our data has a slope very close to -2, consistent with these theoretical models (Cotton). The curve has a clear peak at approximately $q = 0.028$ $\text{Å}^{-1}$, which corresponds to a real space lengthscale, $d$ of 22 nm (where $q = \frac{2\pi}{d}$). The peak likely corresponds to some feature of the polymers in the gel – perhaps the relative distance between them – although ultracentrifugation would likely have had an impact on the size and behavior of the polymers in native gel so, as with the SEM/AFM data, I focused on the order of magnitude of the peak size (between 10 and 100 nm) and not the value itself. The second peak observed on the curve is around 0.1 $\text{Å}^{-1}$, which is roughly 5 nm. Knowing that the gel squeezed from ratfish AoL pores is full of contaminating cells, and that cellular particulate would pellet when centrifuged, I hypothesize that this peak can be explained by cellular debris, namely cell membranes, which are on average approximately 5 nm in thickness (Phillips 2018). I made various attempts to remove cellular contaminant from AoL gel (i.e. filtration, centrifugation), but due to the inevitability of cellular lysis, I was never confident that macromolecular cellular components could be fully separated from those macromolecules that compose the gel itself. Thus, I expected that cellular material as well as polymer AoL gel components would end up in the red pellets observed in the centrifuge tubes of both digested and non-digested gel. The color suggested that, at the very least, hemoglobin from contaminating blood cells was

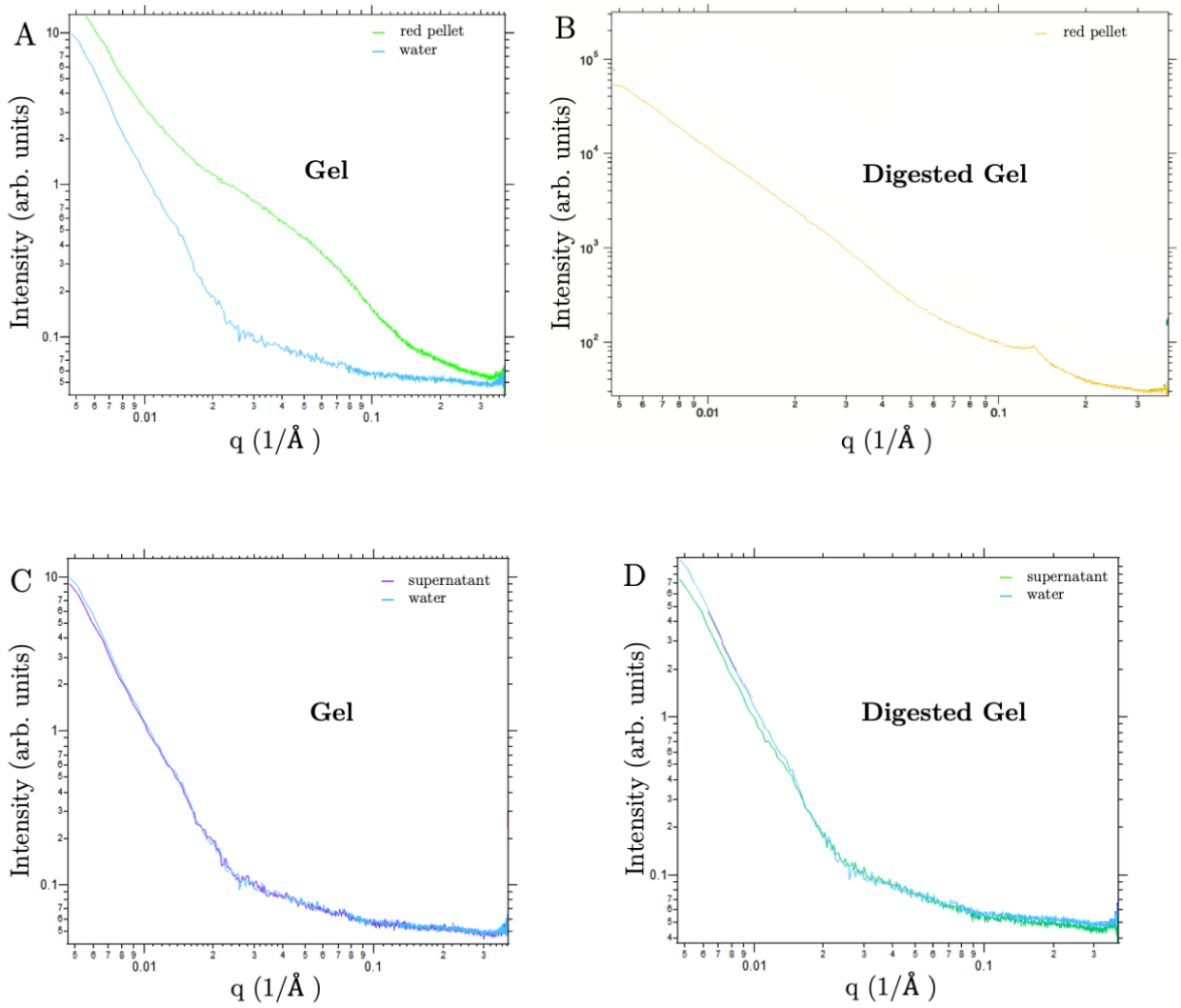


**Figure 3.9** SAXS results from red pellets and supernatant of native vs digested ratfish gel. In all four graphs the scattering intensity is plotted as a function of scattering vector, $q$. **A)** Scattering from the red pellet fraction from ultracentrifuged ratfish gel (green) as compared to water (blue). **B)** Results from red pellet collected after ultracentrifugation of digested ratfish gel. **C)** Supernatant resulting from ultracentrifugation of gel (purple) compared to scattering from water (blue). **D)** Scattering from digested gel supernatant (green) as compared to water (blue).

concentrated to this fraction. The plots resulting from SAXS with both red pellets are shown in Figure 3.9A,B. Interestingly, the plot from the non-digested sample's red pellet had a very broad peak at the same approximate location as was seen for its corresponding white pellet (approximately 22 nm). In contrast, scattering from the digested sample's red peak resulted in a single peak at roughly 5 nm, the same approximate location as the "cell

membrane peak" that was observed in the plot from the non-digested white pellet. The supernatant resulting from centrifuging both non-digested gel and digested gel exhibited scattering patterns identical to water (Figure 3.9C,D). All together, these data suggest that digestion with proteinase K eliminates the ~22 nm peak (from all fractions) and collapses the polymer network. This notion goes hand in hand with the dramatic reduction in gel stiffness observed after treatment with proteinase K.

### *3.4.8 Proton conductivity differences between native gel and proteinase K-digested gel*

After the SAXS experiments revealed marked structural differences between native gel and proteinase K-digested gel, I was interested to see if enzymatic protein removal changed the gel's known proton conductive properties (Josberger et al 2016). I still had an abundance of spotted ratfish AoL gel to analyze, however, given that holocephalans and elasmobranchs diverged some 410 million years ago, I didn't know if native ratfish gel would exhibit comparable proton conductivity to elasmobranch gel (Inoue et al 2010). To perform these experiments, I brought gel samples to Marco Rolandi's lab at UC Santa Cruz where Manping Jia, a graduate student in the lab, performed proton conductivity measurements and compared the proton conductivity of native ratfish gel (that had been dialyzed to remove ions) and proteinase K-treated gel. The results indicated that ratfish gel is proton conductive. Interestingly, we also learned that digested gel is significantly more conductive than native gel. Native gel had an effective conductivity of 2.4 mS/cm compared to digested gel that had a conductivity of 11.9 mS/cm. The native gel sample would have contained keratan sulfate, chitin, and various proteins as compared to the digested sample which theoretically only contained polysaccharides. Given the known proton conductive properties of keratan sulfate (Selberg et al 2019), we suspect that the increase in conductivity

associated with protein removal results from the effect of concentrating keratan sulfate molecules in the digested sample.

### *3.4.9 Structural analysis of polysaccharides extracted from AoL gel with AFM, SEM, & crossed polarized light*

My initial interest in AoL gel structure stemmed from my desire to collect more evidence of chitin's presence in the gel. Therefore, to study the gel's chitinous component in more detail, I chemically extracted chitin from ratfish gel using the same methods as described in Chapter 1. Both the monosaccharide analysis and FTIR experiments reported in Chapter 1 revealed that my extraction methods were effective at removing keratan sulfate and the majority of proteins from the gel and isolating the chitinous component. In the early stages of these extraction experiments, I simply treated samples with 1 M HCl and several rounds of 1 M NaOH at 60°C before dialysis in water. However, I improved the extraction technique by adding a proteinase K digestion step before acid-base treatment which improved the purity of the chitinous product, as evidenced by FTIR (Chapter 1). Although the extraction protocols varied, imaging revealed that material resulting from several different rounds of extraction exhibited repeatable phenomena. When one of the extracted gel solutions was ambiently dried on a surface then scraped up and imaged with SEM, crystals reminiscent of chitin nanowhiskers were readily observed (Figure 3.10A,B) (Mincea et al 2012, Zeng et al 2012). The crystal nanowhiskers appeared to self-organize into aggregates, the degree of which seemingly attributable to the conditions at which the samples were prepared and dried (Figure 3.10B). AFM imaging of gel extract ambiently dried directly onto mica, revealed nanowhiskers similar to those observed with SEM (Figure 3.10C). Interestingly, AFM imaging of a gel sample that had been digested with proteinase K, not chemically treated, but sonicated, showed that crystals can also formed by protein digestion alone

(Figure 3.10D). As I continued adapting the extraction protocols and imaging with both AFM and SEM, crystals of various morphologies were generated, making it clear that crystallization of the nanowhiskers seemed to highly depend on both the extraction process and the desiccation conditions (Figure 3.10E-G). Some crystals took on fine, linear forms (Figure 3.10E), while others were bulkier and more rounded (Figure 3.10F-G). When a sample of chitin extract deposited on mica was imaged with SEM, large branching crystals were observed, many of which closely associated with chunky material distributed widely across the mica surface (Figure 3.10G,H). In fact, in many of the samples, there were far more disordered chunks of amorphous material, like those shown in Figure 3.10H, than crystals. For example, in Figure 3.10A, the material that the whiskers are on top of was a product of the extraction process and thereby also likely composed of chitin. I suspect that chitinous crystals and whiskers form under very specific conditions and by a small subset of the material. The rest of the chitin appeared to exist in an amorphous form. These same two morphologies were observed when a sample of dried gel extract was resuspended, sonicated, then dropped on a glass slide. Upon imaging with light microscopy, I observed fine crystals stemming from a much thicker material that circled the whole edge of the freshly dried droplet (Figure 3.10I,J). Interestingly, when the sample was placed between crossed polarizers and imaged with light microscopy, the crystals exhibited birefringence (Figure 3.10I,J). When the sample was rotated between the polarizers, different crystals transmitted light indicating that they were aligned in several different orientations. Although electron diffraction with transmission electron microscopy (TEM) was attempted to confirm that the observed nanowhiskers/crystals were composed of chitin, the material did not diffract in any detectable way. Therefore, my claim that the observed crystals are chitinous is based on their resemblance to published chitin crystal morphologies, on the FTIR spectra (Chapter 1) which shared peaks with chitin controls, and on the glucosamine

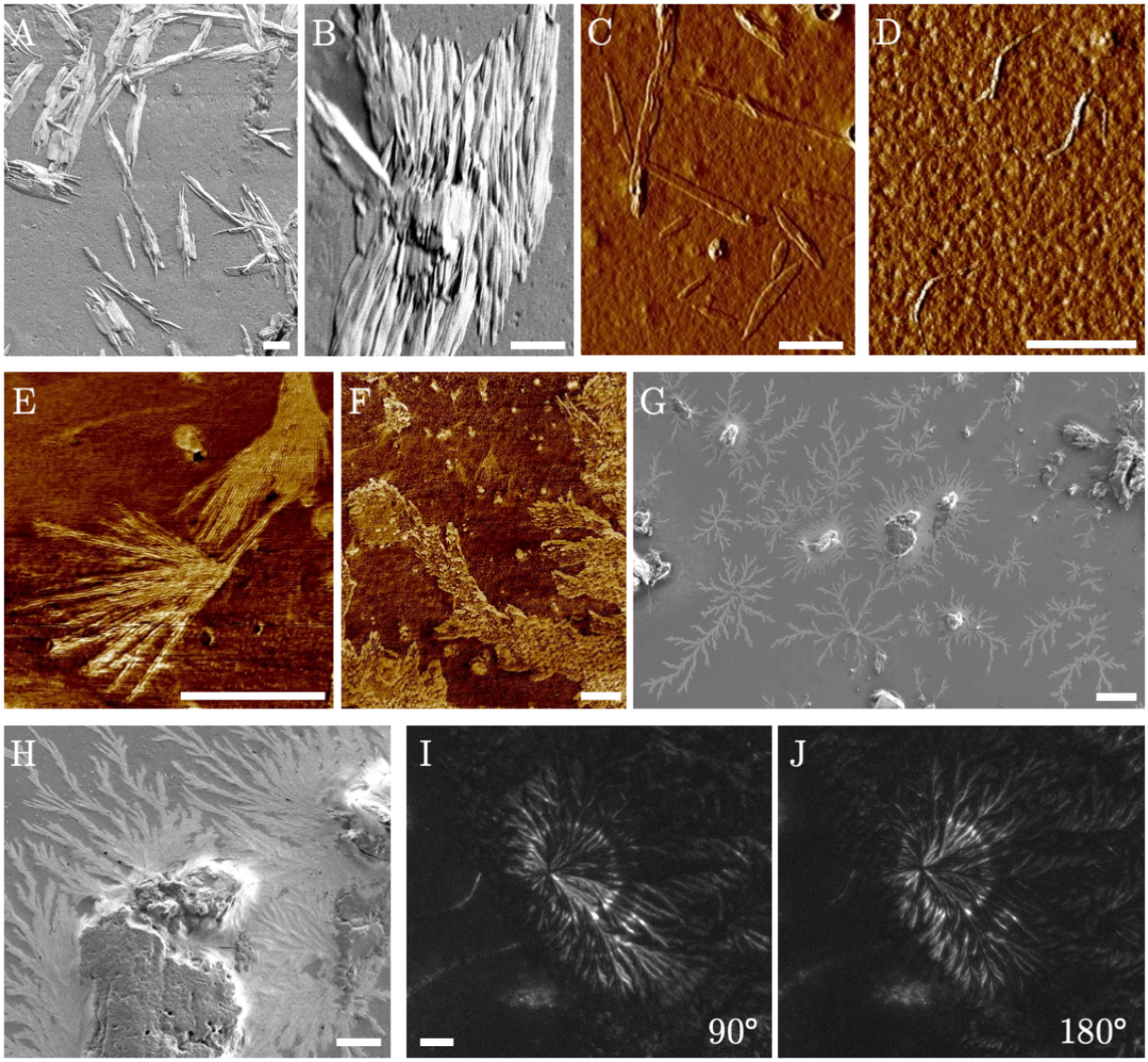


**Figure 3.10** Chitin extracted from AoL gel reveals nanocrystals with SEM and AFM. **A,B)** SEM images of chitin extract that was dried in a petri dish then scraped up and stuck to carbon tape. The images show structures similar in morphology to published images of chitin nanowhiskers. The nanowhiskers readily aggregate (B) with one another. **C)** AFM image (amplitude) showing a different chitin extraction sample than the one shown in (A,B). Sample was dropped onto mica and heat dried before imaging. Once again, structures resembling chitin nanowhiskers were visible with AFM. **D)** AFM image (amplitude) showing more whisker-like structures. This sample was prepared solely by digesting ratfish gel with proteinase K, sonicating the resulting material, dropping it on mica and heat drying. **E,F)** AFM images (phase) showing chitin extraction (without a proteinase K digestion step) that yielded crystal-like structures of highly variable morphology. **G)** Image showing chitin extraction sample that was dropped and heat dried on mica then imaged with SEM. Here, crystals were observed seemingly growing off of dense aggregated material. The chunks of dense material could be composed of amorphous chitin. **H)** Image of the same chitin sample shown in (G) at higher magnification. Here, the dense aggregated amorphous material is centrally positioned with crystals growing off of its edges. **I,J)** Crystals resulting from dried chitin extract resuspended in water, sonicated for 30 minutes, dropped on a glass slide, and heat dried. Transmission images taken with compound light microscope between crossed polarizers. Images demonstrate that the crystals are birefringent because while one part of the crystal transmits light when the polarizer is at 90° (H), when the sample is turned to 180° (I), another part of the crystal transmits light. Scale bars – A-F: 1 $\mu$m; G,I: 10 $\mu$m; H: 2 $\mu$m.

peak resulting from monosaccharide analysis (Chapter 1) performed using the same extracted material observed here with SEM and AFM.

### *3.4.10 Comparison of powder x-ray scattering plots from native gel, extracted gel, and proteinase K-digested gel*

In my continued efforts to confirm chitin's presence in AoL gel, I collected scattering data using a powder x-ray diffractometer with the help of Matthew Robinson. Powder x-ray diffraction (XRD) is similar to SAXS in that the sample of interest is exposed to x-rays and the resulting scattering pattern is collected and plotted. However, dried samples are used with powder XRD, and the method is generally employed to study the crystallinity of materials (Chauhan & Chauhan 2014). Three gel preparations were examined to explore the effects of chitin purity on the diffraction patterns. I started with native ratfish gel that was deposited and dried on a sample holder in three layers. This sample had been dialyzed to remove salts and any other small molecules, but otherwise contained all of the naturally occurring gel components. The next gel sample had been treated with proteinase K (in buffer) and was dried in many layers of ~100 mL aliquots dried at 62°C over the course of several days. These first two samples were left as "flakes" of dried material on the sample holder and not broken up into smaller particulate before analysis. Finally, I used one of extracted gel samples that had been treated with HCl and NaOH but not with proteinase K). XRD with the three samples yielded similar plots containing two broad peaks, one very small and the other more substantial, all located in roughly the same location (Figure 3.11A-C). The broad shape of these peaks contrasted significantly with the spectrum resulting from commercial chitin (from shrimp shells), which showed a characteristic diffraction pattern of several sharp peaks (Figure 3.11D). I expected that the extracted gel sample, and

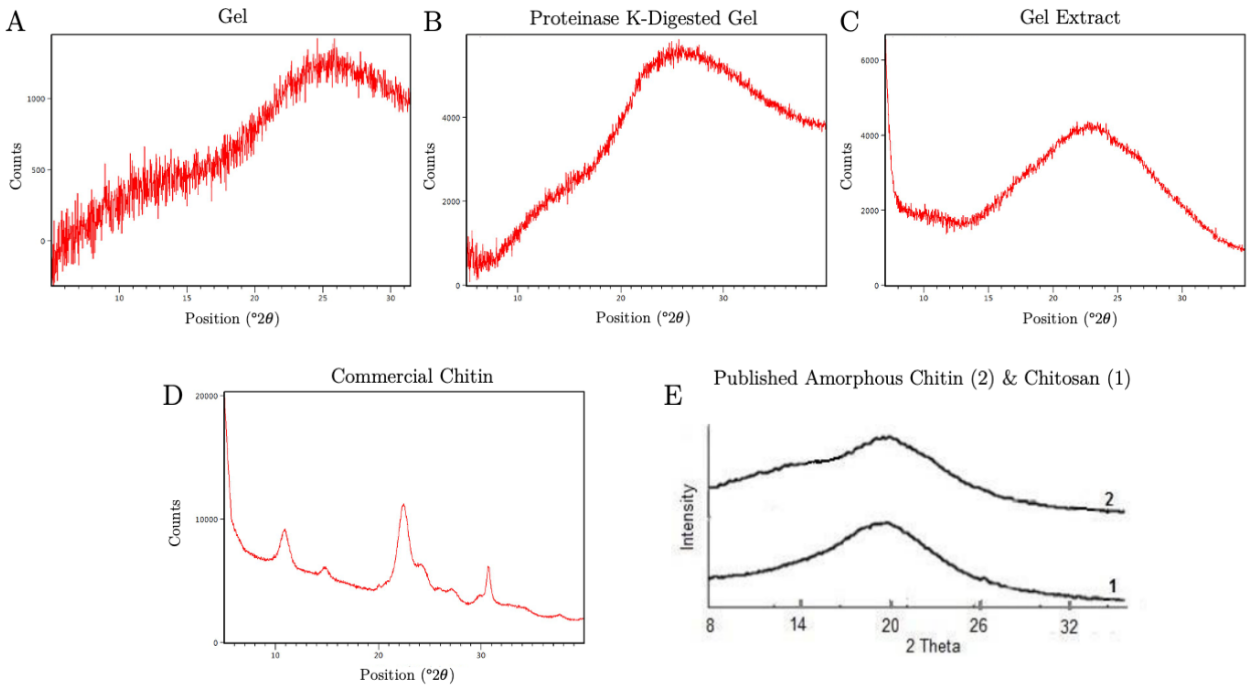


**Figure 3.11** X-Ray scattering plots from AoL gel preparations, commercial chitin, and published amorphous chitin & chitosan. Here, the XRD spectra resulting from three gel samples are compared to a spectrum obtained from commercial chitin – all of the measurements were taken using a Cobalt anode. In contrast, the published spectra from chitin and chitosan were measured with a Copper anode so the x-axis values cannot be directly compared to the chitin/gel samples. **A)** Gel was deposited directly on sample holder in three layers and allowed to ambiently dry. **B)** Proteinase K-treated gel was digested in buffer, dialyzed with 12-14 KDa tubing, then dropped in many 200 $\mu$L aliquots onto a sample holder and heat dried. **C)** Chitin extract was prepared by treating gel once with 1M HCl and several times with 1M NaOH at 50°C followed by many rounds of dialysis in water. Three layers of concentrated sample was then dried on sample holder before analysis by XRD. **D)** Commercial chitin from shrimp shells deposited on sample holder. **E)** Published spectra from amorphous chitosan (1) and chitin (2) that had been ground in a ball mill for 24 hours (Ioelovich 2014).

even the proteinase K-digested sample for that matter, would have exhibited signatures of crystallinity as a subset of the same material had formed visible crystals in earlier experiments using AFM and SEM. Interestingly though, the shapes of the curves from our XRD experiments looked very similar to published diffraction data from "amorphous chitin" (Ioelovich 2014). In his study on the crystallinity of chitin and chitosan (the deacetylated form of chitin), Ioelovich explained that crystallinity could be drastically reduced in the materials if they were subjected to exhaustive ball-grinding. This process would leave behind only amorphous chitin and chitosan as evidenced by XRD. Ioelovich's XRD profiles are

shown in Figure 3.11E, but it is important to point out that while a cobalt anode was used for my analyses (Figure 3.11A-D), Ioelovich used a copper anode, making the x-axis positions not directly comparable to the other plots. Given the similarities of the diffraction patterns between AoL gel samples and Ioelovich's amorphous chitin, I presume that AoL chitin is mostly amorphous, only forming crystals when exposed to particular conditions and only in small quantities.

### *3.4.11 Proteomic datasets from AoL gel of two chondrichthyan species*

I wanted to generate well-annotated proteomes from AoL gel so that I could at least determine which proteins are gel components and then investigate their structural relationships with chitin and keratan sulfate. Therefore, despite the known limitations of cellular contamination, I generated two proteomic datasets using AoL gel from little skate (*Leucoraja erinacea*) and spotted ratfish (*Hydrolagus colliei*) in collaboration with Mike MacCoss and Richard Johnson at the University of Washington (UW). Because there is still no spotted ratfish genome, the proteome from this species was annotated using the genome of the elephant shark (*Callorhincus milii*) and a *de novo* sequencing algorithm developed by Richard Johnson (Johnson et al 2020). Richard's algorithm allowed for the matching of *de novo* proteomic sequences from ratfish gel with related but homologous non-exact sequence matches from, in our case, the elephant shark. Some of the "top hits" in the ratfish proteome included keratin, actin, and myosin, all proteins that could result from cellular contamination, and the top 50 hits are tabulated in Appendix 2. It is important to note that the proteins are listed in a descending order based on a very rough estimation of protein abundance (Total Independent Spectra) in the sample (Appendix 2). Based on my communications with Richard, I gathered that "Percent Coverage" tells us the percent of the elephant shark protein sequence covered by the various *de novo* ratfish peptide

sequences identified, while "Total Independent Spectra" is the approximate number of spectra that could be assigned to a protein, which is a rough guide to protein abundance.

To generate the little skate proteome, I sent a sample of fresh gel to Richard Johnson who once again performed mass spectroscopy. The protein identities of the resulting sequences were predicted by Postdoctoral scholar Daniel Ocampo Daza using an unpublished little skate genome. The data was then merged with the four transcriptomes (AoL pores, AoL canals, AoL alveoli, and pelvic fin skin) that we synthesized and described in Chapter 1. Like the ratfish dataset, the "top hits" were ordered by a rough approximation based on the number of spectra that could be assigned to a given genome sequence. The predicted gene names (in rough protein abundance order) and the transcript per million (TPM) values from our four transcriptomes (Chapter 1) are tabulated in Appendix 2 and allow for the direct comparison between rough protein abundance and transcriptome counts. Many of the top hits in the little skate gel's proteome could be explained by the contamination of cells – keratins were again the top hits. However, Daniel predicted some secreted proteins that can be considered candidate AoL gel components including lactotransferrin and otogelin. Lactotransferrin, a secretory protein known to modulate immune responses in mammals, is both a top hit in the proteome and highly expressed in AoL tissues as compared to pelvic fin skin, indicating that it could be an AoL gel component (Siqueiros-Cendon et al 2014). Otogelin, a glycoprotein component of the gelatinous membrane covering surfaces within mammalian ears, was also an appealing candidate AoL gel component. However, while it was high on the proteome list, interestingly, otogelin exhibited low expression in the AoL transcriptomes (Cohen-Salmon et al 1997). A manuscript detailing the proteomic findings mentioned here will be published soon and the top hits from the little skate proteomic dataset are shown in Appendix 2.

When I first began studying AoL gel, I sought to eliminate cellular contaminants and thereby improve the reliability of proteomic datasets. I tried removing cells from the AoL gel by forcing it through a 5 $\mu$m mesh filter and tried separating the gel from contaminating particulates by running it on a polyacrylamide gel but proteomic analyses with these samples failed to improve our results (data not shown). Human contamination also turned out to be an issue with the little skate proteomic dataset. Although the introduction of human hair/cells was seemingly avoided in the spotted ratfish proteome, my experience has shown that cellular contamination from the source fish is an inevitability. My fluorescent images from gel samples exposed to nuclear label (DAPI) visually confirmed that cells are abundantly distributed in AoL gel extracted from expired fish. Therefore, as it stands right now, I cannot determine whether a given protein in our proteome is a gel component or a product of cell lysis and until the techniques laid out here are improved, AoL gel proteomes should all be interpreted with the understanding that cellular contamination is prevalent.

## 3.5 Discussion

When I first imaged CBD-labeled spotted ratfish AoL gel in tissue sections, I observed the chitinous component of the gel organized into little "packets" similar in shape and size to the cells lining the inside of the AoL canals. Published transmission electron micrographs of AoL tissue sections from bull sharks (*Carcharinus leucas*) revealed similar results, showing that material is seemingly released from the cells lining the inside of the canals, although the gel material from these images is more uniform in structure and not organized into packets (Whitehead et al 2015). Therefore, I was unsure if the observed packet-like structures were reflective of the unfixed aqueous gel configuration, so a preparation of CBD-labeled native gel was also imaged with fluorescence microscopy. CBD

labeling revealed the folding of a multi-layered, fluid structure. I still don't know if the chitinous "packets" seemingly extruded from epithelial canal cells organize over time into the more tightly packed organization seen with aqueous gel or if they were merely products of fixation. It's also important to mention that CBD labeling of unfixed gel does not necessarily inform about the distribution of chitin in the gel *per se*, as the fragility of the gel made rigorous washing impossible. Instead, in this context I used CBD as a non-specific fluorescent label to merely observe the general gel structure. Because the fluorescent microscopic results were somewhat inconclusive, I was encouraged to study the structure of AoL gel at higher magnifications.

I was interested in chitin's contribution to gel structure specifically, so I first tried using fluorescent nanocrystals called quantum dots (Qdots) to label chitin. However, I ran into the same issue as with CBD – the gel material would dissociate quite readily when exposed to liquids, so washing was not practical and therefore labeling was not trustworthy. When Qdot-labeled gel was imaged with AFM, the Qdots seemed to cover the entire surface so it was hard to tell if they were binding in any specific manner. After my chitin-labeling attempts didn't pan out, I focused on documenting the general gel structure. Ambiently dried native ratfish gel was imaged using AFM and SEM and aggregated globules with an average diameter of approximately 100 nm were consistently observed. The sizes of the imaged globules were surely not reflective of the actual size of globules in hydrated gel because desiccation surely had an effect on gel structure. Perhaps the limitations of drying effects could have been overcome if I had been able to image ratfish gel with liquid AFM. Instead, supercritical drying was used to convert AoL hydrogel into an aerogel, where the spaces previously occupied by liquid were theoretically replaced by air after treatment (Sahin et al 2017). The bulk of the supercritically dried gel exhibited a porosity similar to that of published supercritically dried gels (Figure 3.4C) (Cardea et al 2013). The sample's

structure appeared more compacted in some areas as compared to others, and I suspect this could have resulted from the interaction of gel material with the inside surface of the dialysis tubing (Figure 3.4B). Close examination of the supercritically dried gel revealed widespread globular elements similar to those globules observed in the ambiently dried samples.

The major components that make up gels have been shown to exist in various forms. These forms include fibrous or rod-like particles, flexible coils, spherical particles, and linear molecules held together by crystalline junctions (Djabourov 1988). The microscopic evidence described in this chapter suggests that AoL gel is colloidal in nature, with spherical globules representing a substantial portion of the structure. SAXS with concentrated dehydrated gel generated a peak which roughly corresponded to 22 nm. I see that this value likely represents one of two options: the average size of the globules themselves, or the rough size of the spaces between the globules. If the peak represents the size of the globules themselves, instead of taking the value of "22" to heart, it is safer to estimate that they are between 10 and 100 nm in diameter because ultracentrifugation would likely have impacted their actual size. However, globules were still observable by AFM & SEM in many of the digested gel samples despite the fact that the "22 nm" peak was completely absent from the SAXS plot from digested gel. This makes me suspect that the SAXS peak represents the spacing between the spherical globules, not the size of the objects themselves. When ambiently dried gel was imaged with AFM, rope-like structures were observed weaving amongst the globules (Figure 3.3A-C). These structures were absent from the images of proteinase K-digested gel, which might indicate that they consist of proteins involved in holding the polymer network together. Elimination of these tethering protein ropes by enzymatic digestions, seemingly collapsed the polymer network (as evidenced by SAXS) and although the globules remained, they became dispersed at random in solution. A model of this hypothesis is shown in Figure 3.12.

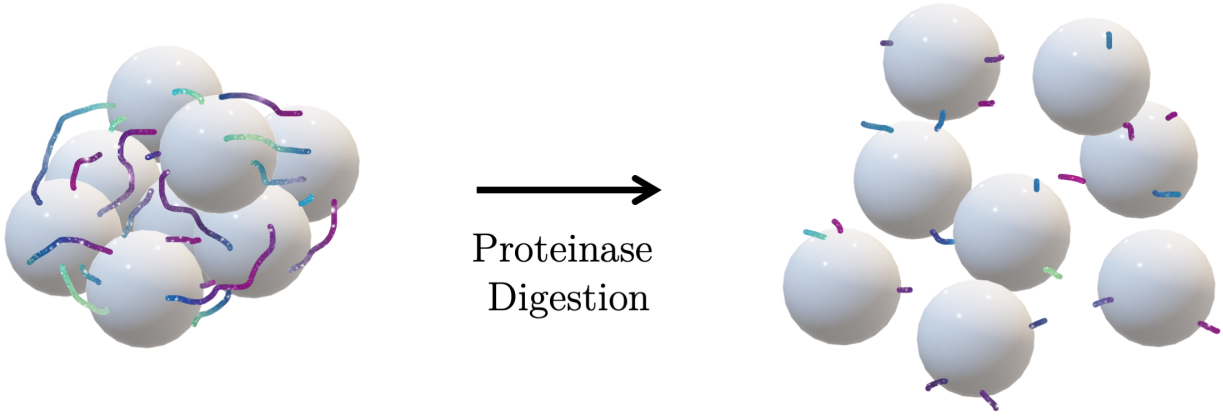


**Figure 3.12** Hypothetical model of AoL gel structure. Globules observed with SEM & AFM are depicted as white spheres. In this model, proteins (represented by multi-colored fibers) are shown holding the globules in close association at a distance between 10 and 100 nm when gel is in its native state (left). Digestion with proteinase K breaks up the majority of these proteins (right) which randomizes their spacing and collapses the organized polymer network.

I still don't know what AoL gel globules are composed of. In many cases, SEM and AFM revealed the presence of globules before and after proteinase K digestion, so I suspect that they are not (at least completely) composed of proteins. The microscopic results were variable, so I can't confidently claim that the globules widely observed in native gel were of the same nature as those observed in some of the digested gel samples. Even if proteins are ruled out, based on the experiments reported in this chapter, it is still unclear if the material remaining after proteinase K digestion was composed of polysaccharides, lipids, or some combination of macromolecules. It is very compelling that the AoL gel globules were similar in morphology to published images of chitosan nanoparticles (Haas et al 2005), so it is possible that the globules are composed of chitin. Following this logic, the fibrous structures that were observed with SEM in some of my digested samples could have been chitin nanofibers that were in a pure enough protein-free state that they became unbound from their previous configuration as globules.

Qualitative evidence from SDS PAGE suggested that proteinase K digestion is more effective in buffer than in water, and that small peptides remain after digestion regardless of the solution. The proteinase K-treated gel used for SAXS had been digested in PBS and wasn't dialyzed, but the polymer network was still collapsed, as evidenced by the shallow slope of the curve and the absence of peaks in the 10-100 nm range. This means that the elimination of large proteins (without removing small peptides/amino acids) was sufficient to drastically reduce the gel's stiffness and alter the molecular structure. However, because the yellow cloudy layer resulting from ultracentrifugation of digested gel was very fluid, it is likely that some of the gel's structural content was lost to the supernatant and any peaks that may have resulted from SAXS would not be present. It is also probable that some of the same material that settled in the native gel's white pellet, settled in the red pellet of the digested sample. That would explain why the two samples shared a ~5 nm peak in their SAXS plots. Because the peak was not eliminated in the proteinase K digested sample, it could be attributed to abundant lipid membranes from contaminating cells.

SDS PAGE is useful for comparing the relative sizes and abundances of protein between two samples on the same gel, however there are limitations if comparing results from two different gels. The two SDS PAG images shown in Figure 3.5 were stained with Coomassie Blue for different amounts of time so colorimetric comparison between gels would be inaccurate. Still, the gel shown in Figure 3.5B demonstrated the pretty intuitive finding that dialysis post-digestion eliminates small peptides and the larger the MWCO of the dialysis tubing, the more peptide is eliminated from the sample. Interestingly, most of the supercritically dried proteinase K-treated gel samples exhibited spherical morphologies as evidenced by SEM imaging. After comparing the three samples, I learned that the more protein pure the preparation, the smaller the observed particle size. Digested, non-dialyzed gel particles were roughly 1 $\mu$m in diameter while digested, 12-14 KDa dialyzed gel particles

were only 100 nm in average diameter. I suspect that the spherical particles result from the supercritical drying process itself and given that this same phenomenon did not occur when native gel was supercritically dried, the material properties seemed to play a role in their generation. When I removed proteins from the gel by digestion and sonicated the resulting material, I observed the formation of crystals that resembled chitin nanowhiskers (Figure 3.11D). This means that by eliminating protein from the gel, endogenous chitin can be manipulated to form characteristic structures such as whiskers, or nanoparticles (Mincea et al 2012, Zeng et al 2012). Hijazi et al supercritically dried chitosan and generated nanoparticles that looked remarkably similar to the spherical structures that were created by supercritically drying proteinase K-digested gel samples (Hijazi et al 2014). After Hijazi et al treated their chitosan samples with supercritical $CO_2$, the resulting nanoparticles were collected in solutions of varying pH, and they observed that the most uniform spherical nanoparticles resulted from solutions that were higher in pH (Hijazi et al 2014). Importantly, the non-dialyzed, digested gel solution had a pH of ~8 because it was maintained in enzyme buffer as compared to the dialyzed samples that were at pH of ~5 before exposure to supercritical $CO_2$. Still, I don't understand why the spherical nanoparticles varied so much in size between the three samples. Given that proteinase K digestion may release chitin from its polymeric network, it is compelling that particles similar in morphology to documented chitosan nanoparticles were generated by our methods.

I synthesized chitin nanowhiskers from AoL gel by extracting polysaccharides from gel samples using chemical (HCl & NaOH) treatments. I varied the extraction protocols over the course of my studies and consequently revealed multiple crystal morphologies (Figure 3.11). FTIR spectra and monosaccharide analyses (Chapter 1) using the same extracted samples revealed that the extraction methods removed keratan sulfate but not chitin. Knowing this, the observed crystal morphologies represent one more line of evidence

that chitin is present in AoL gel. I was intrigued to see that, when imaged with SEM and AFM, chitin appeared to take on a crystallized form far less readily than an amorphous one. This finding was supported by the shallow, wide peaks that were obtained with powder x-ray diffraction that were similar in shape to published images of amorphous chitin (Ioelovich 2014).

Although I was initially focused on identifying chitin's structural role in AoL gel specifically, a number of the experiments described in this chapter expanded our understanding of the gel's protein components. By comparing the proton conductivity of native and proteinase K-digested ratfish gel, for example, it is now understood that proteins do not play a direct role in the conductivity of the material, despite their clear contribution to the gel's stiffness. In fact, the proton conductivity data showed that proteins may actually dampen the gel's potential conductivity by influencing the position and/or availability of keratan sulfate – the component thought to confer the proton conductive abilities – inside the gel. These data, along with the SAXS spectra, did not inform which specific proteins play a role in the gel's structure and function, but they did suggest that proteins in general are critical for making the material gelatinous and for maintaining the structured polymer network, but not critical for proton conductivity.

Sample preparation techniques must be improved in order to reliably use AoL gel proteomes to determine which proteins compose the gel itself and which result from cellular contamination. The little skate proteome (Appendix 2) offered some interesting new evidence of a few proteins that may be candidate gel components based on their presence in AoL-specific transcriptomes and absence from the pelvic fin skin transcriptome. Given that many of the supposed contaminating proteins (e.g. keratins, actins) were highly expressed in both the AoL pore and pelvic fin skin transcriptomes, I presume that these proteins result from skin cells distribute throughout the gel samples. Proteins that are highly

expressed in AoL-specific transcriptomes and not in pelvic fin transcriptomes, are likely either gel components or proteins specific to AoL cells. Further, those proteins that are secretory in nature (e.g. lactotransferrin, otogelin) are more likely to be gel component candidates than those known nuclear or cytoplasmic proteins. Regardless, these determinations are still inference-based and imperfect and new methods must be explored to isolate the gel components from cellular debris. For example, it would be interesting to see if gel component proteins could be identified by pulling chitin and/or keratan sulfate out of gel solution and sequencing those proteins that are bound to the polysaccharides. No matter what, until we know which proteins are secreted into the AoL gel, it will be challenging to develop a structural model of the gel's molecular arrangement.

## 3.6 Acknowledgments

I want to thank our collaborators at the University of California, Merced (UCM). First, thanks to Linda Hirst, who helped familiarize me with her lab's atomic force microscope and fluorescence microscope and took some of the AFM and fluorescence images shown in the chapter. Linda and Alauna Wheeler went to UC Berkeley and performed the synchrotron experiments. Linda provided invaluable advice on how to interpret all data collected in this chapter. Thanks to Valerie Leppert, who provided technical SEM and XRD expertise. Thank you to Matthew Robinson, who captured all SEM images and ran the powder X-ray diffractometer at UC Merced. Matt was the mastermind behind our use of supercritical drying methodologies and always had enthusiastic ideas about how to interpret our results. Thank you to Richard Johnson and Mike MacCoss at the University of Washington for running proteomics analyses and helping us interpret our data using non-homologous alignment algorithms. Daniel Ocampo Daza annotated the little skate proteome (UW) and analyzed the significance of the top hits. This research used beamline 7.3.3 of

the Advanced Light Source, which is a DOE Office of Science User Facility under contract no. DE-AC02-05CH11231 (Hexemer et al 2010).

## 3.7 Chapter 3 References

Bodznick D, Northcutt RG. 1980. Segregation of Electro- and Mechanoreceptive Inputs to the Elasmobranch Medulla. *Brain Research* 195: 313-21

Brown BR, Hughes ME, Russo C. 2005. Infrastructure in the electric sense: admittance data from shark hydrogels. *J Comp Physiol A Neuroethol Sens Neural Behav Physiol* 191: 115-23

Buchtova N, Budtova T. 2016. Cellulose aero-, cryo- and xerogels: towards understanding of morphology control. *Cellulose* 23: 2585-95

Cardea S, Baldino L, De Marco I, Pisanti P, Reverchon E. 2013. Supercritical Gel Drying of Polymeric Hydrogels for Tissue Engineering Applications. *Chemical Engineering Transactions* 32: 1123-28

Chauhan A, Chauhan P. 2014. Powder XRD Technique and its Applications in Science and Technology. *Journal of Analytical and Bioanalytical Techniques* 5

Cohen-Salmon M, El-Amraoui A, Leibovici M, Petit C. 1997. Otogelin: a glycoprotein specific to the acellular membranes of the inner ear. *Proc Natl Acad Sci U S A* 94: 14450-5

Collin SP, Whitehead D. 2004. The functional roles of passive electroreception in non-electric fishes. *Animal Biology* 54: 1-25

Cotton JP. Small Angle Scattering and Polymers. 144-61

Djabourov M. 1988. Architecture of gelatin gels. *Contemporary Physics* 29: 273-97

Doyle J. 1967. The 'Lorenzan Sulphates' - A New Group of Vertebrate Mucopolysaccharides. *Biochemical Journal* 103: 325-30

Doyle J. 1968. The Lorenzan Sulphates: A Comparative Study. *Comparative Biochemistry and Physiology* 24: 479-85

Ganesan K, Budtova T, Ratke L, Gurikov P, Baudron V, et al. 2018. Review on the Production of Polysaccharide Aerogel Particles. *Materials (Basel)* 11

Ganesan K, Dennstedt A, Barowski A, Ratke L. 2016. Design of aerogels, cryogels and xerogels of cellulose with hierarchical porous structures. *Materials and Design* 92: 345-55

Gauthier ARG, Whitehead DL, Tibbetts IR, Cribb BW, Bennett MB. 2018. Morphological comparison of the ampullae of Lorenzini of three sympatric benthic rays. *J Fish Biol* 92: 504-14

Haas J, Ravi Kumar MN, Borchard G, Bakowsky U, Lehr CM. 2005. Preparation and characterization of chitosan and trimethyl-chitosan-modified poly-(epsilon-caprolactone) nanoparticles as DNA carriers. *AAPS PharmSciTech* 6: E22-30

Hexemer A, Bras W, J G, Schaible E, Gann E, et al. 2010. A SAXS/WAXS/GISAXS Beamline with Multilayer Mnochromator. *Journal of Physics: Conference Series* 247

Hijazi N, Rodier E, Letourneau J, Louati H, Sauceau M, et al. 2014. Chitosan nanoparticles generation using CO2 assisted processes. *Journal of Supercritical Fluids* 95: 118-28

How MJ, Jones JVS. 1969. Comparative Studies of Lorenzini Jelly from 2 Species of Elasmobranch .I. Preparation of Glycopeptides. *Carbohydrate Research* 11: 207-&

How MJ, Jones JVS, Stacey M. 1970. Comparative Studies of Lorenzini Jelly From Two Species of Elasmobranch. *Carbohydrate Research* 12: 171-81

Ifuku S, Saimoto H. 2012. Chitin nanofibers: preparations, modifications, and applications. *Nanoscale* 4: 3308-18

Inoue JG, Miya M, Lam K, Tay BH, Danks JA, et al. 2010. Evolutionary origin and phylogeny of the modern holocephalans (Chondrichthyes: Chimaeriformes): a mitogenomic perspective. *Mol Biol Evol* 27: 2576-86

Ioelovich M. 2014. Crystallinity and Hydrophility of Chitin and Chitosan. *Research and Reviews: Journal of Chemistry* 3: 7-14

Johnson RS, Searle BC, Nunn BL, Gilmore JM, Phillips M, et al. 2020. Assessing Protein Sequence Database Suitability Using De Novo Sequencing. *Mol Cell Proteomics* 19: 198-208

Josberger EE, Hassanzadeh P, Deng Y, Sohn J, Rego MJ, et al. 2016. Proton Conductivity in ampullae of Lorenzini jelly. *Science Advances* 2: e1600112: 1-6

Kalmijn AJ. 1974. The Detection of Electric Fields from Inanimate and Animate Sources Other Than Electric Organs In *Handbook of Sensory Physiology: Electroreceptors and Other Specialized Receptors in Lower Vertebrates*, pp. 147-200

Kikhney AG, Svergun DI. 2015. A practical guide to small angle X-ray scattering (SAXS) of flexible and intrinsically disordered proteins. *FEBS Lett* 589: 2570-7

Mincea M, Negrulescu A, Ostafe V. 2012. Preparation, Modification, and Applications of Chitin Nanowhiskers: A Review. *Reviews on Advanced Materials Science* 30: 225-42

Murray RW, Potts WTW. 1961. The Composition of the Endolymph, Perilymph, and Other Body Fluids of Elasmobranchs. *Comparative Biochemistry and Physiology* 2: 65-75

Newton KC, Gill AB, Kajiura SM. 2019. Electroreception in marine fishes: chondrichthyans. *J Fish Biol* 95: 135-54

Phillips R. 2018. Membranes by the Numbers In *Physics of Biological Membranes*, ed. P Bassereau, P Sens, pp. 73-105. Switzerland: Springer Nature

Quignard F, Valentin R, Di Renzo F. 2008. Aerogel materials from marine polysaccharides. *New Journal of Chemistry* 32: 1300-10

Sahin I, Ozbakir Y, Inonu Z, Ulker Z, Erkey C. 2017. Kinetics of Supercritical Drying of Gels. *Gels* 4

Selberg J, Jia M, Rolandi M. 2019. Proton conductivity of glycosaminoglycans. *PLoS One* 14: e0202713

Siqueiros-Cendon T, Arevalo-Gallegos S, Iglesias-Figueroa BF, Garcia-Montoya IA, Salazar-Martinez J, Rascon-Cruz Q. 2014. Immunomodulatory effects of lactoferrin. *Acta Pharmacol Sin* 35: 557-66

Tricas TC, Michael SW, Sisneros JA. 1995. Electrosensory optimization to conspecific phasic signals for mating. *Neuroscience Letters* 202: 129-32

Waltman B. 1966. Electrical properties and fine structure of the ampullary canals of Lorenzini. *Acta physiologica Scandinavica* 66: 3-60

Whitehead DL, Gauthier AR, Mu EW, Bennett MB, Tibbetts IR. 2015. Morphology of the ampullae of Lorenzini in juvenile freshwater Carcharhinus leucas. *J Morphol* 276: 481-93

Wueringer BE, Tibbetts IR, Whitehead DL. 2008. Ultrastructure of the ampullae of Lorenzini of Aptychotrema rostrata (Rhinobatidae). *Zoomorphology* 128: 45-52

Zeng JB, He YS, Li SL, Wang YZ. 2012. Chitin Whiskers: An Overview. *Biomacromolecules* 13: 1-11

Zhang X, Xia K, Lin L, Zhang F, Yu Y, et al. 2018. Structural and Functional Components of the Skate Sensory Organ Ampullae of Lorenzini. *ACS Chem Biol*

# Conclusions & Future Directions

When the discovery of vertebrate chitin was first published in 2015, it came with a plethora of new questions about the nature, distribution, and evolution of the versatile polysaccharide (Tang et al 2015). At the time that this dissertation was submitted (June 2020), chitin had only been described in less than a dozen vertebrate species even though a simple BLAST search would reveal that chitin synthase (*CHS*) genes are widespread in numerous vertebrate clades – a detailed documentation of vertebrate *CHS* genes will soon be published by researchers in the Amemiya lab. Therefore, the study of vertebrate chitin is an emerging field of science and the findings laid out in this dissertation, many of which descriptive in nature, highlight chitin's distribution and characteristics within an anatomic system where it had not previously been observed before.

The Ampullae of Lorenzini were discovered centuries ago and have been thoroughly studied for decades, yet the details of how they function have remained a complete black box. We still do not understand how electric field signals "enter" the pores, move through the organs and trigger responses within the specialized electrosensory cells of the alveoli. Electric field signals must pass through a stiff, proton conductive hydrogel to be detected at the distal end of the canals, and in my view, a deeper understanding of the gel's properties will inevitably shed light on the overall function of the Ampullae of Lorenzini themselves. To that end, the discovery of chitin within AoL gel progresses our knowledge of both the electrosensory system itself and the various roles of chitin within the vertebrate lineage.

When I set out to study the synthesis of chitin in the AoL of cartilaginous fishes five years ago, I was fixated on determining what role it played in the system as a whole. There were three main hypotheses that I wanted to test, and I only scratched the surface of two of them. First, I tried to test if chitin is involved in the establishment and maintenance of the tubular structure of the AoL in a similar way that chitin expands and shapes the

spiracles in insects (Devine et al 2005). To study this, I exposed developing little skate embryos to CHS-inhibiting drugs with the hope of disrupting chitin synthesis, but a combination of outside variables prevented my ability to draw any major conclusions. In retrospect, it seems unlikely that chitin plays a major (or even minor) role in the establishment of AoL shape given that, unlike insect spiracles, a layer of collagen makes up the outermost layer of AoL tubes and provides a rigidity that is hard to break even with forceps and the force of a human hand (I know this from experience)!

Upon learning about the proton conductivity of AoL gel, I hypothesized that chitin plays either a direct role in the movement of protons or perhaps it plays a supporting role as a scaffold decorated with units of proton conductive keratan sulfate. Studies have shown that chitin is not itself proton conductive (Zhong et al 2011), however it is possible that AoL chitin is modified in a way that confers proton conductivity (i.e. *via* sulfation). With researchers at UC Santa Cruz, I learned that when proteins are removed from AoL gel, the conductivity of the remaining solution is markedly higher than that of native gel. Although these results are informative and compelling, it is still unclear which remaining components, of which there are two main candidates: keratan sulfate and chitin, confer the observed proton conductivity. Based on its known proton conductivity (Selberg et al 2019), keratan sulfate is inevitably a major contributor, but to what extent chitin contributes is still unclear. And so, like the first, my second hypothesis was not completely tested. I originally wanted to compare the proton conductivity of proteinase K-digested gel to gel treated with both chitinase and proteinase K. I figured that this method might allow me to discern slight differences between the gel's keratan sulfate component and the gel's total polysaccharide component (keratan sulfate + chitin). Maybe then chitin's contribution to the proton conductivity could be subtracted from the two values. However, there is an inevitable variation in the starting volumes of gel samples which makes direct comparisons of the

resulting conductivity values somewhat inaccurate. Instead, it seems more feasible and more informative to determine whether or not AoL gel chitin is modified and then assess whether or not those modifications might make the molecules proton conductive (or at the very least, soluble).

Some evidence has shown that chitin has bacteriostatic effects on several microbial species (Benhabiles et al 2012). Therefore, a third hypothetical role of chitin in AoL gel is that it offers the organs (and the material itself) some protection from pathogens that could easily invade from the environment. I did not explore this potential function in my dissertation studies but hope to someday learn if any of my proposed hypothetical roles, or perhaps a combination of these roles can explain the presence of chitin in AoL gel.

So far, chitin has been documented in the guts of several vertebrate species where it was inferred to form a barrier separating the gut epithelium from potentially pathogenic ingested microbes (Nakashima et al 2018, Tang et al 2015). I did not search for chitin in the guts of cartilaginous fishes although, given the phylogenetic distribution of the trait, I expect that it would also be found there. The chitinous barrier membrane observed in fish guts is unlike chitinous AoL gel in that it consists of characteristic chitin nanofibers composing a rigid network more similar to the chitinous structures of invertebrates than the amorphous structure of AoL gel.

Researchers in the Amemiya lab published some observations on the distribution of chitin in the skin of fish and salamanders (Tang et al 2015) and since then, we have continually observed highly specific signals from chitin binding probes (CBD) in the skin of many more fish species (see Figure 1.9, for example). The implications of chitinous secretions on the skin are still unknown. Perhaps, as is also possible with AoL gel, chitin on and in fish skin serves an antimicrobial role. I am currently under the impression that the mysterious chitinous organs described in Chapter 2 and referred to as “blobs,” secrete chitin

as a mucosal component on the skin. However, if this is the case, it is peculiar that CBD labeling is always observed brightly just on top of the blobs and not in a dispersed gradient around the structures. Regardless, although the study of vertebrate chitin has just begun, the polysaccharide has already been observed in a diverse distribution of anatomic systems and in various forms. For this reason, vertebrate chitin can be compared to a sort of Swiss Army Knife, but with many of its retractable tools still undiscovered.

It is important to address the ecological implications of our discovery of vertebrate chitin. In Chapter 2, I discussed the widespread use of CHS inhibitors as pesticides in both terrestrial agriculture and aquaculture. Studies have shown that these CHS inhibitors are not lethal to fish when ingested, but in the context of fish farms, they accumulate dramatically in the natural environment surrounding the fish enclosures (Olsvik et al 2013, Selvik et al 2002). Importantly, these studies precede 2015, so researchers were operating under the assumption that chitin is not synthesized by vertebrates! In light of our findings about the distribution of chitin amongst vertebrates, particularly in aqueous ecosystems, it is imperative that the potential impacts of CHS inhibitors are addressed more widely. Due to a number of variables described in Chapter 2, I was unable to determine whether or not two CHS inhibitors (diflubenzuron and nikkomycin Z) had an effect on chitin synthesis in little skate embryos. However, some preliminary data collected by researchers in the Amemiya lab showed that diflubenzuron and another CHS inhibitor called, "pseurotin A" had drastic effects when zebrafish were reared in water containing 0.1 $\mu$M drug solutions (unpublished data). The eyes of the drug-treated zebrafish were greatly reduced, they exhibited signs of cardiac edema, and were generally shrunken as compared to wild-type animals. These initial findings raise many questions and imply that further chitin synthase inhibition experiments with diverse vertebrate taxa are all the more urgent.

I am fascinated by the untold evolutionary story of chitin in the AoL. I serendipitously examined the distribution of CBD signals in a number of diverse chondrichthyans and yet there were many orders, and the vast majority of species, that remain unsampled (see Figure 1.2D). Still, based on the sampling that was accomplished, the most parsimonious scenario would suggest that chitinous AoL gel evolved in the ancestors to all chondrichthyans. Therefore, the distribution of this trait outside the class Chondrichthyes it is still unknown and of great interest. I attempted some preliminary CBD histochemistry experiments with paddlefish (fish that possess ancestral electrosensory organs) as well as two species of electrosensory teleost fishes and in all cases, my findings were inconclusive. To learn if the gel inside these electrosensory organs contains chitin, in addition to CBD histochemistry, spatial *CHS* expression analyses must be conducted with both electroreceptive teleost fishes as well as non-chondrichthyan fishes that possess ancestral electrosensory systems (i.e. sturgeons, paddlefish, etc). The morphologies of electrosensory organs amongst fishes are very diverse (especially when comparing the ancestral ampullary organs to teleost tuberous organs) and yet, most types contain a stiff gel (Baker et al 2013). Whether teleost fishes independently evolved a chitinous gel inside their electrosensory organs or not, the finding is still very interesting. In one potential outcome, chitin is such an essential electrosensory organ gel component that it evolved multiple times. On the other hand, if teleosts do not use chitin in the gel of their electrosensory organs, then that could imply that the function of chitin in ancestral ampullary organs is replaceable.

When I began this research in early 2016, the little skate (*Leucoraja erinacea*), a benthic Atlantic species, the whale shark (*Rhincodon typus*), the largest fish in the world, and the elephant shark (*Callorhincus milii*), a deep-sea chimaera, were the only cartilaginous fish species with available genomes. Although it arguably had the most poorly annotated

genome of the three, I performed the most exhaustive *CHS* expression studies on little skates simply because they are relatively easily accessible and culturable. I don't think I necessarily would have used a different study system, but it is interesting to consider that available chondrichthyan genomes have more than tripled in just a few short years. The biggest limitation of my *CHS* experiments was the fact that I couldn't use injection-based gene knockdown experiments to observe the effects of removing chitin synthase enzymes from developing little skate embryos. I am hopeful that, as more and more vertebrate chitin synthase genes become identified, it is only a matter of time until knockdowns are performed on chondrichthyans and the wide-reaching impacts of chitin synthesis can be explored.

Innumerable questions remain about the structure of AoL gel. Firstly, do the features described in Chapter 3 hold true for all chondrichthyan species? Both published accounts and my own experiences have shown that there is a large variation in the stiffness of gel from different chondrichthyan species (Doyle 1967). It is unclear how the molecular components and structure translate to the observed stiffnesses of each species gel. Next, I am still plagued by the question that launched my structural inquiries in the first place: how are the molecules arranged in AoL gel? To glean a deeper understanding of both chitin's function, and more broadly, the gel's function in the context of electrosensory organs, we need to know how the molecules interact and organize. When I first began exploring the structure of native gel with AFM and SEM, I was operating with a loose hypothesis that the gel structure might take on a form similar to that of aggrecan in cartilage (Morgelin et al 1994, Ng et al 2003). Aggrecan is a proteoglycan consisting of a protein core bound by molecules of chondroitin sulfate and keratan sulfate (Kiani et al 2002). In cartilage, aggrecan molecules connect to a "backbone" of hyaluronic acid, a polysaccharide similar to chitin in that it is non-sulfated and composed of *N*-acetylglucosamine in addition to glucuronic acid.

These hyaluronic acid molecules connect to aggrecan proteoglycans *via* so-called linker proteins and form a large complex.

Given that AoL gel contains keratan sulfate and chitin, we figured that perhaps it was comprised of a somewhat similar proteoglycan structure. Well, I never achieved an appropriate dilution, the proper conditions, nor the right resolution to resolve individual molecules within AoL gel using either SEM or AFM. Instead, the only structural consistency observed with native gel was the widespread distribution of globules, the presence of which were confirmed by SAXS. I can't say definitively what the globules are composed of specifically as images of proteinase K-digested gel revealed a number of artefacts and some unexplained observations. However, the fact that globules were observed within many of the proteinase K-digested samples could suggest that they are composed, at least in part, of chitin. The bulk of my structural gel analyses focused on the polysaccharide and protein components of AoL gel, but the lipid content of AoL gel must be considered going forward. In some circumstances with SEM, large droplets of material were observed dotted across the stub surface and with various gel preparations. These droplets resembled the appearance of oil on a wet plate but were never studied. Lipidomic analysis of gel material would certainly help to fill in some blanks, however, as with proteomics, it would be challenging to distinguish between cellular contaminant and potential lipid components in the gel. Alternatively, the addition of a phenol/chloroform extraction step to our established chitin isolation protocol would likely increase the purity of extracted polysaccharide content in future analyses.

When proteins were removed from the gel material, crystals that resembled chitin nanowhiskers were formed by a small percentage of the remaining material, while the rest appeared to aggregate in an amorphous form. It is still unclear if the amorphous material failed to crystalize due to the presence of small peptides that somehow remained after

extraction or if it was simply a property of the chitinous material itself. Further methods should be employed to explore the properties of this amorphous material so that we can truly understand the nature of the chitin synthesized inside the Ampullae of Lorenzini.

## Conclusions & Future Directions References

Baker CV, Modrell MS, Gillis JA. 2013. The evolution and development of vertebrate lateral line electroreceptors. *J Exp Biol* 216: 2515-22

Benhabiles MS, Salah R, Lounici H, Drouiche N, Goosen MFA, Mameri N. 2012. Antibacterial activity of chitin, chitosan and its oligomers prepared from shrimp shell waste. *Food Hydrocolloids* 29: 48-56

Devine WP, Lubarsky B, Shaw K, Luschnig S, Messina L, Krasnow MA. 2005. Requirement for chitin biosynthesis in epithelial tube morphogenesis. *PNAS* 102: 17014-19

Doyle J. 1967. The 'Lorenzan Sulphates' - A New Group of Vertebrate Mucopolysaccharides. *Biochemical Journal* 103: 325-30

Kiani C, Chen L, Wu YJ, Yee AJ, Yang BB. 2002. Structure and function of aggrecan. *Cell Res* 12: 19-32

Morgelin M, Heinegard D, Engel J, Paulsson M. 1994. The cartilage proteoglycan aggregate: assembly through combined protein-carbohydrate and protein-protein interactions. *Biophys Chem* 50: 113-28

Nakashima K, Kimura S, Ogawa Y, Watanabe S, Soma S, et al. 2018. Chitin-based barrier immunity and its loss predated mucus-colonization by indigenous gut microbiota. *Nat Commun* 9: 3402

Ng L, Grodzinsky AJ, Patwari P, Sandy J, Plaas A, Ortiz C. 2003. Individual cartilage aggrecan macromolecules and their constituent glycosaminoglycans visualized via atomic force microscopy. *Journal of Structural Biology* 143: 242-57

Olsvik PA, Samuelsen OB, Erdal A, Holmelid B, Lunestad BT. 2013. Toxicological assessment of the anti-salmon lice drug diflubenzuron on Atlantic cod Gadus morhua. *Dis Aquat Organ* 105: 27-43

Selberg J, Jia M, Rolandi M. 2019. Proton conductivity of glycosaminoglycans. *PLoS One* 14: e0202713

Selvik A, Hansen PK, Ervik A, Samuelsen OB. 2002. The stability and persistence of diflubenzuron in marine sediments studied under laboratory conditions and the

dispersion to the sediment under a fish farm following medication. *Sci Total Environ* 285: 237-45

Tang WJ, Fernandez J, Sohn JJ, Amemiya CT. 2015. Chitin is endogenously produced in vertebrates. *Curr Biol* 25: 897-900

Zhong C, Deng Y, Roudsari AF, Kapetanovic A, Anantram MP, Rolandi M. 2011. A polysaccharide bioprotonic field-effect transistor. *Nat Commun* 2: 476

# Appendix 1

## Proton Conductivity of Little Skate (*Leucoraja erinacea*) Gel

While studying the differences in proton conductivity between native ratfish gel and proteinase K-digested gel with Manping Jia at UC Santa Cruz, I had brought a sample of gel extracted from a little skate (*Leucoraja erinacea*) and figured that it would be interesting to determine whether or not the material was proton conductive. Josberger et al had previously examined the proton conductive properties of gel from bonnethead shark (*Sphyrna tiburo*), big skate (*Raja binoculata*), and longnose skate (*Raja rhina*) but did not study gel from the little skate (Josberger et al 2016). We used a different assay to investigate the proton conductivity of little skate gel than the one used with ratfish gel in Chapter 3. The assay employed an electrical device and methodologies very similar to those described in (Josberger et al 2016). AoL gel was positioned on top of the device so that it pooled between two palladium contacts. When voltage was applied to the source contact, protons were injected from the source contact into the jelly. These protons were then drained into the second contact where the displacement of electrons could be measured as current. The relative humidity (RH) of the environment was controlled around the device and the difference between 50% and 90% humidity were compared. A slight increase in current was observed when the humidity was increased, which is what would be expected from a proton conductive material as water vapor offers a small supply of protons to the environment (Figure A1). Subsequently, when protons were introduced to the device by the addition of $H_2$ gas to the chamber, Manping and I observed a marked increase in current (Figure A1). These observations indicated that little skate AoL gel is proton conductive.

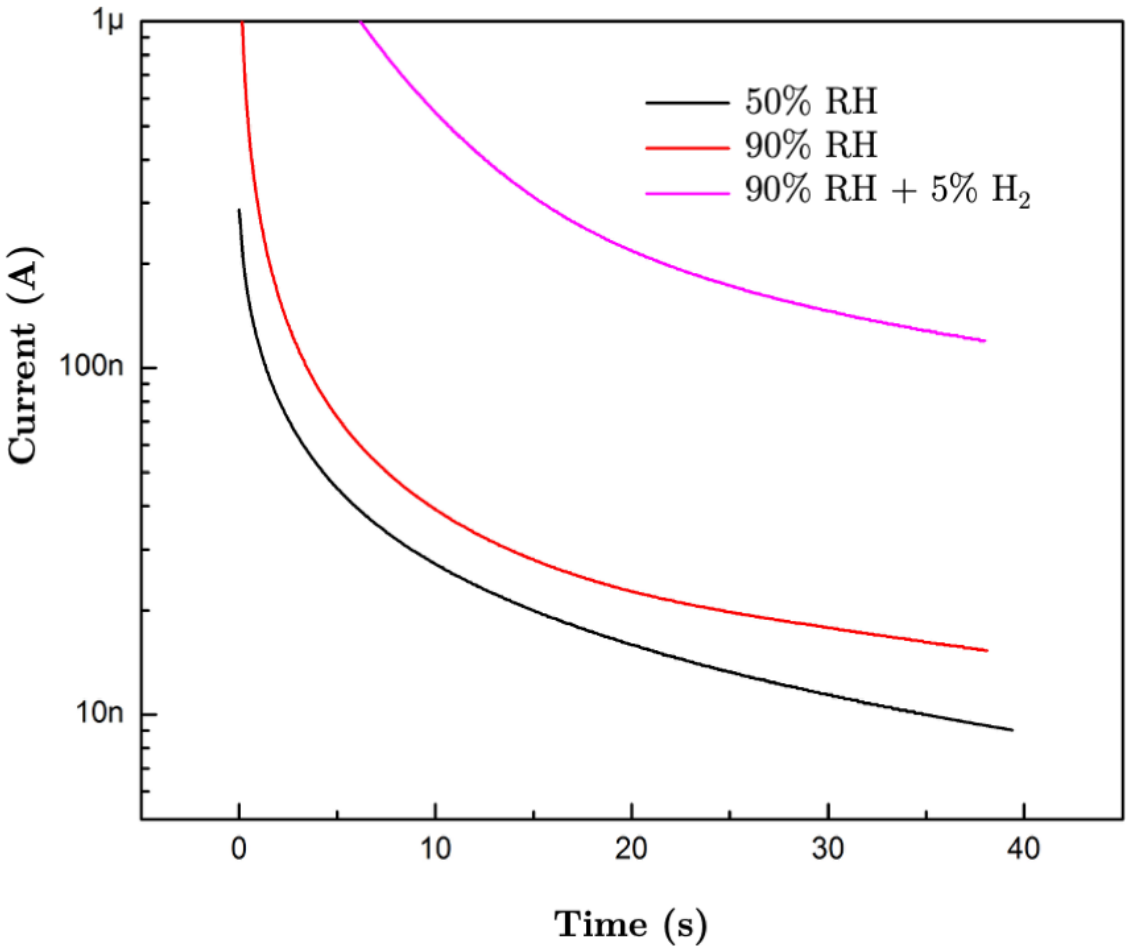


**Figure A1** Little skate AoL gel response rate to voltage under various conditions. We observed a slight increase in current when we increased the humidity from 50% to 90% (black & red). After protons were introduced to the environment by adding 5% H2 gas, we saw a very large increase in current (pink).

## Appendix 1 References

Josberger EE, Hassanzadeh P, Deng Y, Sohn J, Rego MJ, et al. 2016. Proton Conductivity in ampullae of Lorenzini jelly. *Science Advances* 2: e1600112: 1-6

# Appendix 2

## Proteomes

### Top 50 hits of proteome from spotted ratfish (*Hydrolagus colliei*) AoL gel

| Protein | Protein Description | Percent Coverage | Tot Indep Spectra |
|---|---|---|---|
| tr\|V9KJC7\|V9KJC7_CALMI tr\|V9KNJ0\|V9KNJ0_CALMI | Keratin, type II cytoskeletal 8 OS=Callorhinchus milii PE=2 SV=1;Keratin, type II cytoskeletal 8 OS=Callorhinchus milii PE=2 SV=1 | 46.1 | 251 |
| tr\|V9KMR0\|V9KMR0_CALMI | Keratin, type II cytoskeletal 8 OS=Callorhinchus milii PE=2 SV=1 | 45.2 | 228 |
| tr\|V9K7R6\|V9K7R6_CALMI | Myosin-9-like protein OS=Callorhinchus milii PE=2 SV=1 | 18 | 82 |
| tr\|V9K8N6\|V9K8N6_CALMI | Neuroblast differentiation-associated protein AHNAK-like protein (Fragment) OS=Callorhinchus milii PE=2 SV=1 | 27.9 | 106 |
| tr\|K4FTZ1\|K4FTZ1_CALMI tr\|K4GFR7\|K4GFR7_CALMI | Actin, cytoplasmic 1 OS=Callorhinchus milii PE=2 SV=1;Actin, cytoplasmic 1 OS=Callorhinchus milii PE=2 SV=1 | 46.9 | 88 |
| tr\|V9KMT3\|V9KMT3_CALMI | Type I keratin K18 OS=Callorhinchus milii PE=2 SV=1 | 29.8 | 80 |
| tr\|V9KBM8\|V9KBM8_CALMI | Alpha-actinin-1-like protein OS=Callorhinchus milii PE=2 SV=1 | 23.6 | 47 |
| tr\|K4G587\|K4G587_CALMI tr\|K4GDF4\|K4GDF4_CALMI tr\|K4GEN0\|K4GEN0_CALMI | Actin, alpha 2, smooth muscle, aorta OS=Callorhinchus milii PE=2 SV=1;Actin, alpha 2 OS=Callorhinchus milii PE=2 SV=1;Actin, alpha 2 OS=Callorhinchus milii PE=2 SV=1 | 29.4 | 70 |
| sp\|K2C1_HUMAN\|K2C1_HUMAN | K2C1 OS=HUMAN GN=None PE=None SV=None | 27.2 | 53 |
| tr\|V9L6V6\|V9L6V6_CALMI | Type I keratin K18 (Fragment) OS=Callorhinchus milii PE=2 SV=1 | 47.7 | 63 |
| tr\|V9L895\|V9L895_CALMI | Keratin, type I cytoskeletal 42-like protein (Fragment) OS=Callorhinchus milii PE=2 SV=1 | 30.7 | 55 |
| tr\|V9KBJ1\|V9KBJ1_CALMI tr\|V9KD83\|V9KD83_CALMI | Alpha-actinin-1-like protein OS=Callorhinchus milii PE=2 SV=1;Alpha-actinin-1-like protein OS=Callorhinchus milii PE=2 SV=1 | 20.9 | 32 |
| tr\|K4GC47\|K4GC47_CALMI | Heat shock cognate protein OS=Callorhinchus milii PE=2 SV=1 | 24 | 30 |
| tr\|K4G3P3\|K4G3P3_CALMI tr\|K4GH77\|K4GH77_CALMI | Keratin, type I cytoskeletal 42 OS=Callorhinchus milii PE=2 SV=1;Keratin, type I cytoskeletal 42-like protein OS=Callorhinchus milii PE=2 SV=1 | 25.3 | 25 |
| tr\|V9KFV0\|V9KFV0_CALMI | Gelsolin-like protein OS=Callorhinchus milii PE=2 SV=1 | 13.4 | 26 |
| tr\|V9KGV8\|V9KGV8_CALMI | Heat shock protein 90kDa alpha (Cytosolic), class B member 1 OS=Callorhinchus milii PE=2 SV=1 | 9.5 | 26 |
| tr\|V9K7C1\|V9K7C1_CALMI | Filamin-B OS=Callorhinchus milii PE=2 SV=1 | 6.7 | 18 |
| tr\|V9KDP3\|V9KDP3_CALMI | Protein-arginine deiminase type-2-like protein OS=Callorhinchus milii PE=2 SV=1 | 12.4 | 19 |
| tr\|V9KCA6\|V9KCA6_CALMI | Transitional endoplasmic reticulum ATPase OS=Callorhinchus milii PE=2 SV=1 | 9.4 | 15 |
| sp\|K22E_HUMAN\|K22E_HUMAN | K22E OS=HUMAN GN=None PE=None SV=None | 6.7 | 24 |
| tr\|V9KBN2\|V9KBN2_CALMI tr\|V9KDC4\|V9KDC4_CALMI | Transketolase OS=Callorhinchus milii PE=2 SV=1;Transketolase OS=Callorhinchus milii PE=2 SV=1 | 13.9 | 21 |
| tr\|V9KIX2\|V9KIX2_CALMI | 14-3-3 protein theta-like protein OS=Callorhinchus milii PE=2 SV=1 | 22.6 | 18 |
| tr\|K4FSH1\|K4FSH1_CALMI tr\|K4G4H2\|K4G4H2_CALMI | Tubulin beta chain OS=Callorhinchus milii PE=2 SV=1;Tubulin beta chain OS=Callorhinchus milii PE=2 SV=1 | 21.6 | 15 |
| tr\|K4G9R8\|K4G9R8_CALMI | Elongation factor 1-alpha OS=Callorhinchus milii PE=2 SV=1 | 19.3 | 34 |
| tr\|K4FYM9\|K4FYM9_CALMI | Tubulin alpha chain OS=Callorhinchus milii PE=2 SV=1 | 15.1 | 15 |
| tr\|K4G0N9\|K4G0N9_CALMI tr\|K4GEV1\|K4GEV1_CALMI | RhoA OS=Callorhinchus milii PE=2 SV=1;RhoA-like protein OS=Callorhinchus milii PE=2 SV=1 | 30.1 | 15 |
| tr\|V9K7A9\|V9K7A9_CALMI | Clathrin heavy chain OS=Callorhinchus milii PE=2 SV=1 | 8.2 | 15 |
| tr\|V9K7U2\|V9K7U2_CALMI | Desmoplakin OS=Callorhinchus milii PE=2 SV=1 | 4.8 | 13 |
| tr\|V9L0F5\|V9L0F5_CALMI | Protein-glutamine gamma-glutamyltransferase 2 (Fragment) OS=Callorhinchus milii PE=2 SV=1 | 15.4 | 10 |
| tr\|V9K7B7\|V9K7B7_CALMI | Apolipoprotein B OS=Callorhinchus milii PE=2 SV=1 | 2.3 | 10 |
| tr\|V9LIG4\|V9LIG4_CALMI tr\|V9LJI3\|V9LJI3_CALMI | Histone H2B OS=Callorhinchus milii PE=2 SV=1;Histone H2B (Fragment) OS=Callorhinchus milii PE=2 SV=1 | 30.4 | 20 |
| tr\|K4FSQ1\|K4FSQ1_CALMI tr\|K4GDC7\|K4GDC7_CALMI tr\|K4GDU2\|K4GDU2_CALMI tr\|K4GHP7\|K4GHP7_CALMI tr\|V9KL59\|V9KL59_CALMI | Asparaginyl-tRNA synthetase-like protein OS=Callorhinchus milii PE=2 SV=1;Asparaginyl-tRNA synthetase, cytoplasmic-like protein OS=Callorhinchus milii PE=2 SV=1;Asparaginyl-tRNA synthetase, cytoplasmic-like protein OS=Callorhinchus milii PE=2 SV=1;Asparaginyl-tRNA synthetase, cytoplasmic-like protein OS=Callorhinchus milii PE=2 SV=1;Asparaginyl-tRNA synthetase, cytoplasmic-like protein OS=Callorhinchus milii PE=2 SV=1 | 10.2 | 18 |
| tr\|V9KG52\|V9KG52_CALMI tr\|V9KID9\|V9KID9_CALMI | Gelsolin OS=Callorhinchus milii PE=2 SV=1;Gelsolin OS=Callorhinchus milii PE=2 SV=1 | 9.5 | 17 |
| tr\|V9K8Q4\|V9K8Q4_CALMI | Myosin-10 (Fragment) OS=Callorhinchus milii PE=2 SV=1 | 4.4 | 17 |
| sp\|K1C10_HUMAN\|K1C10_HUMAN | K1C10 OS=HUMAN GN=None PE=None SV=None | 19.7 | 11 |
| tr\|V9KJM0\|V9KJM0_CALMI | Tropomyosin alpha-4 chain-like protein OS=Callorhinchus milii PE=2 SV=1 | 27.8 | 10 |
| tr\|K4G460\|K4G460_CALMI tr\|K4GHK2\|K4GHK2_CALMI | Anterior gradient protein 3-like protein OS=Callorhinchus milii PE=2 SV=1;Anterior gradient protein 3-like protein OS=Callorhinchus milii PE=2 SV=1 | 17 | 18 |
| tr\|K4FT44\|K4FT44_CALMI | Transferrin OS=Callorhinchus milii PE=2 SV=1 | 9.4 | 16 |
| tr\|K4GC64\|K4GC64_CALMI tr\|K4GJZ4\|K4GJZ4_CALMI | ATP synthase subunit alpha OS=Callorhinchus milii PE=2 SV=1;ATP synthase subunit alpha OS=Callorhinchus milii PE=2 SV=1 | 7.9 | 13 |
| tr\|K4G067\|K4G067_CALMI tr\|K4G3M7\|K4G3M7_CALMI tr\|K4GEZ7\|K4GEZ7_CALMI | Tubulin alpha chain OS=Callorhinchus milii PE=2 SV=1;Tubulin alpha chain OS=Callorhinchus milii PE=2 SV=1;Tubulin alpha chain OS=Callorhinchus milii PE=2 SV=1 | 15.1 | 13 |
| tr\|V9K787\|V9K787_CALMI tr\|V9K7C4\|V9K7C4_CALMI tr\|V9K7D2\|V9K7D2_CALMI | Spectrin alpha chain, brain OS=Callorhinchus milii PE=2 SV=1;Spectrin alpha chain, brain OS=Callorhinchus milii PE=2 SV=1;Spectrin alpha chain, brain-like protein OS=Callorhinchus milii PE=2 SV=1 | 4.4 | 12 |
| tr\|V9L801\|V9L801_CALMI | 14-3-3 protein beta/alpha-like protein OS=Callorhinchus milii PE=2 SV=1 | 21 | 8 |
| tr\|V9KIH1\|V9KIH1_CALMI | 78 kDa glucose-regulated protein-like protein OS=Callorhinchus milii PE=2 SV=1 | 13.2 | 7 |
| tr\|V9KM01\|V9KM01_CALMI | 14-3-3 protein epsilon OS=Callorhinchus milii PE=2 SV=1 | 16.9 | 3 |
| tr\|V9KUA9\|V9KUA9_CALMI | Tubulin alpha chain OS=Callorhinchus milii PE=2 SV=1 | 14.5 | 13 |
| tr\|V9KCM1\|V9KCM1_CALMI | Alpha-actinin-3-like protein OS=Callorhinchus milii PE=2 SV=1 | 7 | 11 |
| tr\|V9K962\|V9K962_CALMI | Filamin-A (Fragment) OS=Callorhinchus milii PE=2 SV=1 | 5.8 | 10 |
| tr\|V9KCD6\|V9KCD6_CALMI | Serine/threonine-protein kinase PAK 2-like protein OS=Callorhinchus milii PE=2 SV=1 | 12.7 | 10 |
| tr\|V9K784\|V9K784_CALMI tr\|V9K7I0\|V9K7I0_CALMI | Spectrin beta chain OS=Callorhinchus milii PE=2 SV=1;Spectrin beta chain OS=Callorhinchus milii PE=2 SV=1 | 3.1 | 9 |

Top 100 hits of proteome from little skate (*Leucoraja erinacea*) AoL gel

| | Transcriptome Data | | | |
|---|---|---|---|---|
| **Predicted Gene Name** | **Pore TPM** | **Canal TPM** | **Hyoid TPM** | **Pelvic Fin TPM** |
| Krt17-2 | 19162.4 | 1818.54 | 592.029 | 19457.8 |
| Krt17-2 | 7506.31 | 1345.26 | 459.832 | 6828.81 |
| Krt8-2 | 6501.13 | 1126.99 | 551.28 | 5060.54 |
| Ltf-3 | 191.621 | 4427.65 | 457.394 | 2.1257 |
| Tgm2-6 | 5437.48 | 762.719 | 226.974 | 2482.26 |
| UnkProt_6932 | 725.983 | 30626.4 | 27148.6 | 0 |
| Dsp | 277.613 | 80.2141 | 30.2427 | 187.221 |
| Ppl-2 | 147.492 | 249.026 | 95.8073 | 71.1206 |
| Cast | 359.578 | 72.0221 | 43.5819 | 194.631 |
| Scin-2 | 429.845 | 115.686 | 43.8497 | 387.654 |
| Scin-2 | 2.11E-06 | 5.63068 | 9.56247 | 4.60859 |
| Cndp2-1 | 67.9702 | 14.1211 | 14.5332 | 429.579 |
| Otog | 13.3307 | 61.782 | 36.9083 | 0.396625 |
| Hspa8-6 | 1603.37 | 1615.57 | 1496.61 | 1962.34 |
| Fbn2-4 | 46.4788 | 281.625 | 84.9649 | 0.0523783 |
| Actb-6 | 1532.35 | 596.984 | 246.913 | 1651.23 |
| Myh9 | 167.021 | 61.9851 | 21.8524 | 64.3457 |
| Actb-5 | 560.199 | 279.986 | 107.443 | 497.475 |
| Actg1-1 | 604.082 | 419.501 | 162.289 | 587.824 |
| Capn2-3 | 602.638 | 105.081 | 71.576 | 494.173 |
| Hephl1 | 1.36621 | 45.1185 | 10.4739 | 1.02659 |
| Ltf-1 | 0 | 6.07E-07 | 0 | 0 |
| Actn4 | 271.428 | 326.443 | 139.504 | 216.838 |
| Krt18-2 | 10545.7 | 67.4247 | 3.07395 | 1636.47 |
| Krt8-3 | 619.772 | 651.372 | 126.381 | 421.748 |
| Ahnak-16 | 128.204 | 156.075 | 101.767 | 46.62 |
| Fbn2-5 | 11.118 | 63.8637 | 19.0418 | 0 |
| Actg1-5 | 41.5724 | 11.2704 | 5.91119 | 54.8151 |
| Actb-2 | 0 | 0 | 0 | 0.58836 |
| Hbd-3 | 93.1676 | 9062.58 | 12181.8 | 148.419 |
| Flnb | 136.729 | 48.3137 | 24.8124 | 68.8142 |
| Actb-1 | 541.363 | 300.906 | 227.927 | 636.115 |
| Krt17-1 | 841.261 | 346.401 | 48.1301 | 593.973 |
| Epx-2 | 594.069 | 43.2454 | 2.54137 | 214.26 |

| | | | | |
|---|---|---|---|---|
| Actc1-2 | 0 | 0 | 0 | 0.0226745 |
| Rnpep-1 | 830.558 | 110.153 | 112.008 | 1617.11 |
| Evpl-2 | 197.752 | 360.174 | 118.9 | 92.4863 |
| Hbd-1 | 84.2292 | 8908.24 | 11511.6 | 142.931 |
| Mslnl-2 | 19.2459 | 0.44628 | 0.797395 | 5.21412 |
| Timp2-2 | 73.5661 | 431.231 | 500.551 | 68.7189 |
| Hspa8-2 | 22.0617 | 11.11 | 387.981 | 21.7527 |
| Actg1-8 | 6.18229 | 2.46069 | 6.89105 | 2.40935 |
| Alox5-3 | 35.6501 | 13.7097 | 19.8193 | 9.00376 |
| Cd109 | 0.0660639 | 11.8572 | 9.06827 | 0.0310794 |
| Ppif-1 | 1538.13 | 747.694 | 460.946 | 2071.26 |
| Uba1 | 133.745 | 24.3017 | 27.692 | 88.4948 |
| Evpl-1 | 96.318 | 158.579 | 55.2678 | 51.1796 |
| Col1a2-1 | 166.844 | 272.567 | 329.42 | 106.474 |
| Tubb2b-1 | 133.827 | 159.028 | 174.568 | 118.45 |
| P4hb-2 | 352.395 | 439.231 | 310.194 | 315.403 |
| Myh6-4 | 0.926785 | 1.14095 | 0.958662 | 0.295202 |
| Hspa5 | 108.846 | 101.379 | 172.165 | 76.2314 |
| Eef2 | 2.99571 | 1.26201 | 8.33E-05 | 1.18188 |
| Avil-3 | 147.704 | 67.1063 | 56.8037 | 77.4826 |
| Cltc-1 | 78.7694 | 43.2337 | 155.246 | 35.6511 |
| Rnpep-2 | 256.728 | 25.5343 | 29.978 | 490.304 |
| Tgm2-5 | 262.654 | 12.381 | 14.0482 | 152.948 |
| Dsc3 | 537.915 | 102.491 | 58.9908 | 190.815 |
| Hsp90ab1 | 1227.41 | 1371.55 | 1528.68 | 1386.7 |
| Calr-3 | 366.852 | 477.26 | 414.225 | 342.649 |
| Serpinb9-1 | 911.212 | 407.399 | 193.743 | 757.092 |
| C3-7 | 0 | 0 | 0 | 0 |
| Muc5ac-3 | 12.4463 | 0.611649 | 0.0826848 | 3.96884 |
| Anpep-3 | 14.2236 | 110.174 | 49.1015 | 1.93639 |
| Gstp1 | 1941.71 | 521.566 | 508.386 | 1005.51 |
| Dsg2-1 | 498.346 | 75.8354 | 34.2995 | 177.964 |
| Ywhab-3 | 803.236 | 245.709 | 173.75 | 838.617 |
| Sord-4 | 394.651 | 58.7779 | 53.7112 | 288.466 |
| Atp5f1b | 272.681 | 180.149 | 293.123 | 326.025 |
| Hba2-2 | 105.023 | 10495 | 14001.4 | 169.269 |
| Pdia3 | 192.962 | 149.921 | 160.376 | 183.788 |
| S100z-2 | 8087.53 | 1009.54 | 839.853 | 10521.4 |
| Tgm2-4 | 369.323 | 143.691 | 27.2622 | 208.076 |

| | | | | |
|---|---|---|---|---|
| Col1a1 | 0 | 0 | 0.838605 | 0 |
| Atp2a1 | 116.917 | 71.6503 | 46.7446 | 69.1671 |
| Ywhaq | 186.106 | 68.5708 | 20.9672 | 308.005 |
| Capn9-2 | 130.406 | 108.334 | 28.2618 | 88.409 |
| Cdh17 | 270.789 | 61.8143 | 13.6603 | 138.841 |
| Hba2-3 | 53.1068 | 6063.15 | 8057.08 | 93.7599 |
| Ctnnb1-2 | 404.998 | 74.129 | 72.0081 | 266.948 |
| Gdi2 | 339.22 | 158 | 161.906 | 304.056 |
| Plec-2 | 43.9705 | 47.1939 | 23.5636 | 11.1972 |
| Msln-2 | 138.398 | 4.56314 | 2.6682 | 66.5282 |
| Ugdh-2 | 131.954 | 38.5586 | 26.0796 | 87.8228 |
| Lmnb2 | 56.3878 | 22.0274 | 21.5501 | 43.4213 |
| Scel | 656.614 | 209.929 | 109.558 | 447.896 |
| Pdcd6ip | 132.665 | 33.6621 | 15.2036 | 93.108 |
| Wdr1 | 92.2613 | 52.3629 | 49.7111 | 85.427 |
| Prdx6-2 | 374.482 | 252.448 | 269.545 | 465.765 |
| Dync1h1 | 22.0701 | 20.9436 | 29.7196 | 11.8575 |
| Gsto1 | 316.908 | 101.734 | 77.9551 | 145.125 |
| Glud1 | 135.02 | 60.2954 | 46.8464 | 85.3181 |
| Capn2-1 | 637.064 | 209.138 | 154.481 | 496.401 |
| Atp5f1a | 285.407 | 191.689 | 394.273 | 300.729 |
| Tkt | 68.7012 | 26.8621 | 47.6788 | 30.5079 |
| Tubb2b-2 | 0.0029242 | 0.96579 | 0 | 0.00093629 |
| S100p | 58839.4 | 52966.4 | 18308.7 | 59253 |
| Otogl | 0.661837 | 5.70516 | 3.27701 | 0 |